División de Fotónica
Centro de Investigaciones en Óptica, A.C.
Loma Del Bosque 115, Col. Lomas del Campestre León,Gto. Mex.

Synchronization of External-Cavity Semiconductor Lasers and its Applications in Secure Communications

by

Flavio Rodrigo Ruiz Oliveras

A thesis submitted in partial satisfaction of the requirements for the degree of Doctor in Science.

Advisor:
Dr. Alexander N. Pisarchik

September, 2009

This thesis is dedicated to G-d and to my parents.

Acknowledgments

I would first like to express my gratitude to G-d and to my parents for all their support.

I wish to thank Prof. Alexander N. Pisarchik for his guidance during my graduate studies. My gratitude also goes to Professors Bernardo Mendoza Santoyo and Alejandro R. Femat Flores for their service on my committee. I also like to thank Prof. Alexander V. Kir'yanov for his commentaries.

I would also like to express my thanks to all my teachers and partners at Centro de Investigaciones en Óptica, A.C., specially to Prof. Francisco Javier Cuevas de la Rosa, Guillermina Muñiz, Laura González and Dr. Guillermo Huerta Cuellar. I wish to thank Professors Claudio R. Mirasso, Pere Colet, Ingo Fischer, Vasile Tronciu and Dr. Miguel C. Soriano. I wish to thank my aunt Martha Oliveras and Prof. Ramiro Sandoval for their support and teaching me to see life in a different way. I also wish to thank my teachers Jesús and León Castro

Abstract

Synchronization of External-Cavity Semiconductor Lasers and its Application in Secure Communication
by
Flavio Rodrigo Ruiz Oliveras
Doctor in Science, Optics
Centro de Investigaciones en Óptica, A.C.
Dr. Alexander N. Pisarchik, chair

A numerical study of dynamics, synchronization and applications of semiconductor lasers with external cavities in secure communication systems is presented in this dissertation. The dynamics of an external-cavity semiconductor laser is studied through bifurcation diagrams using the feedback strength, length of the external cavity and the initial phase of the electric field as control parameters. A second cavity is then added, and it is showed that it is a simple mechanism to stabilize chaotic orbits into fix points. Synchronization between a master and a slave external-cavity semiconductor laser is studied for different conditions. It is first studied in monostable regions where these lasers are operating in a CW, periodic or chaotic regime. Then the synchronization is studied in regions of multistability. The applications of external-cavity semiconductor lasers in secure communications is then studied when these lasers behave in a chaotic way. A one-channel communication system (all-optical) is compared with a two channel communication system (all optical and optoelectronic) using different message transmission techniques.

The outline of this dissertation is as follows: In chapter 1 a brief introduction of lasers, external-cavity semiconductor lasers, synchronization and communication systems is given. In chapter 2 the dynamics of an external-cavity semiconductor laser is analyzed according to different control parameters. Chapter 3 is dedicated to the study of optical injection from a master laser (ML) to a slave laser (SL). Different scenarios are looked according to the dynamics of the ML or the SL; not only when they have chaotic behavior, but also when they have fix point or periodic regimes are studied. We study the case where lasers are operating in monostable and multistable regions. On chapter 4 applications of synchronization of chaotic lasers in secure optical communications are studied. Different scenarios, like one channel and two channels using pure optical elements, and a two-channel optoelectronic system are studied. Finally, global conclusions of the results are given.

Contents

List of Figures

Chapter 1

Introduction

Contents

1.1 Lasers

The word *Laser* stands for Light Amplification by Stimulated Emission of Radiation. Gourdon Gould was the first person who used the word *laser* while he was a student under Charles Townes, the inventor of the *MASER* (Microwave Amplification by Stimulated Emission of Radiation). In 1960, Theodore Maiman invented the ruby laser, considered to be the first successful quantum generator. The concept of stimulated emission as the fundamental mechanism to produce laser light was first introduced by Albert Einstein in 1917 [Siegman 1986, Aboites 2007, Thyagarajan 1981, Beesley 1971, Saford 1988]. Other processes such as absorption and spontaneous emission also occur during the production of laser light.

To explain these mechanisms the Bohr atomic model is used, where the electrons are arranged around the nucleus similar to a planetary system. The orbits of the electrons define specific energy levels where the electrons can move to by absorbing or emitting radiation, in our case photons. Electrons in the outer orbits are at higher energy levels than those in inner orbits. Let us suppose a system where only two energy levels exist, where $\Sigma_1$and Σ_2 stand for the energy of the respective levels. For the case of absorption, the initial state of an electron is at the lower level, or the level with less energy (Σ_1). When a photon of energy $\Sigma = \Sigma_2 - \Sigma_1$, interacts with this electron, this photon will be absorbed by the electron, and it will jump to the Σ_2 energy level (see figure 1.1 a)).

Now, when the electron is located in the upper level, spontaneous or stimulated emission can occur, i.e. an electron tends to return to its initial state, that is to level 1.

In this case a photon with energy $\Sigma = \Sigma_2 - \Sigma_1$ will be emitted (see figure 1.1 b)). Light produced by spontaneous emission is called luminescence, equal to around one-tenths to one-third of the total laser's output power. For the case of stimulated emission, another photon with energy $\Sigma = \Sigma_2 - \Sigma_1$ will come and interact with the electron located on the upper level. This will cause the electron to return to the lower level, and during this process a photon will be emitted, at the end there will be two photons with the same characteristics (see figure 1.1 c)). Since both photons have the same characteristics, the same phase and frequency, the light emitted by a laser has temporal and spatial coherence, that are important characteristics of the laser light. Due to the wave-particle duality of photons, the frequency of the emitted photons will be given by:

$$\upsilon = \frac{\Sigma_2 - \Sigma_1}{h} \tag{1.1}$$

where $h = 6.63 \times 10^{-34}$ J·s is Planck's constant.

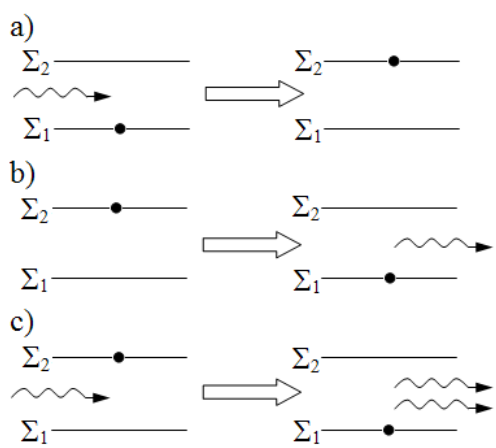

Figure 1.1: a) Absorption, b) spontaneous emission and c) stimulated emission.

The absorption process depends on the energy density of radiation (density of photons) at frequency υ, denoted as $u(\upsilon)$. Absorption is proportional to the number of electrons found in level 1 (N_1). The amount of absorptions per time, per volume can be written as:

$$N_1 B_{12} u(\upsilon), \tag{1.2}$$

where B_{12} is a proportionality coefficient, characteristic of the energy levels. If N_2 is the number of electrons in level 2, then spontaneous emission will be described as:

$$N_2 A, \tag{1.3}$$

where A is the proportionality coefficient. Finally, the process of stimulated emission depends on the energy density of radiation and on the number of electrons in level 2:

$$N_2 B_{21} u(\upsilon), \tag{1.4}$$

where B_{12} is the proportionality coefficient. The coefficient A, B_{12} and B_{21} are called Einstein coefficients and depend on the atomic system. Now that these three processes have been described, the rate equation to model the exchange of electrons between the levels Σ_2 and Σ_1 can be obtained. For energy level 2, the population increases due to absorption, and decreases due to spontaneous and stimulated emission. Taking this into consideration, the rate equation of population inversion can be written as:

$$\frac{dN(t)}{t} = N_1 B_{12} u(\upsilon) - N_2 A - N_2 B_{21} u(\upsilon). \tag{1.5}$$

The above equation expresses the electronic transition per volume per time. Sometimes it is convenient to express equation (1.5) in transitions per time. To do this, equation (1.5) should just be multiplied by the volume of the active medium, and the energy required for absorption and stimulated emission will now be in number of photons.

In thermal equilibrium, the number of transitions from level 1 to level 2 is the same as the number of transitions from level 2 to level 1. Taking this into account:

$$N_1 B_{12} u(\upsilon) = N_2 A + N_2 B_{21} u(\upsilon), \tag{1.6}$$

and from this last expression the radiation density is:

$$u(\upsilon) = \frac{A}{\left(\frac{N_1}{N_2}\right) B_{12} - B_{21}}. \tag{1.7}$$

From the law of Boltzman, the population ratios for both energy levels is given as:

$$\frac{N_1}{N_2} = \exp\left(\frac{h\upsilon}{kT}\right), \tag{1.8}$$

where $k = 1.38$ J/K is Boltzman's constant, and T is the temperature. Substituting equation (1.8) into equation (1.7) we obtain:

$$u(\upsilon) = \frac{A}{\exp\left(\frac{h\upsilon}{kT}\right) B_{12} - B_{21}}, \tag{1.9}$$

According to the law of Planck, the energy density is:

$$u(\upsilon) = \frac{8\pi h\upsilon^3}{c^3} \frac{A}{\exp\left(\frac{h\upsilon}{kT}\right) - 1}, \tag{1.10}$$

where c is the speed of light. Comparing equations (1.9) and (1.10), we have that $B_{12} = B_{21} = B$, and $A/B = 8\pi h\upsilon^3/c^3$. A dimensional analysis from equation (1.10), shows that the units of A is second^{-1}, so $\tau_{\mathrm{e}} = 1/A$ is the life time of an electron in level 2.

Laser light is generated when population inversion is reached. For a two level system, as the one mentioned before, this means that the population of electrons in level Σ_2 will be greater than the population in level Σ_1. All these phenomena occur in the active medium of a laser. Now we need a mechanism to produce a permanent population inversion. In the case of semiconductor lasers, an electric current is used to inject electrons to the higher energy level. This electric current is known as the "pump current". For other types of lasers, such as the ruby laser, a flash light can be used as the pump mechanism.

Once population inversion is obtained, electrons from energy level Σ_2 will descend to energy level Σ_1, and photons will be produced by spontaneous emission. Therefore a way to maintain the photons in the active media is needed in order to obtain stimulated emission. Photons are contained in the active media by means of a resonator (optical cavity), which can be formed by a pair of mirrors. The active media is placed between the mirrors, this way the photons will travel back and forth reflecting from the mirrors and going through the active media. While photons travel through the active medium, these will interact with the electrons located in energy level Σ_2, and stimulated emission will increase the number of photons and light amplification will take place. At least one of the mirrors needs to have a reflectivity less than 100%, allowing some photons to escape from the resonator. The length of the resonator is of extreme importance so that the photons can oscillate inside the cavity. Its length must be a multiple of the wave length associated with the photons:

$$L = q\frac{\lambda}{2}, \tag{1.11}$$

where L is the distance between the two mirrors, $q = 1, 2, 3,...$, and λ is the wave length. If $L >> \lambda$, then a great number of modes will be able to oscillate inside the resonator. The wave length can be defined as $\lambda = c/\upsilon n_{\mathrm{c}}$, where n_{c} is the refractive index, and the angular frequency is $\omega = 2\pi\upsilon$. Inserting these two equations into equation (1.11),we get the different mode frequencies that can be held in the resonator:

$$\omega_{\mathrm{m}} = q\frac{\pi c}{L n_{\mathrm{c}}}. \tag{1.12}$$

Thus, a laser consists of three main parts: the active medium where the population inversion is created, the pump which is in charge of creating the inversion population, and a resonator which contains the photons so that light amplification and stimulated

emission can occur. Figure 1.2 shows a typical scheme of a ruby laser containing this three elements.

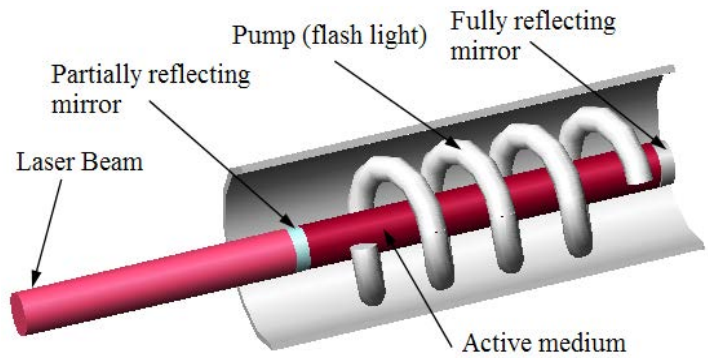

Figure 1.2: Scheme showing the principal components of a laser.

To derive the equation that describes the evolution of the complex electric field [Rogister 2001, Soriano 2006] normalized so that $|E(t)|^2$ is the intensity in number of photons, let us consider a travelling wave inside a resonator. Figure 1.3, shows the scheme of an electric field propagating inside a cavity of length L. $R_1 = r_1^2$ and $R_2 = r_2^2$ denote the mirror power or intensity reflection coefficients, where r_1 and r_2 are the amplitude reflection coefficients. This complex field propagates in an active medium whose complex refractive index is $n_\mathrm{c} = n + n'$, n is the real part and $n' = \frac{c}{2\omega}(g - \mu)$ is the imaginary part. Where g is the gain due to stimulated emission and μ is the optical loss inside the cavity. We consider the forward and backward travelling complex field $\Xi(x,t) = E(t)\exp(-in\omega x/c)$ inside the resonator.

For the travelling forward complex field:

$$\Xi_\mathrm{f}(x,t) = E_\mathrm{fo}(t)\exp\left(-i\frac{n\omega}{c}x + \frac{1}{2}x\,(g-\mu)\right), \tag{1.13}$$

and for the backward:

$$\Xi_\mathrm{b}(x,t) = E_\mathrm{bo}(t)\exp\left(-i\frac{n\omega}{c}\,(L-x) + \frac{1}{2}\,(L-x)\,(g-\mu)\right), \tag{1.14}$$

where ω is the angular frequency of the electric field and c is the speed of light. The conditions $E_\mathrm{fo} = r_1 E_\mathrm{bo}(0)$ and $E_\mathrm{bo} = r_2 E_\mathrm{fo}(L)$ must be satisfied. This leads to the well known equation:

$$r_1 r_2 \exp\left(-2i\frac{n\omega}{c}L + L(g-\mu)\right) = 1, \tag{1.15}$$

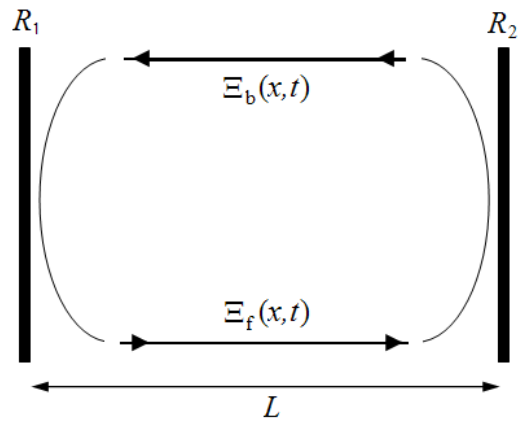

Figure 1.3: Schematic arrangement of the complex field travelling forward and backward in a resonator.

where gain and losses are equal.

To obtain the threshold gain, now we consider the intensities instead of the complex electric field. Starting with an intensity I_0 at R_1, the intensity after a complete round trip is:

$$I = I_0 R_1 \exp\left(gL - \mu L\right) R_2 \exp(gL - \mu L). \tag{1.16}$$

The threshold gain needed for laser emission is reached at $I = I_0$, then:

$$g_{\text{th}} = \mu + \frac{1}{2L} \ln\left(\frac{1}{R_1 R_2}\right). \tag{1.17}$$

From equation (1.15) the total gain experienced by the traveling complex field after one round trip inside the cavity is defined as:

$$G = r_1 r_2 \exp\left(-2i\frac{n\omega}{c}L + L(g - \mu)\right). \tag{1.18}$$

Next, a first order Taylor expansion is done to the term $n\omega/c$ around the lasing threshold:

$$\begin{aligned}\frac{n\omega}{c} &\approx \frac{(n\omega)\,|_{\text{th}}}{c} + \frac{1}{c}\frac{\partial\,(n\omega)}{\partial\omega}|_{\text{th}}\,(\omega - \omega_{\text{th}}) + \frac{1}{c}\frac{\partial\,(n\omega)}{\partial N}|_{\text{th}}\,(N - N_{\text{th}}) \\ &= \frac{n_{\text{th}}\omega_{\text{th}}}{c} + \frac{n_{\text{g}}}{c}\,(\omega - \omega_{\text{th}}) + \frac{\omega_{\text{th}}}{c}\frac{\partial n}{\partial N}|_{\text{th}}\,(N - N_{\text{th}})\,.\end{aligned} \tag{1.19}$$

Equation (1.19) contains the angular frequency at threshold ω_{th}, the population inversion at threshold N_{th}, and the refractive group index n_{g}:

$$n_{\mathrm{g}} = n + \omega \frac{\partial n}{\partial \omega}. \tag{1.20}$$

Inserting equation (1.19) into equation (1.18) and separating G into two gain factors, one is constant and another depends on the frequency, this is:

$$G = G_{\mathrm{c}} G_{\omega,} \tag{1.21}$$

$$G_{\mathrm{c}} = \exp\left[\frac{1}{2}\ln(R_1 R_2) + L(g-\mu) - 2i\frac{\omega_{\mathrm{th}}}{c}\frac{\partial n}{\partial N}|_{\mathrm{th}}\left(N - N_{\mathrm{th}}\right)\right], \tag{1.22}$$

$$G_{\omega} = \exp\left[-2i\frac{n_{\mathrm{th}}\omega_{\mathrm{th}}L}{c}\right]\exp\left[-2i\frac{n_{\mathrm{g}}L}{c}\left(\omega - \omega_{\mathrm{th}}\right)\right], \tag{1.23}$$

Equation (1.23) can be written in a simpler manner. From equation (1.12), $n_{\mathrm{th}}\omega_{\mathrm{th}}L/c$ is a multiple of 2π, the first factor equals to 1, and

$$\tau_{\mathrm{d}} = 2\frac{n_{\mathrm{g}}L}{c}, \tag{1.24}$$

is the laser cavity round trip time. Then G_{ω} is:

$$G_{\omega} = \exp\left[-(\omega - \omega_{th})\tau_{\mathrm{d}}\right], \tag{1.25}$$

and the complex gain reads:

$$G = G_{\mathrm{c}}\exp\left[-(\omega - \omega_{\mathrm{th}})\tau_{\mathrm{d}}\right]. \tag{1.26}$$

The term g depends on the population N, and it is linearized around its threshold value giving:

$$g(N) = g_{\mathrm{th}} + \frac{\partial g(N)}{\partial N}|_{N\mathrm{th}}(N - N_{\mathrm{th}}). \tag{1.27}$$

Once the gain for one round trip inside the cavity is obtained, after one round trip the complex amplitude is:

$$E(t + \tau_d) = GE(t). \tag{1.28}$$

For a slow varying complex amplitude $\omega \approx \omega_{\mathrm{th}}$, with $G = G_{\mathrm{c}}$. Since $E(t)$ is the amplitude of a slow varying filed, we can approximate:

$$\frac{dE(t)}{dt} \approx \frac{E(t + \tau_{\mathrm{d}}) - E(t)}{\tau_{\mathrm{d}}}. \tag{1.29}$$

Substituting equation (1.28) into equation (1.29), we get:

$$\frac{dE(t)}{dt} = \frac{(G-1)}{\tau_{\mathrm{d}}} E(t). \tag{1.30}$$

Since G is close to unity, it can be expanded leading to:

$$G \cong 1 + \ln(G_{\mathrm{c}}). \tag{1.31}$$

Using equations (1.17), (1.24), (1.27), (1.31) and $\omega \approx \omega_{\mathrm{th}}$, the term $(G-1)/\tau_{\mathrm{d}}$ is given by:

$$\frac{(G-1)}{\tau_{\mathrm{d}}} = \frac{c}{2n_{\mathrm{g}}} \frac{\partial g(N)}{\partial N}|_{N\mathrm{th}}(N - N_{\mathrm{th}}) - i\frac{\omega}{n_{\mathrm{g}}} \frac{\partial n}{\partial N}|_{N\mathrm{th}}(N - N_{\mathrm{th}}) \tag{1.32}$$

Inserting this last equation into equation (1.30), the equation for the slow varying complex amplitude is given by:

$$\frac{dE(t)}{dt} = \left[\frac{c}{2n_{\mathrm{g}}} \frac{\partial g(N)}{\partial N}|_{N\mathrm{th}}(N - N_{\mathrm{th}}) - i\frac{\omega}{n_{\mathrm{g}}} \frac{\partial n}{\partial N}|_{N\mathrm{th}}(N - N_{\mathrm{th}})\right] E(t) \tag{1.33}$$

1.2 Semiconductor lasers

The active media of semiconductor lasers [Saleh 1991, Wilson 1998, Singh 1995] is made by the union of N-type with P-type materials. As mentioned before, electrons, also called charge carriers, can only occupy levels with specific energies. The levels with less energy are filled first, and the electrons that occupy the highest energy levels are called valence electrons. In a semiconductor material, the valence electrons do not belong to a specific atom in the crystalline web, but belong to all the system of atoms. The place where these electrons are found is called a valence band. The next energy level from the valence band is called a conduction band, and in between these two levels there is a prohibited band called a band gap, where electrons cannot be found. Impurities added to this crystal structure can modify its properties. If different atoms with more valence electrons than those that form the crystal structure are added, then there is more probability to find electrons in the conduction band, this is a N-type material. On the other hand if atoms with less valence electrons are added, then there is less probability to find electrons in the conduction band and an absence of charge carrier called holes appear in the valence band, this is a P-type material. Atoms that belong to group IV of the periodic table, such as silicon and germanium, are used to form the main crystalline structure. To obtain N-type material, atoms that belong to group V of the periodic table, such as phosphorus and arsenic, are added as impurities to the crystal structure. To create the P-type material, the atoms from group III, such as boron and indium, are added to the crystalline structure.

As we mentioned before, there is a certain probability to find electrons in the valence or conduction band. This probability is indicated with the Fermi level, which is described by:

$$f(\Sigma) = \frac{1}{\exp\left(\frac{\Sigma - \Sigma_{\mathrm{f}}}{k_{\mathrm{B}}T}\right) + 1}, \tag{1.34}$$

where k_{B} is the Boltzman constant, Σ_{f} is the Fermi energy, T is the temperature, and Σ is the energy corresponding to the energy level. Under normal conditions, the Fermi level is located in the middle of the band gap, meaning that there is exactly the same probability to find an electron in the valence or conduction band. For the N-type material, the Fermi level is located closer to the conduction band (see figure 1.4 a)), so there is higher probability to find and electron in the conduction band. For the P-type material, the Fermi level is near the valence band, so there is a greater probability to find an electron in the valence band (see figure 1.4 b)).

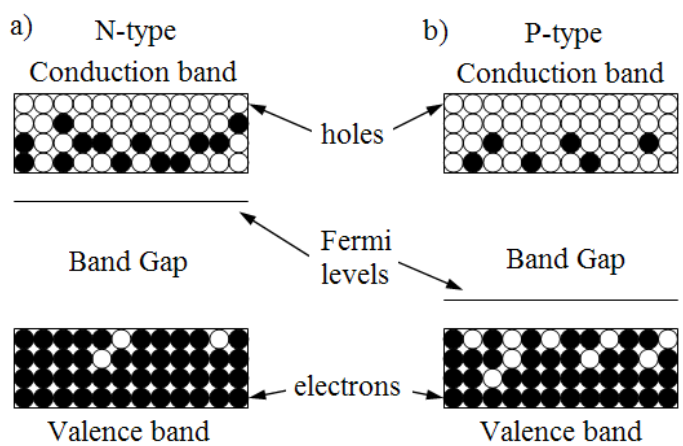

Figure 1.4: Fermi levels for a) N-type and b) P-type materials.

Once the N-type and P-type materials are joined, the excess of electrons found in the N-type material diffuse towards the holes of the P-type material, and by a similar way some holes of the P-type material diffuse into the N-type material. The junction of the N-type with P-type material is known as a diode. The zone where this electrons and holes diffuse is called a depletion region. Once the union is made, the Fermi level is kept constant in each material, producing a potential with difference V_0 between the two materials at the depletion region (see figure 1.5).

If the positive side of a battery is connected with the P-type and the negative side with the N-type, this causes a decrease in the potential of the depletion area, and both

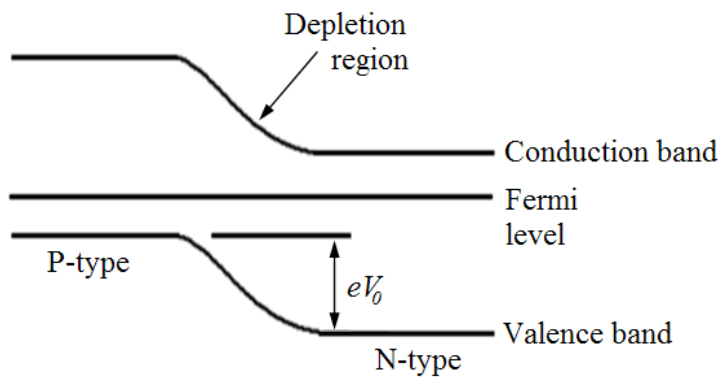

Figure 1.5: Potential formed at depletion region.

Fermi levels of the diode will not be at the same level; the holes of the P-type side and the electrons of N-type side will be repelled to the depletion region. Since the electrons and holes are found at the union and the potential decrease, the electrons from the conduction band will drop to the valence band combining with the holes. The electron will be able to emit a photon during the transition because the electrons are moving from a high energy level to a low energy level. In this case the battery supplies the pump current of the semiconductor laser. Finally, for this type of lasers, the facets act as the reflecting mirrors to form the resonator, some reflective coatings can also be added on the laser facets. When the rate of injected electrons and stimulated emission are equal, the semiconductor medium is said to be transparent. Table 1 [Sale 1995] shows some of the materials used in semiconductor lasers, as well as the wavelengths.

Material	Wavelength
AlGaAs/GaAs	680-690 nm
InGaAs/GaAs	950-1100 nm
InGaAsP/InP	1000-1700 nm
AlGaInP/GaAs	600-700 nm
ZnCdSSe	450-550 nm
AlGaInN	200-640 nm
GaInNAs/GaAs	1300-1500 nm
GaN/AlGaN	400-550 nm

Table 1. Materials used for semiconductors

A very important dynamical parameter of a semiconductor lasers is the α factor, which takes into account the changes of the refractive index induced by carriers [Henry 1982, Fleming 1981, Osinski 1987, Masoller 1997]. It is also known as

the linewidth enhancement factor because it is responsible for the increasing spectral linewidth in semiconductor lasers. It is defined as:

$$\alpha = \frac{\partial n/\partial N}{\partial n'/\partial N} = -2\frac{\omega}{c}\frac{\partial n/\partial N}{\partial g/\partial N} \tag{1.35}$$

and:

$$\frac{\partial n}{\partial N} = -\alpha\frac{c}{2\omega}\frac{\partial g}{\partial N}. \tag{1.36}$$

Substituting equation (1.36) into equation (1.33), the evolution of the slow varying amplitude of the complex field is:

$$\frac{dE(t)}{dt} = (1+i\alpha)\left[\frac{c}{n_{\mathrm{g}}}\frac{\partial g}{\partial N}|_{\mathrm{th}}\,(N-N_{\mathrm{th}})\right]\frac{E(t)}{2}. \tag{1.37}$$

Lets define the gain per second as:

$$v_{\mathrm{g}}g(N) = v_{\mathrm{g}}g_{\mathrm{th}} + G_{\mathrm{N}}(N(t)-N_{\mathrm{th}}) = G_N(N(t)-N_0), \tag{1.38}$$

where $G_{\mathrm{N}} = v_{\mathrm{g}}\frac{\partial g}{\partial N}|_{N_0} \approx v_g\frac{\partial g}{\partial N}|_{N_{\mathrm{th}}}$, the group velocity is $v_{\mathrm{g}} = c/n_{\mathrm{g}}$ and N_0 is the carrier number at transparency. Most losses in semiconductor lasers are through the facet mirrors, so we can define the total loss rate of photons as the photon lifetime:

$$\tau_{\mathrm{p}} = \frac{1}{v_{\mathrm{g}}g_{\mathrm{th}}}. \tag{1.39}$$

Introducing equations (1.38) and (1.39) into (1.37), we have:

$$\frac{dE(t)}{dt} = (1+i\alpha)\left[G_{\mathrm{N}}\,(N(t)-N_0) - \frac{1}{\tau_{\mathrm{p}}}\right]\frac{E(t)}{2}. \tag{1.40}$$

High light intensities saturate the gain. This is due to physical phenomena as hole burning and dynamic carrier heating. Hole burning accounts for a local depletion of the carrier number due to the fact that the optical field does not have the same intensity through the active layer. Dynamic carrier heating account for temporary loss of carriers which jump to higher energy bands where it is impossible to recombine with holes in the valence bands. This new gain [Vicente 2008, Heil 2001] is given by:

$$G_{\mathrm{s}} = \frac{G_{\mathrm{N}}}{1+s|E(t)|^2}, \tag{1.41}$$

where s is the saturation. Finally, to simulate the noise [Heil 2001, Heil 2002, Locuet 2002, Buldú 2009] from spontaneous emission:

$$\sqrt{2\beta N(t)}\xi(t), \tag{1.42}$$

where β is the spontaneous emission rate and $\xi(t)$ is a Gaussian white noise having unity intensity. The amplified spontaneous emission can be neglected in common semiconductor lasers [Siegman 1986]. Only in high-gain semiconductor lasers in which the reflectivity of the laser facets have been deliberately manipulated, the amplified spontaneous emission has to be taken into consideration..

The equation that describes the carrier rate is very similar to equation (1.5), only some things need to be taken into consideration. First of all as mentioned before, in semiconductor lasers the pumping is done trough an electric current I, so the number of electrons, or carriers, injected to the high energy level is given by I/e_c, where e_c is the charge of the electrons. The process of spontaneous emission is the same as equation (1.3), and $A = 1/\tau_\mathrm{n}$, where τ_n is the carrier lifetime. The stimulated emission will be given by $G_\mathrm{N}(N(t) - N_0)|E|^2$. If the above are used for the carrier rate equation and inserting equations (1.41) and (1.42) into equation (1.40), we get the rate equations for a semiconductor laser:

$$\frac{dE(t)}{dt} = (1 + i\alpha)\left[\frac{G_\mathrm{N}\left(N(t) - N_0\right)}{1 + s|E(t)|^2} - \frac{1}{\tau_\mathrm{p}}\right]\frac{E(t)}{2} + \sqrt{2\beta N(t)}\xi(t), \tag{1.43}$$

$$\frac{dN(t)}{dt} = \frac{I}{e_\mathrm{c}} - \frac{N(t)}{\tau_\mathrm{n}} - \frac{G_\mathrm{N}(N(t) - N_0)|E|^2}{1 + s|E(t)|^2}. \tag{1.44}$$

Typical values used for the parameters [Revuelta 2002, Vicente 2005] of these two equations are shown in table 2.

Parameter	Value
α [1]	3
G_N	1.5×10^{-8} ps^{-1}
N_0 [1]	1.5×10^{8}
s [1]	10^{-7}
τ_p	2 ps
β	1.1×10^{-6} ps^{-1}
I	29 mA
e_c	1.6×10^{-19} C
τ_n	2 ns

Table 2. Parameter values for rate equations.

[1] Dimensionless parameters

The solution of equations (1.43) and (1.44) result in relaxation oscillations as shown in figure 1.6.

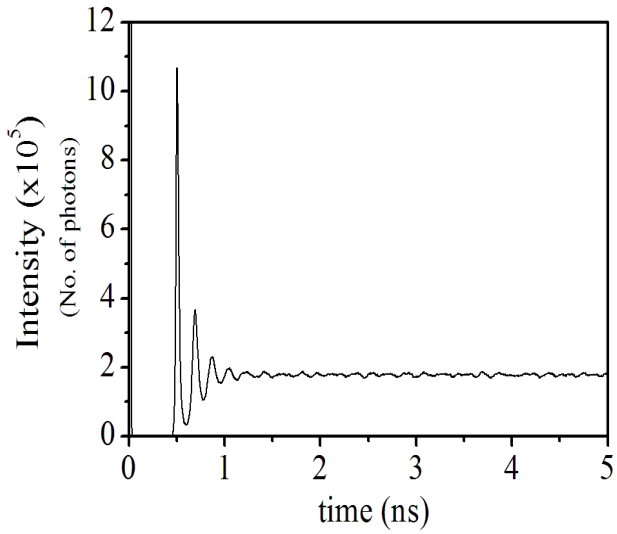

Figure 1.6: Relaxation oscillations of a semiconductor laser.

1.3 External-cavity semiconductor laser

External cavities are added to semiconductor lasers to produce optical feedback. This consists in injecting the semiconductor laser output back into its own cavity after the reflection from an external mirror (see figure 1.7).

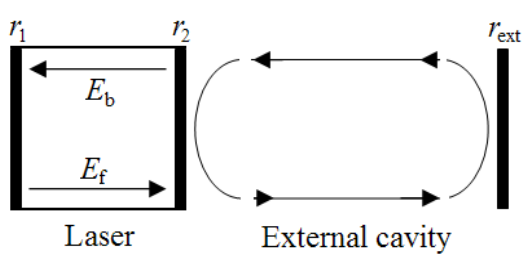

Figure 1.7: Semiconductor laser with external cavity

The amplitude of E_b is the result of both the reflection of E_f at r_2 and the entering of the amplitude of the complex field inside the external cavity, containing an infinite

number of contributions due to the round trips of the external cavity, E_b can be written as[Lang 1980, van Tartwijk 1995]:

$$\begin{aligned} E_\mathrm{b} &= r_2 E_\mathrm{f} \\ &+ (1-r_2^2) r_\mathrm{ext} E_\mathrm{f} \exp(-i\omega\tau) \\ &+ (1-r_2^2) r_\mathrm{ext} (r_2 r_\mathrm{ext}) E_\mathrm{f} \exp(-i2\omega\tau) \\ &+ (1-r_2^2) r_\mathrm{ext} (r_2 r_\mathrm{ext})^2 E_\mathrm{f} \exp(-i3\omega\tau) \\ &+ \dots , \end{aligned} \tag{1.45}$$

where τ is the round trip time of the external cavity. When the feedback is weak, then it can be approximated by taking into account just one external round trip, this is:

$$E_\mathrm{b} = r_2 \left[1 + \frac{(1-r_2^2) r_\mathrm{ext}}{r_2} \exp(-i\omega\tau) \right] E_\mathrm{f}. \tag{1.46}$$

The term $\phi = \omega\tau$ is the phase of the complex field in the external cavity. The effective amplitude reflectivity r_eff can be defined as the ratio $E_\mathrm{b}/E_\mathrm{f}$ [Kobayashi 1976, Wang 1994, Petermann 1991]. The total cavity loss rate for the compound cavity can be derived in a similar manner as equation (1.17):

$$\mu_\mathrm{cav} = \frac{c}{2nL} \ln \left(\frac{1}{r_1 r_\mathrm{eff} \exp(-i\omega\tau)} \right), \tag{1.47}$$

which leads to:

$$\mu_\mathrm{cav} = \frac{c}{2nL} \left[\ln \left(\frac{1}{r_1 r_2} \right) - \ln \left(1 + (1-r_2^2) \frac{r_\mathrm{ext}}{r_2} \exp(-i\omega\tau) \right) \right]. \tag{1.48}$$

The term $\ln(1/r_1 r_2)$ stands for the cavity loss without the external mirror and has already been taken into account, when equation (1.33) was derived previously. If $(1-r_2^2) r_3/r_2 << 1$ and $\tau << 1$, then the feedback rate is given as:

$$\kappa = \frac{1-r_2^2}{\tau_\mathrm{d}} \frac{r_\mathrm{ext}}{r_2}. \tag{1.49}$$

Inserting the feedback rate into equation (1.43) and taking into consideration the lag of the external cavity for the amplitude of the complex field we get the Lang-Kobayashi[Lang 1980, Mirasso 1996] model for a semiconductor laser with optical feedback:

$$\begin{aligned} \frac{dE(t)}{dt} &= (1+i\alpha) \left[\frac{G_\mathrm{N} (N(t) - N_0)}{1 + s|E(t)|^2} - \frac{1}{\tau_\mathrm{p}} \right] \frac{E(t)}{2} \\ &+ \kappa E(t-\tau) \exp(-i\omega\tau) + \sqrt{2\beta N(t)} \xi(t). \end{aligned} \tag{1.50}$$

Optical feedback introduces a degree of freedom, therefore it can have more rich dynamics[Weiss 1991]. With the appropriate parameters of the external cavity, constant wave (CW), periodic, quasi-periodic, chaotic behavior, and low frequency fluctuations can be obtained [Jesper 1992]. Chaotic behavior is obtained due to the coherence collapse[Cohen 1991, Besnard 1993, Giudici 1997, Salathe 1979, Lenstra 1985], which is a catastrophic broadening of the linewidth that can be up to 10 GHz. Figure 1.8 shows time series for different regimes that can be achieved. The rich dynamics that external-cavity semiconductor lasers exhibit, can be used for different applications, such as interferometric sensors and in optical communications[Ohtsuko 2006, Colet 1998, Gouaux 1998].

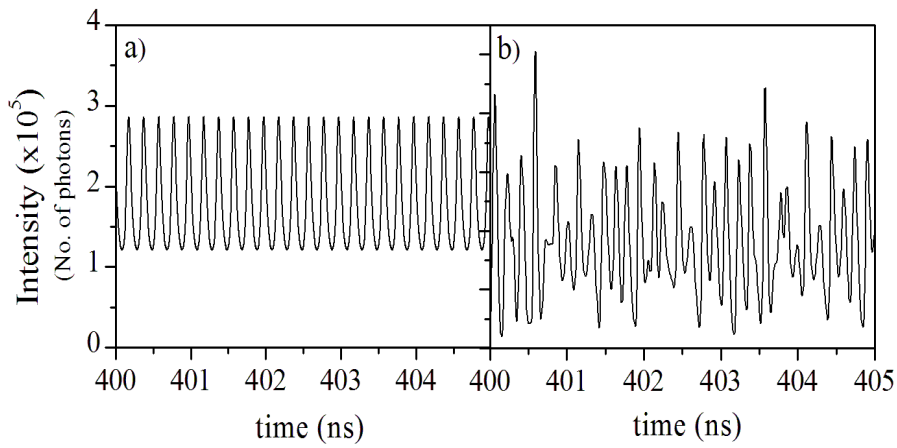

Figure 1.8: Time series showing a) period 1 and b) chaos.

To stabilize the output of this type of lasers, a second external cavity can be used [Rogister 1999, Rogister 2000, Ruiz-Oliveras 2005]. The advantage of this technique to stabilize the laser is that the position and reflectivity of the second mirror are not necessary to be very accurate. Figure 1.9 shows a scheme for a semiconductor laser with two external cavities, and the model is given as:

$$\begin{aligned}\frac{dE(t)}{dt} &= (1+i\alpha)\left[\frac{G_{\mathrm{N}}\left(N(t)-N_0\right)}{1+s|E(t)|^2}-\frac{1}{\tau_{\mathrm{p}}}\right]\frac{E(t)}{2} \\ &+ \kappa_1 E(t-\tau_1)\exp(-i\omega\tau_1)+\kappa_2 E(t-\tau_2)\exp(-i\omega\tau_2) \\ &+ \sqrt{2\beta N(t)}\xi(t),\end{aligned} \tag{1.51}$$

where κ_1 and κ_2 are the feedback parameters for the first and second external cavities, and τ_1 and τ_2 are the respective round trip times.

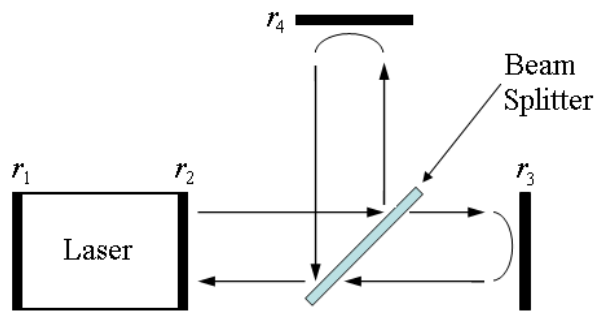

Figure 1.9: Semiconductor laser with two external cavities.

1.4 Synchronization

Synchronization was studied [Peterson , Bennet 2002] by Christian Huygens in 1665. At this time Huygens patented his design of the pendulum clock with the solution of the longitude problem in mind. The longitude problem consisted in knowing in an accurate way the distance one had travel after setting sail. It is said that one day he was confined in his house, due to sickness, and meanwhile he was observing two pendulum clocks that where hanged on the wall. Huygens noticed that the pendulums of the two clocks were swinging together; when one pendulum swung to the left, the other went to the right. The pendulums remained precisely in opposite phase.

After deliberately disturbing the pendulums, so that no longer one mirrored the movement of the other pendulum, it was only a matter of time that the pendulums were back in opposite-phase motion. Huygens suspected that the clocks where influencing each other. His first thought was that the air currents produced by the motion of the pendulum were the responsible of this. After further researching, he made an experiment (figure 1.10), where two clocks were suspended on a common frame. Then he realized that the vibrations of their common support, which he called "imperceptible movements" where the responsible of the synchronization between the clocks.

Recently the research on synchronization of chaotic systems has driven the attention. One of the characteristics of a chaotic system is its sensibility to initial conditions, also known as the butterfly effect. For a specific chaotic system, having slightly different initial conditions, the trajectories experience an exponential divergence. As a result, chaotic systems defy synchronization. Recent studies have shown that chaotic systems can be synchronized with the appropriate coupling [Pecora 1990, Roy 1994]. Usually an output signal from one chaotic system is introduced to the other system. The system whose signal is introduced to the other one is called the driver or master system, and the other system that receives the signal is the driven or slave system

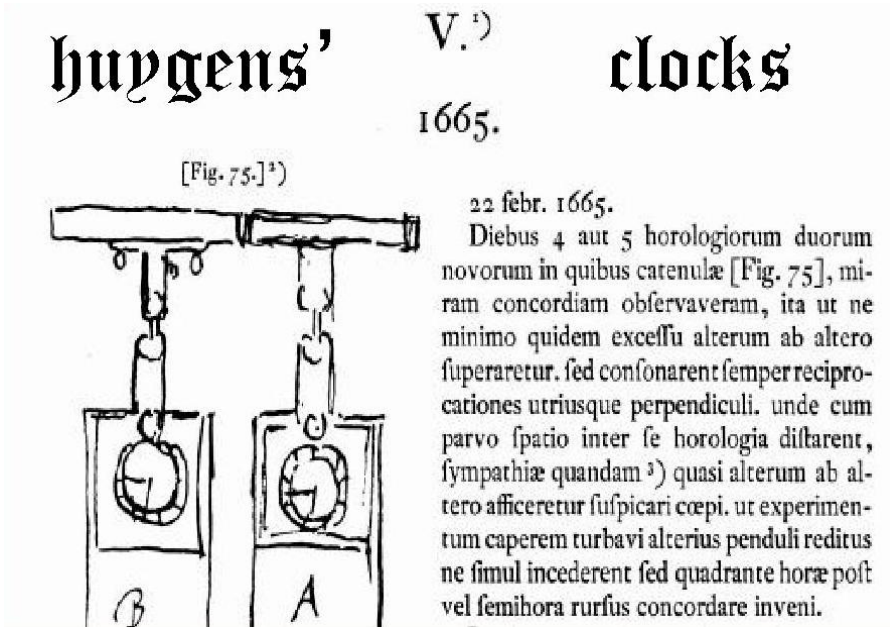
huygens' V.[1] clocks

1665.

[Fig. 75.][2]

22 febr. 1665.

Diebus 4 aut 5 horologiorum duorum novorum in quibus catenulæ [Fig. 75], miram concordiam obſervaveram, ita ut ne minimo quidem exceſſu alterum ab altero ſuperaretur. ſed conſonarent ſemper reciprocationes utriusque perpendiculi. unde cum parvo ſpatio inter ſe horologia diſtarent, ſympathiæ quandam [3]) quasi alterum ab altero afficeretur ſuſpicari cœpi. ut experimentum caperem turbavi alterius penduli reditus ne ſimul incederent ſed quadrante horæ poſt vel ſemihora rurſus concordare inveni.

Figure 1.10: Huygens' clocks experiment.

If there are two coupled chaotic oscillators, whose outputs are $y_1(t)$ and $y_2(t)$, different types of synchronization[Boccaletti 2002] can exist between them:

1. Identical or complete synchronization: it is defined as the identity between the trajectories of the driven system (slave) with the driver systems (master). The existence of complete synchronization implies that:

$$\lim_{t\to\infty} [y_1(t) - y_2(t)] = 0. \tag{1.52}$$

In other words, the driven (slave) system forgets its initial conditions, though evolving on a chaotic attractor. This type of synchronization is only observed for identical chaotic systems. To measure the complete synchronization one can use the cross-correlation between signals or the mean synchronization error. The cross-correlation is defined as[Soriano 2008]:

$$C(t) = \frac{\langle y_1(t')y_2(t'-t) - \overline{y}_1\overline{y}_2\rangle_{t'}}{\sigma_{y_1}\sigma_{y_2}}, \tag{1.53}$$

where $\overline{y}_{1,2}$and $\sigma_{y_{1,2}}$ are the mean and standard deviations. The cross correlation has a value between 0 (no synchronization) and 1 (complete synchronization). On the other hand the mean synchronization error is:

$$\langle e \rangle = \left\langle \sqrt{(y_1 - y_2)^2} \right\rangle . \tag{1.54}$$

2. Phase synchronization: this expresses that the phase difference between two irregular oscillators is bounded, this is:

$$|\phi_1 - \phi_2| < const. \tag{1.55}$$

It is important to emphasize that although the phases of the two oscillators are locked, the amplitudes are uncorrelated.

3. Lag synchronization: here we compare the two oscillators at different times. If we can find a time τ such that $y_1(t) = y_2(t-\tau)$, then the system $y_1(t)$ is said to lag (advance) the dynamics of system $y_2(t)$. There can also be the case when $y_1(t-\tau) = y_2(t)$, this case $y_2(t)$ anticipates the dynamics of $y_1(t)$. In this case when the cross-correlation is computed, the maximum cross correlation will be at $C(\tau)$ or $C(-\tau)$ due to the lag or anticipation; while for identical synchronization its maximum value will be at $C(0)$.
4. Generalized Synchronization: in coupled non-identical systems there is no hope of

having a manifold in the phase space attracting the system trajectories. Generalized synchronization is said to exist if there exists a transformation $\psi : y_1(t) \to y_2(t)$ which is able to map asymptotically the trajectories of the driver attractor into the ones of the driven attractor $y_2(t) = \psi(y_1(t))$, regardless of the initial conditions.

Studies have been made for synchronization of different types lasers, e.g. , CO_2 [Sugawara 1994, Meucci 2006], fiber [Luo 2000], and semiconductors [Mirasso 1996]. Semiconductor lasers have caught particular attention because its relaxation oscillations frequency is very high (several gigahertz), which is approximately four orders of magnitude higher than the fundamental frequencies of gas, solid-state, and fiber lasers. For the case of semiconductor lasers with external cavities and operating in a chaotic regime, synchronization can be achieved between two of these lasers [Sivaprakasam 2002, Murakami 2002, Liu 2002, Locquet 2002]. The coupling of these lasers is done through optical injection. This is, the output signal of the master or driver laser (ML) is injected into the slave or driven laser (SL), as it is shown in figure 1.11.

The equation that describes the behavior of the slow varying amplitude of the complex field for the master laser is the same as (1.50). For the slave laser, an extra term simulating the optical injection coming from the master laser has to be added, which turns out to be:

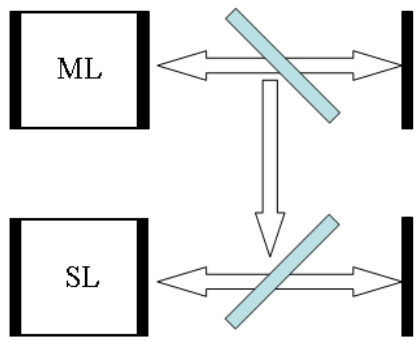

Figure 1.11: Master-Slave laser configuration to obtain synchronization.

$$\frac{dE_{\mathrm{s}}(t)}{dt} = (1+i\alpha)\left[\frac{G_{\mathrm{N}}\left(N_{\mathrm{s}}(t)-N_0\right)}{1+s|E(t)|^2} - \frac{1}{\tau_{\mathrm{p}}}\right]\frac{E_s(t)}{2} \tag{1.56}$$

$$+\kappa E_{\mathrm{s}}(t-\tau)\exp(-i\omega\tau) + \gamma E_m(t) + \sqrt{2\beta N(t)}\xi(t),$$

where "m" and "s" stand for master and slave, and γ is the coupling parameter between master and slave laser, defined as [Mirasso 2000]:

$$\gamma = \eta\frac{\sqrt{1-R}}{\tau_{\mathrm{d}}\sqrt{R}}, \tag{1.57}$$

where R is the facet laser power reflectivity, η are the losses different than those introduced by the lase facet and τ_{d} is the laser cavity round trip time. R is usually around 30% for semiconductor lasers and $\tau_{\mathrm{d}} = 6.6$ ps.

When ML and SL are operating in a chaotic regime and have a low coupling between them, the signal trajectories evolve independently. Due to the butterfly effect as mentioned above, slightly different initial conditions will result in an exponential divergence between the two trajectories. If we plot master laser vs. slave laser intensities, there is no correlation between them as in figure 1.12 a). For this case the cross-correlation obtained is close to zero. When the coupling between them is strong enough complete synchronization will be obtained.(Figure 1.12 b)). This will give a cross-correlation close to one (Figure 1.12 c),) and the maximum occurs at $C(0)$.

Phase synchronization between ML and SL is shown on figure 1.13. The amplitudes are uncorrelated, as shown in figure 1.13 a). Figure 1.13 b) shows the cross-correlation between the two lasers which is $C(0) = 0.67$. Looking at the time series of both lasers in figure 1.13 c), it is clearly seen that the amplitudes are different, but the phases are

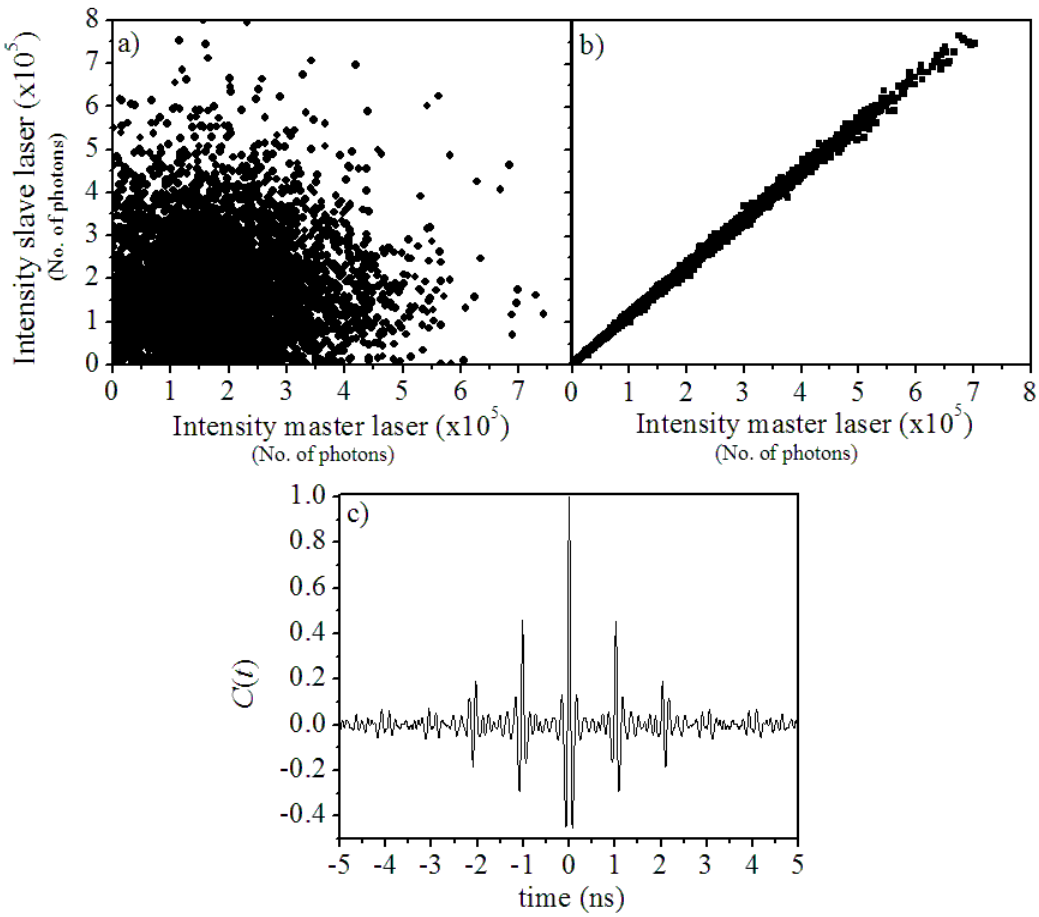

Figure 1.12: a) ML vs SL intensities without coupling, b) ML vs SL intensities when coupling $\gamma = 70$ ns^{-1} and c) the cross-correlation between ML and SL.when $\gamma = 70$ ns^{-1}.

the same. This type of synchronizations between ML and SL occurs before the coupling is strong enough to obtain complete synchronization.

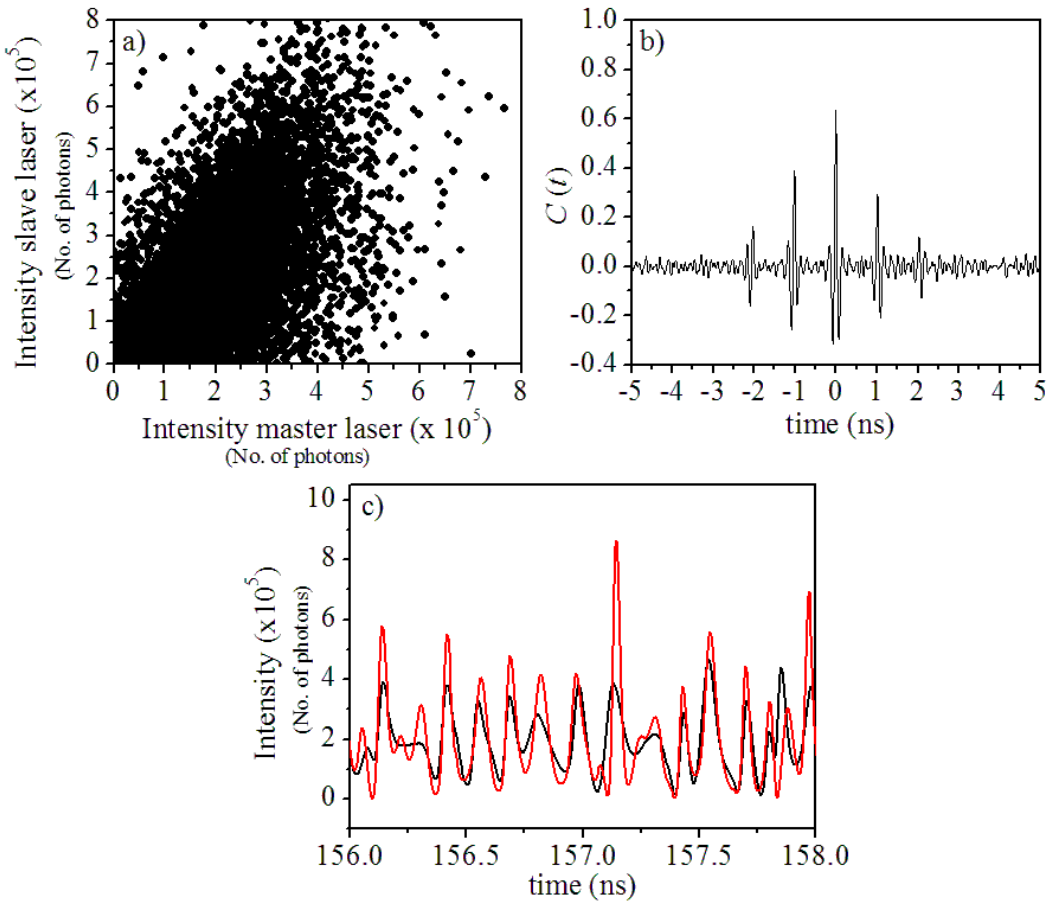

Figure 1.13: a) The intensities of ML vs. SL showing how they are uncorrelated, b) the cross-correlation between the two signals and c) time series showing phase synchronization.

1.5 Communication systems

The use of light to send information [Dutton 1998] is not new, flashlights to send messages between warships were already used in the XVIII century. Alexander Graham Bell had the idea of glass fiber to carry optical communication signals. This idea had to wait 80 years for its realization, when the laser was invented (1960), low loss optical fiber (1970's) and other technological devices were developed. A communication system

consists of a transmitter and a receiver. In the transmitter, a series of bits in electrical form are send to the modulator. The modulator drives the laser according to the series of bits and the light is focused into an optical fiber. The light after travelling through the fiber, is fed to a detector at the receiver, and it is converted back to electrical form. Finally, a decoder is used to reconstruct the original bit stream.

The application of chaotic synchronization may be used to send information in a secure way. Since synchronization of chaotic lasers is possible, and its compatibility with the existing optical fiber communication technology, semiconductor lasers are very attractive for secure communications. Two semiconductor lasers with external feedback are coupled through optical fiber. To be able to transmit a message, both lasers need to be completely synchronized. The message then is added to the chaotic laser in the transmitter. Then comparing the signal of the laser from the transmitter with the one from the receiver, the message can be recovered, figure 1.14 shows how this works. For this type of systems there are three main encoding and decoding schemes that can be used: chaotic modulation, chaotic masking and shift keying.

Chaotic modulation resembles the typical AM for radio. The message is added by modulating the emitter's chaotic carrier according to the expression:

$$M(t) = (1 - \varepsilon m(t))P_{\mathrm{t}}(t) \tag{1.58}$$

where ε is the amplitude of the message encoded, $m(t)$ is the message and $P_{\mathrm{t}}(t)$ is the intensity of the transmitter laser. In this type of scheme, the message $m(t)$ and the intensity $P_{\mathrm{t}}(t)$ have the same phase. Since the laser at the transmitter is synchronized with the one at the receiver, the recovered message is obtained as follows:

$$m_{\mathrm{r}}(t) = \frac{1}{\varepsilon}\left(1 - \frac{M(t)}{P_{\mathrm{r}}(t)}\right), \tag{1.59}$$

where $P_{\mathrm{r}}(t)$ is the intensity of the laser at the receiver and $m_{\mathrm{r}}(t)$ is the recovered message. For chaotic masking, the message is just added to the intensity of the transmitter laser:

$$M(t) = P_{\mathrm{t}} + \varepsilon m(t). \tag{1.60}$$

To recover the message at the receiver one needs to subtract the intensity of the laser at the receiver from the incoming signal of the transmitter:

$$m_{\mathrm{r}}(t) = \frac{M(t) - P_r(t)}{\varepsilon}.$$

The schemes for chaotic modulation and chaotic masking shown in figure 1.15 a) are very similar.

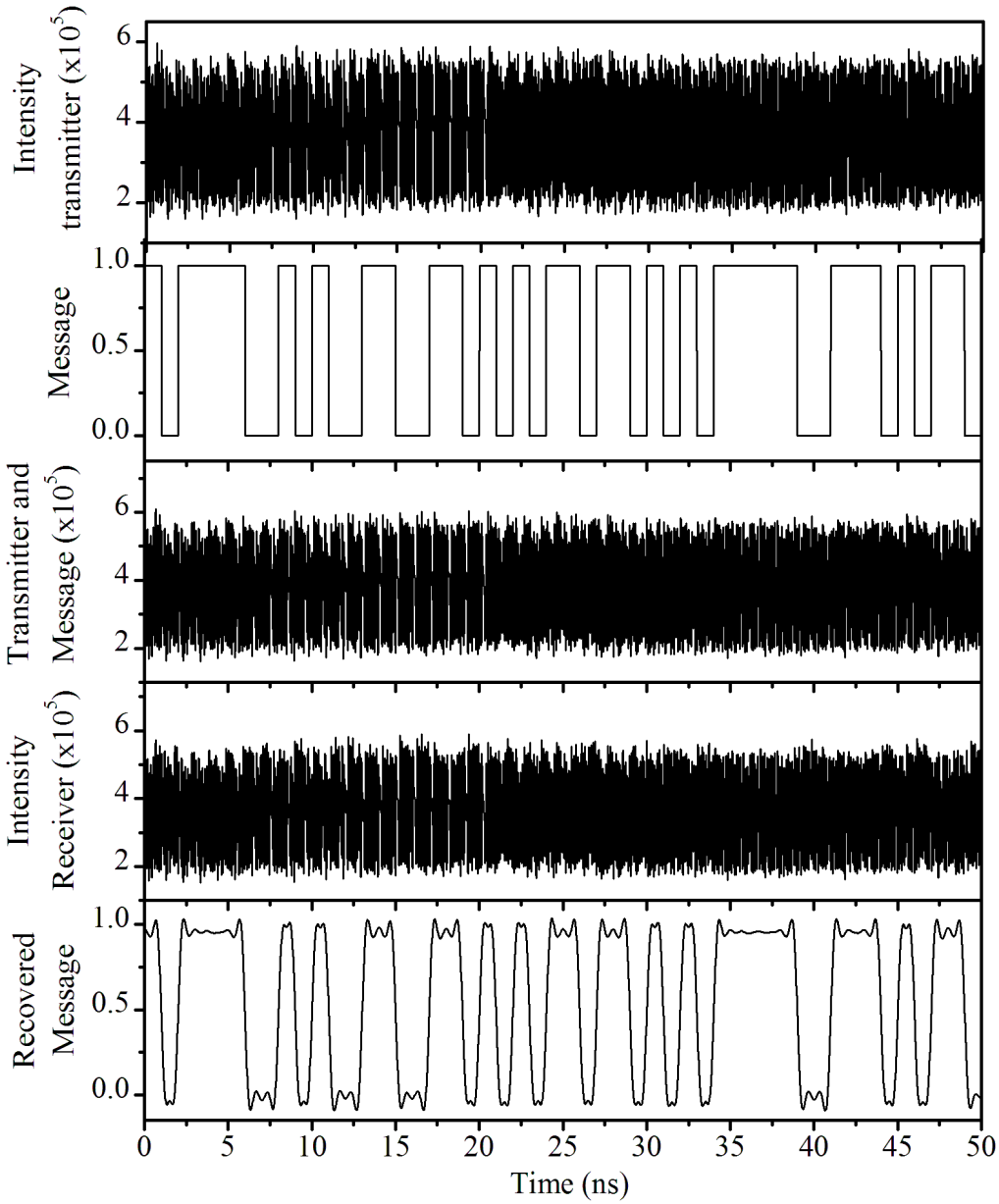

Figure 1.14: Encoding and decoding message in a chaotic carrier.

Finally, chaotic shift keying refers to when the signal is added to the transmitter itself, but not to the out coming signal from it (see figure 1.15 b)). In our case this can be done by adding the message to the pump current of the laser at the transmitter:

$$I(t) = I + \varepsilon m(t) \tag{1.61}$$

where I is the constant pump current, ε is the amplitude, and $m(t)$ is the message To the recover the message one just needs to subtract the intensities of the lasers:

$$m_{\mathrm{r}}(t) = P_{\mathrm{t}}(t) - P_{\mathrm{r}}(t) \tag{1.62}$$

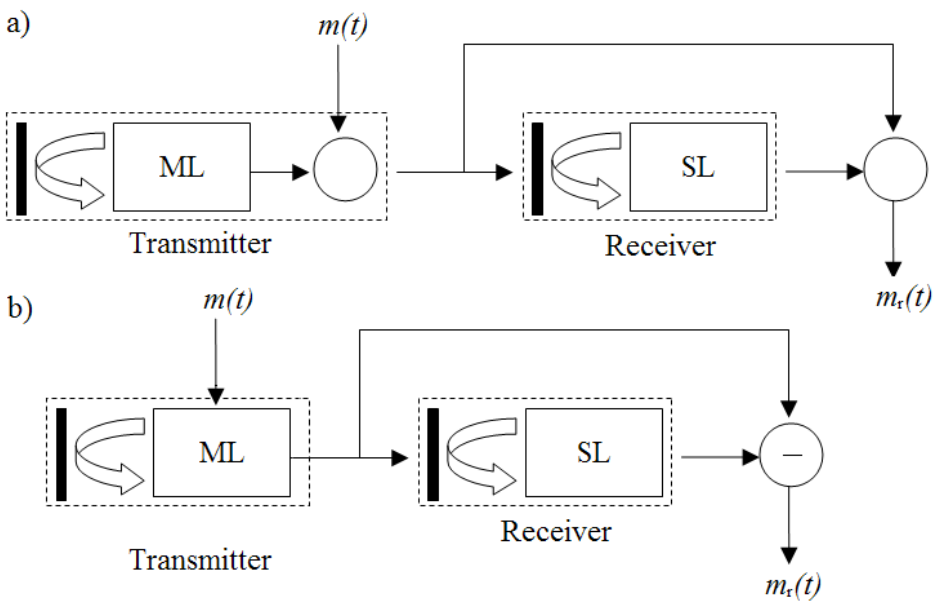

Figure 1.15: Scheme for a) chaotic masking and modulation, and b) shift keying.

The communication schemes mentioned above use only one channel to synchronize the lasers and to add the message. This may result in a problem since the added message can be seen as an outside disturbance that can affect the synchronization between the lasers, and this will affect the quality of the recovered message. Two channel systems using identical synchronization have been suggested for electronic circuits. [García-López 2005, García-López 2008]. The main advantage of this type of systems is that one channel is used to synchronize the chaotic oscillators, and the second one is used to transmit the message. Since the message is not sent through the synchronization channel, the synchronization error is kept low. The disadvantage of this system

is that a bit rate speed at which the message is transmitted is slow, as compared with other optical systems.

Two channel communication systems using generalized synchronization have been suggested [Terry 2001]. There are two main schemes for this type of communications systems. The first scheme, shown in figure 1.16, consists of a transmitter with a master (X_{T}) and slave (Y_{T}) chaotic oscillators. The transmitter contains only one oscillator (Y_{R}), which is the same as the slave oscillator (Y_{T}) in the transmitter. The master oscillator is coupled with the other two oscillators. Since the master oscillator is different than the other two chaotic oscillators, generalized synchronization can be obtained. On the other hand, the two slave oscillators, which are identical are completely synchronized. The message is then transmitted by modulating the coupling between X_{T} and Y_{T}. The coupling variation causes a synchronization error between Y_{T} and Y_{R}. When synchronization error is small, a bit "1" is send, and when it is large a bit "0" is send. The main problem with this system is that the distance between X_{T} and Y_{T},Y_{R} has to be the same, otherwise the synchronization error between Y_{T} and Y_{R} will be large too.

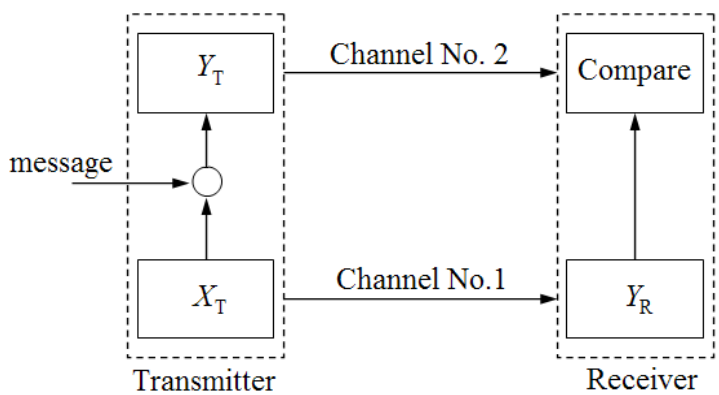

Figure 1.16: Communication system using generalized synchronization with one master oscillator.

The second scheme contains a transmitter with master (X_{T}) and slave (Y_{T}) chaotic oscillators, and a receiver with master (X_{R}) and slave (Y_{R}) chaotic oscillators, as shown in figure 1.17. Since X_{T} and X_{R} are identical, there is complete synchronization between them. The slave oscillators Y_{T} and Y_{R} are different than the master oscillators X_{T} and X_{R}. Therefore generalized synchronization can be obtained between X_{T}, Y_{T} and X_{R}, Y_{R}, and complete synchronization between Y_{T} and Y_{R}. The message again produces the synchronization error between Y_{T} and Y_{R}, when the coupling of X_{T} and Y_{T} is varied. The problem with this two methods is again the speed of the transmission because there is a re-synchronization time between Y_{T} and Y_{R}, that limits speed transmission.

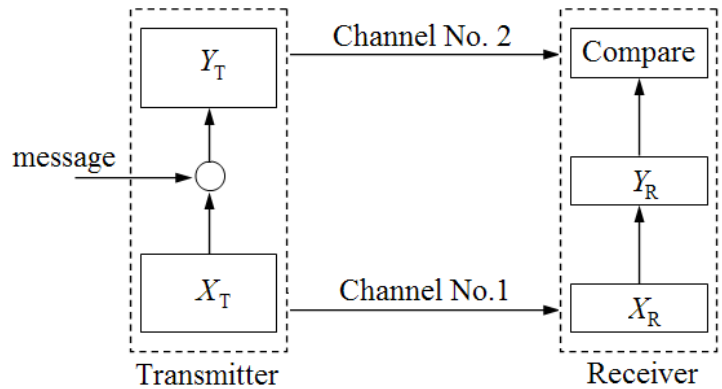

Figure 1.17: Communication system using generalized synchronization with two master oscillators.

There are several methods to analyze the quality of a recovered signal. One of them is eye diagrams[Breed 2005] which consists in splitting up the message in a series of fix intervals. Then all the intervals are overlapped, as shown in figure 1.18, where the message was splitted into series of 5 bits. This is an easy method to concentrate all the bits from the message in a small time interval. The quality of the transmitted message can be characterized by the Q-factor [Kanakidis 2003]:

$$Q = \frac{S_1 - S_0}{\sigma_1 + \sigma_0}, \tag{1.63}$$

where S_1 and S_0 are the average optical intensities of bits "1" and "0", and σ_1 and σ_0 are the corresponding standard deviations. Figure 1.19 shows the eye diagram formed with series of 3 bits with a transmission rate of 1Gb/s and $Q = 16$.

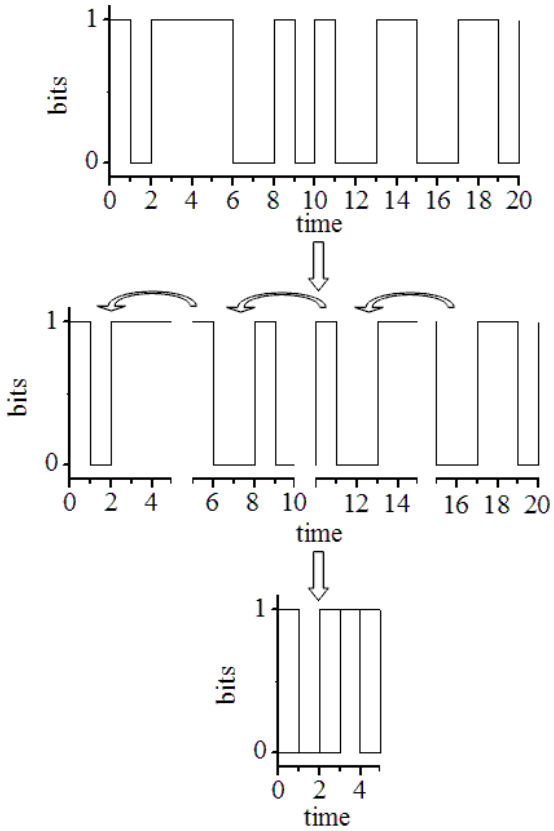

Figure 1.18: Forming an eye diagram from a message.

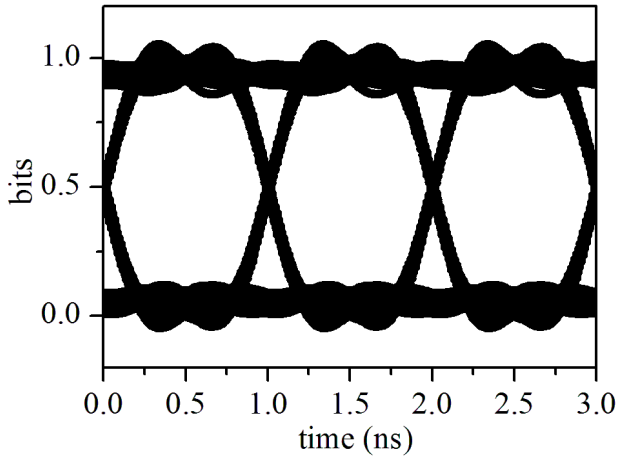

Figure 1.19: Eye diagram taking series of 3 bits for a recovered message whose transmission rate is 1Gb/s.

Chapter 2

Dynamics of an external-cavity semiconductor laser

Contents

This section is dedicated to study the dynamics of a semiconductor laser with optical feedback. For this study we use the Lang-Kobayashi equations. The analysis is performed by calculating bifurcation diagrams as a function of different control parameters, such as the coupling strength, the feedback round trip time and the initial phase [Nagashima 1999, Strogatz 1994, Ohtsuko 2006]. Depending on these parameters, the dynamics of external–cavity semiconductor lasers displays fix points, periodic, quasi-periodic, and chaotic regimes.

Then we add a second cavity to the semiconductor laser, and it shows how the laser dynamics can be stabilize. The linear stability analysis of the fix points analysis of the Lang-Kobayashi equations is performed. We describe this analysis in the appendix.

2.1 One external cavity

The dynamics of an external-cavity semiconductor laser is studied with the model equations (1.44) and (1.50), which describe the evolution of the carrier rate and slow varying complex electrical field. The parameters used in the simulations are in table 2. As mentioned in section 1.3, optical feedback in a laser induces an additional degree of freedom that makes its dynamics richer. The dynamics of such lasers is defined by the phase (ϕ) of the external complex wave, the round trip time (τ) and the feedback strength (κ) of the external cavity.

Figure 2.1 shows the bifurcation diagram as a function of the external cavity round trip time (τ), where $\tau = 1$ ns corresponds to an external cavity of 15 cm. with air.

The phase $\phi = 0$ and the feedback $\kappa = 10$ ns^{-1} are kept constant. One can see that by adding an external cavity we can obtain either CW or fix point (FP), period 1 (P1), period 2 (P2), period 3 (P3), period 4 (P4), quasi periodic (QP) or chaos (CH).

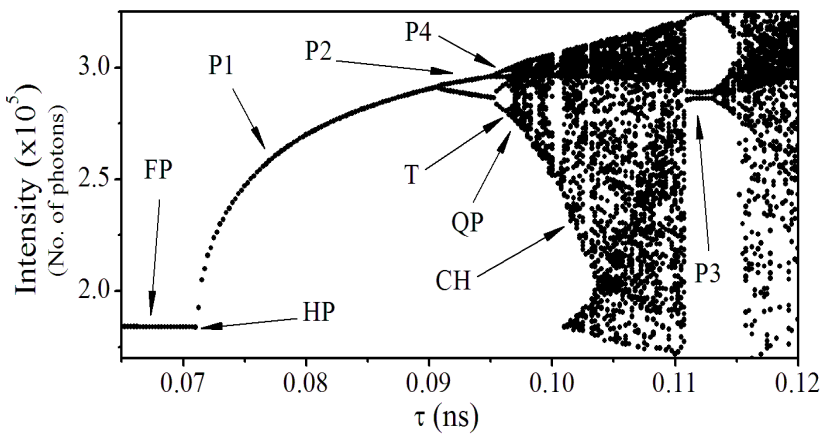

Figure 2.1: Bifurcation diagram with respect of external cavity round trip time τ.

The bifurcation diagram from figure 2.1 shows a period doubling route to chaos. If the length of the external cavity is small enough, the laser works in a CW marked as FP on the bifurcation diagram. When $\tau = 0.071$ ns, a Hopf bifurcation (HP) appears and the laser starts to oscillate in a P1 regime. For larger τ two period doubling bifurcations appear, the first one at $\tau \approx 0.09$ ns, where the laser goes from a P1 to a P2; and the second one at $\tau \approx 0.095$ ns where it goes from a P2 to a P4. Then the laser goes through a toroid bifurcation (T) to a QP state and becomes chaotic. At $\tau = 0.111$ ns there is crisis and then a P3 regime appears, which then turns into QP through a toroid bifurcation and finally goes into chaos.

The power spectra found in figure 2.2 clearly show the dynamics for some specific values of τ. Figure 2.2 a) shows the power spectrum of a P1 regime $\tau = 0.08$. The oscillation frequency is around $f_{\mathrm{m}} = 6$ GHz, which corresponds to the frequency of the relaxation oscillations of the semiconductor laser without an external cavity. Figure 2.2 b) shows the power spectrum of a P2 regime when $\tau = 0.092$. Again the frequency of relaxation oscillations appears together with its subharmonic frequency of $f_{\mathrm{m}}/2 = 3$ GHz. At $\tau = 0.112$ ns there is a P3 which spectrum is shown in figure 2.2 c). The frequency f_{m} appears with its two subharmonics $f_{\mathrm{m}}/3 = 2$ GHz and $2f_{\mathrm{m}}/3 = 4$ GHz. At $\tau = 0.096$ ns a P4 regime appears, with three subharmonics $f_{\mathrm{m}}/4$, $f_{\mathrm{m}}/2$ and $3f_{\mathrm{m}}/4$ as shown in figure 2.2 d).

A QP region at $\tau = 0.097$ ns and its spectrum are shown in figure 2.2 e). In the QP

regime the ratio frequencies between f_{m} and other frequencies is an irrational number ($\mathbb{Q}$). The frequencies marked with the arrows in figure 2.2 d) correspond to 2.47 GHz and 3.654 GHz, the ratios of these frequencies with f_{m} are: $f_{\mathrm{m}}/2.47 = 2.42914...$ and $f_{\mathrm{m}}/3.654 = 1.64203...$, which belong to $\mathbb{Q}$. Figure 2.2 f) corresponds to a chaotic regime when $\tau = 0.105$ ns where the range of frequencies is broad, but the dominant one is still f_{m}.

Figure 2.3 shows the bifurcation diagram with respect to the feedback strength κ. If a reflectivity of 30% is considered for the laser facets, and a round trip time in side the semiconductor laser cavity is $\tau_{\mathrm{d}} = 6.6$ ps, then a feedback strength of $\kappa = 10$ ns^{-1} corresponds to a reflectivity of 0.3% for the external cavity mirror. For this bifurcation diagram, the round trip time of the external cavity is kept to $\tau = 0.35$ ns and the phase $\phi = \pi$. This bifurcation diagram shows a FP→HP→P1→T→QP→CH route to chaos. When the feedback is small enough, $\kappa < 2.8$ ns^{-1}, the laser remains in the CW regime. At $\kappa = 7$ ns^{-1} there is crisis and P1, then for $\kappa \gtrsim 7.4$ ns^{-1} there is chaos.

The next bifurcation diagram is done with respect to phase ϕ. Even though this phase was defined as $\phi = \omega\tau$ in the previous chapter, where ω is the natural laser frequency; this phase can be changed experimentally just by applying an electric field to the external cavity [Pérez 2006, Tronciu 2008a, Tronciu 2008b]. The round trip time of the external cavity and the feedback strength are kept constant to: $\tau = 0.35$ ns and $\kappa = 10$ ns^{-1}. In the bifurcation diagram shown in figure 2.4 we can see chaotic windows separated by the crisis and a P1 regime, then we get inverse Hopf bifurcations (IHP) points that lead to FP dynamics. FP is converted in chaos in the crisis point. This process repeats itself every 2π.

Similar to many other dynamical systems, such as electronic circuits, turbulent flows, etc. [Maurer 1980, Ravelet 2004] semiconductor lasers with external cavities also exhibit coexistence of two [Ruiz-Oliveras 2009] or more attractors. This phenomenon is referred to as multistability, where a particular state can be found by varying the initial conditions. Figure 2.5 shows two bifurcation diagrams as functions of the feedback strength κ. In figure 2.5 a) the phase is $\phi = 0$ and the external round trip time is $\tau = 0.2$ ns, and in figure 2.5 b) the phase is $\phi = \pi$ and the external round trip time is $\tau = 0.4$ ns. From these bifurcation diagrams the coexistence of FP with P1, P2, P4, CH; and the coexistence of P1 with P2 attractors is clearly seen.

For a better understanding of the dynamics of the external-cavity semiconductor laser, figure 2.6 [3d]shows a three dimensional bifurcation diagram with respect to κ, τ, and ϕ. The black regions correspond to a FP behavior, yellow regions indicate P1, blue regions are P2, red regions are P3, and white regions are QP or chaos. For small feedback strengths ($\kappa \lesssim 7.5$) the dynamics has a regular behavior (steady states and

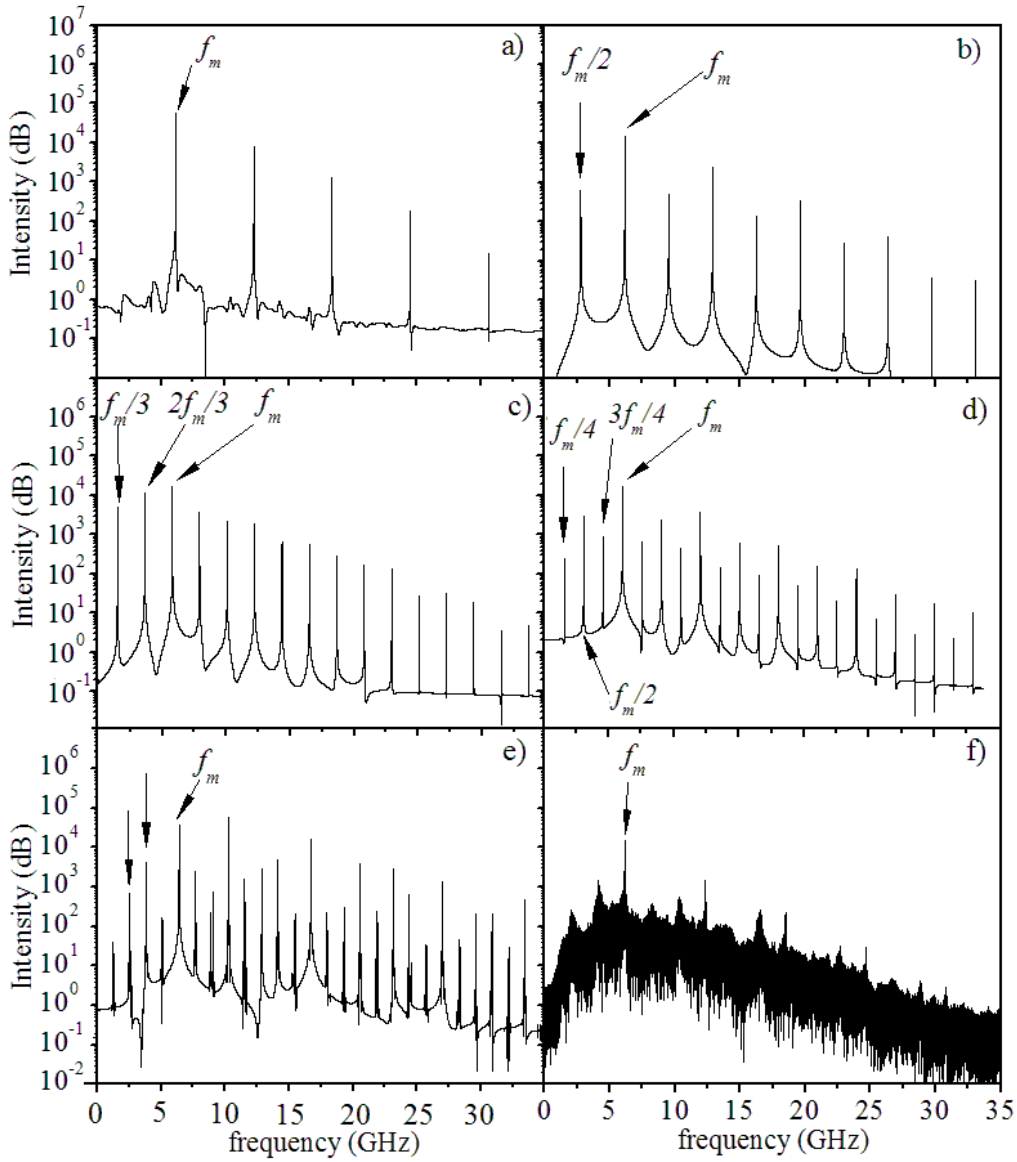

Figure 2.2: Power spectrum for a) period 1, b) period 2, c) period 3, d) quasi-periodic, and e) chaotic regimes.

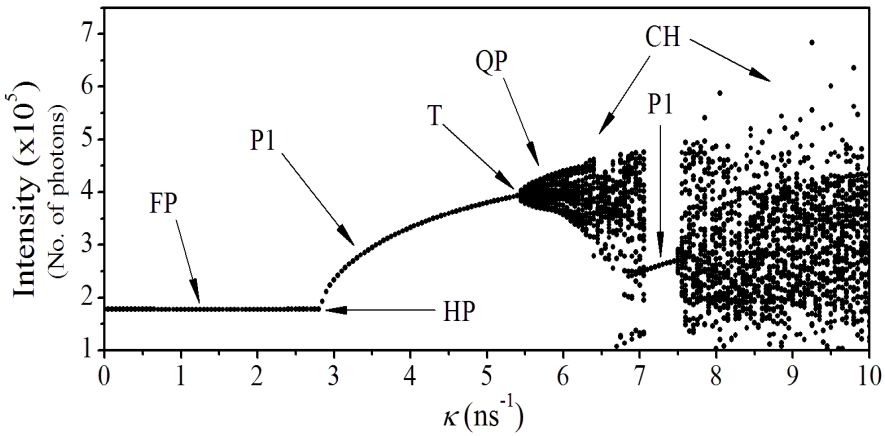

Figure 2.3: Bifurcation diagram with respect of the feedback rate κ.

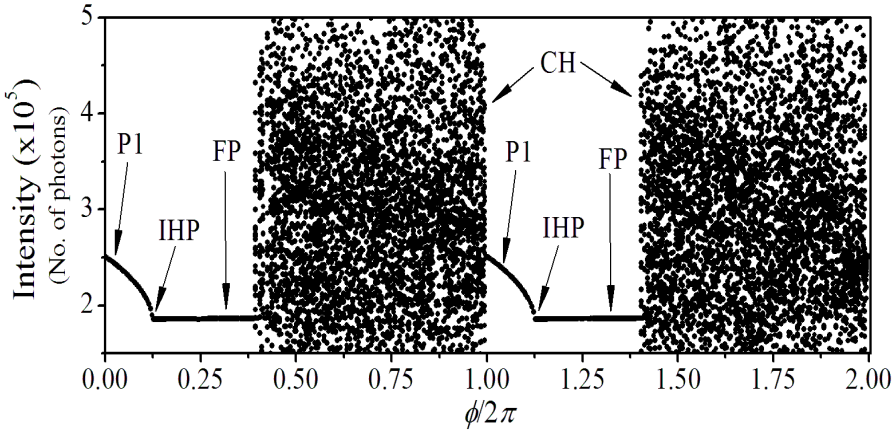

Figure 2.4: Bifurcation diagram with respect to the phase ϕ of the external cavity.

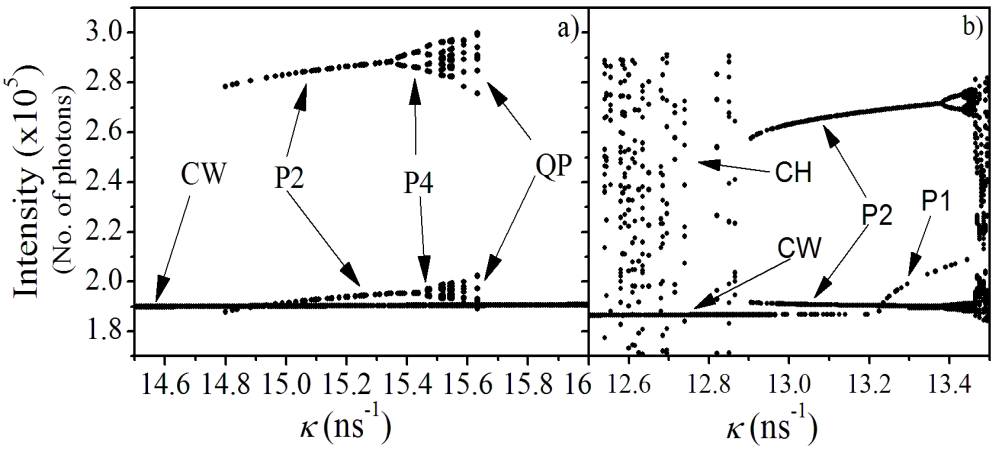

Figure 2.5: Bifurcation diagrams with respect to feedback strength κ showing multistability regions, for a) $\phi = 0$ and $\tau = 0.2$ ns and for b) $\phi = \pi$ and $\tau = 0.4$ ns.

periodic orbits),and for larger feedback strengths ($\kappa > 7.5$), we have QP or chaos. The boundaries between black and yellow regions are Hopf bifurcations, between yellow and blue regions are period doubling, and white regions with any color regions indicate crisis or quasiperiodicity.

The projections of figure 2.6 taken in different directions form codimensional-2 bifurcation diagrams and are shown in figure 2.7. Figure 2.7 a) is the state diagram in the parameter space of the feedback strength κ and the external round trip time τ, with $\phi = m\pi$, with $m = 0, 2, 4, ...$, since the dynamics of the external-cavity semiconductor laser repeats every 2π. Figure 2.7 b) is in the space parameter of the ϕ and τ with $\kappa = 25$ ns^{-1} and figure 2.7 c) is in the space parameter of κ and ϕ with $\tau = 0.25$ ns.

2.2 Two external cavities

For the case of two external cavities [Ruiz-Oliveras 2006b, Ruiz-Oliveras 2006a] equation (1.51) is used to model the slow varying complex electric field. For this analysis the phases of each cavity are not kept independent and are related to the lengths of the external cavity. The phases are given by $\phi_{1,2} = \omega\tau_{1,2}$, where $\phi_{1,2}$ are the phases of the first and second cavity and $\tau_{1,2}$ are the external round trip times for the first and second cavity. Figure 2.8 a) shows the bifurcation diagram with respect to the ratio τ_2/τ_1, the round trip time of the first external is kept constant at $\tau_1 = 0.22$ ns. The feedback strengths for both cavities is $\kappa_{1,2} = 25$ ns^{-1}. When $\tau_2/\tau_1 < 0.4$, the dynamics is very sensitive to the ratio between the external round trip times. Figure 2.8 b) shows

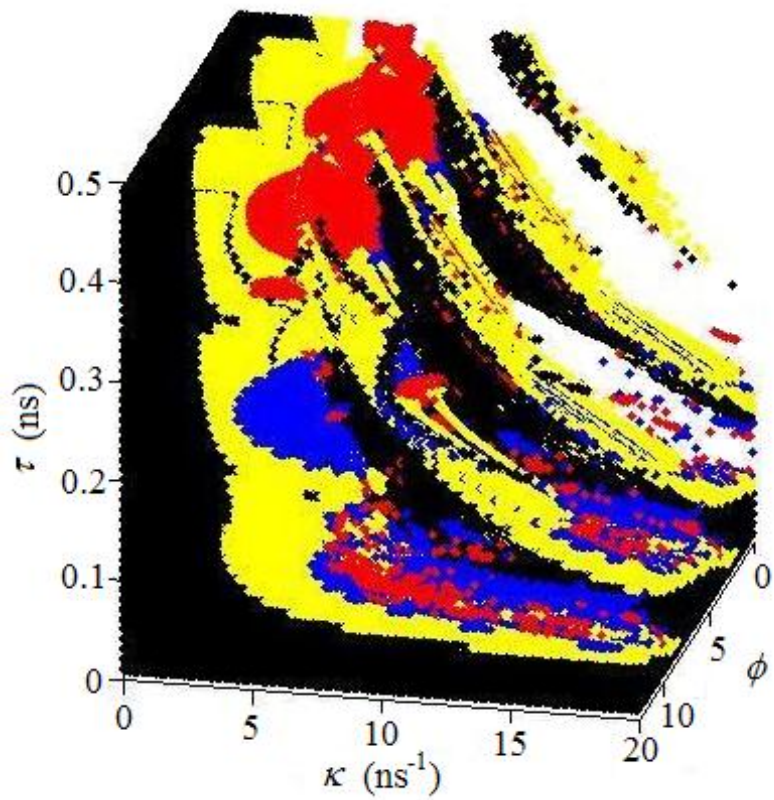

Figure 2.6: Three dimensional bifurcation diagram with respect to the feedback strength κ, external cavity round trip time τ and phase ϕ. The black regions are FP, yellow are P1, blue are P2, red are P3, and white are QP or CH.

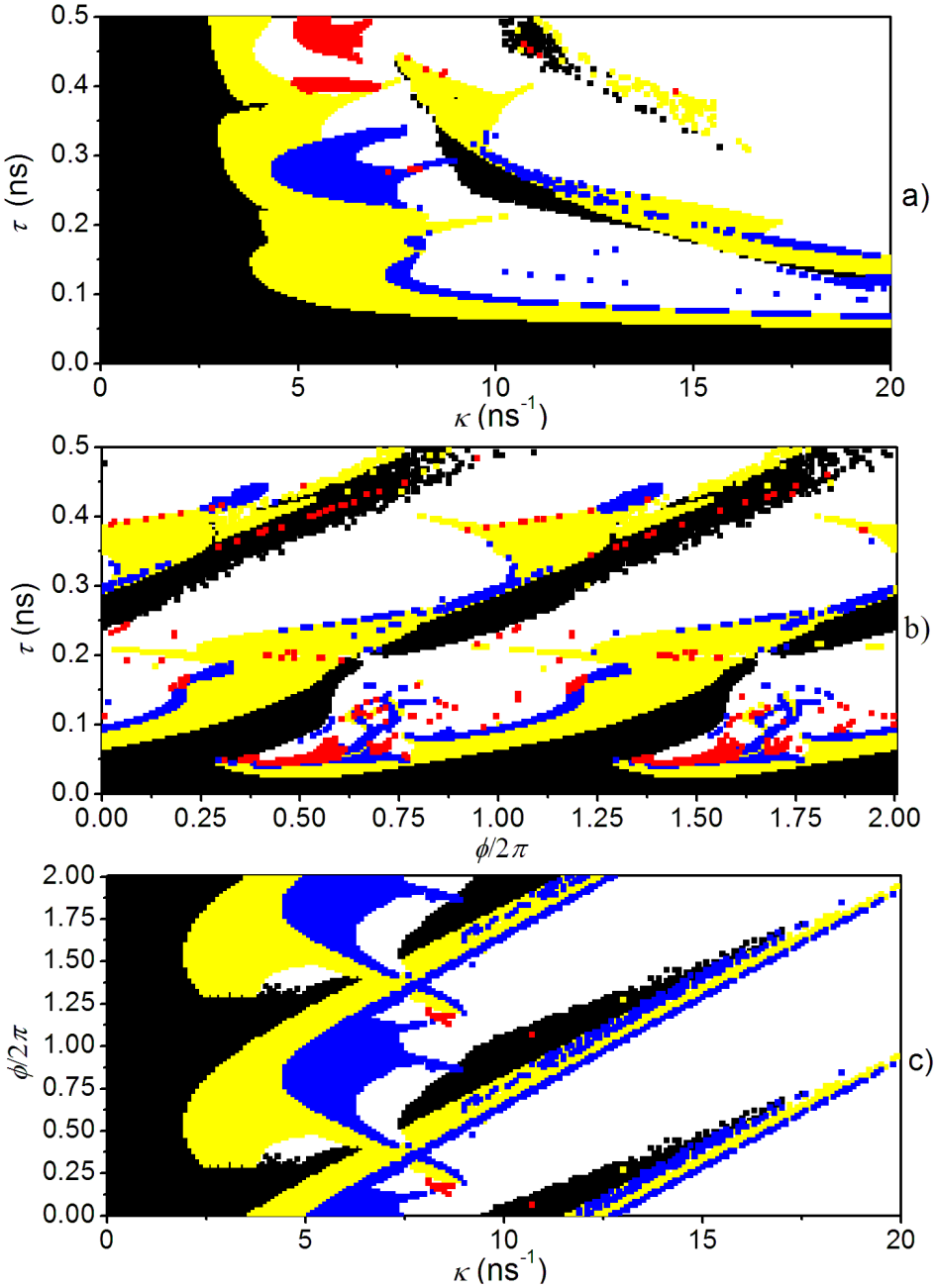

Figure 2.7: State diagrams in parameter spaces of a) κ and τ with $\phi = 0$, b) ϕ and τ with $\kappa = 10$ ns^{-1}, and c) κ and ϕ with $\tau = 0.25$ ns.

an amplification of the bifurcation diagram, when $\tau_2/\tau_1 < 0.4$. A series of torus, inverse torus, crisis, Hopf, and inverse Hopf bifurcations are found. In the region near the ratio $\tau_2/\tau_1 = 1$, there is a chaotic window.

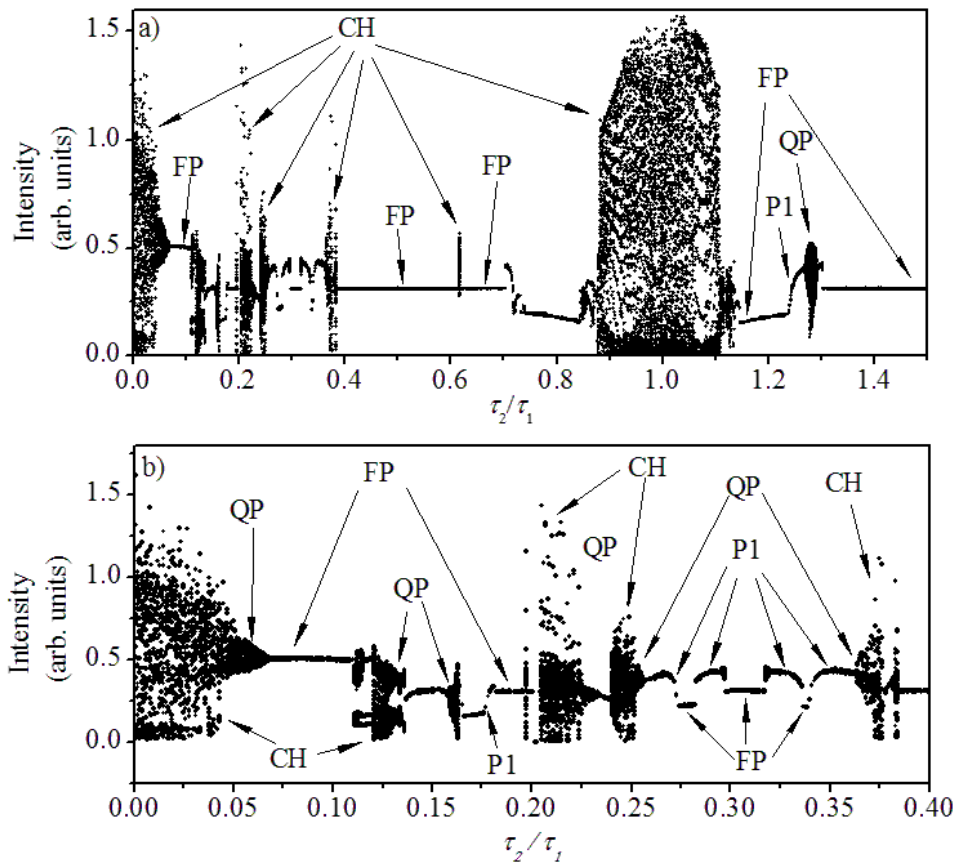

Figure 2.8: Bifurcation diagram with respect of τ_2/τ_1 where $\tau_1 = 0.22$ ns, and the feedback strengths are $\kappa_{1,2} = 25$ ns^{-1}.

Figure 2.9 is the state diagram in the parameter space of the ratios of the external cavity round trip times τ_2/τ_1, and the ratio of the feedback strengths κ_2/κ_1. The parameters of the first external cavity are fixed to $\tau_1 = 0.22$ ns and $\kappa_1 = 25$ ns^{-1}. Phase locking is a phenomena where the frequencies of two coupled oscillators are some rational multiples of each other. The combined locked motion then becomes periodic, and the locking regions are called Arnold tongues. When the frequencies are not rational multiples of each other then the behavior is quasi-periodic or chaotic. The color nomenclature of figure 2.9 is the same one used before.

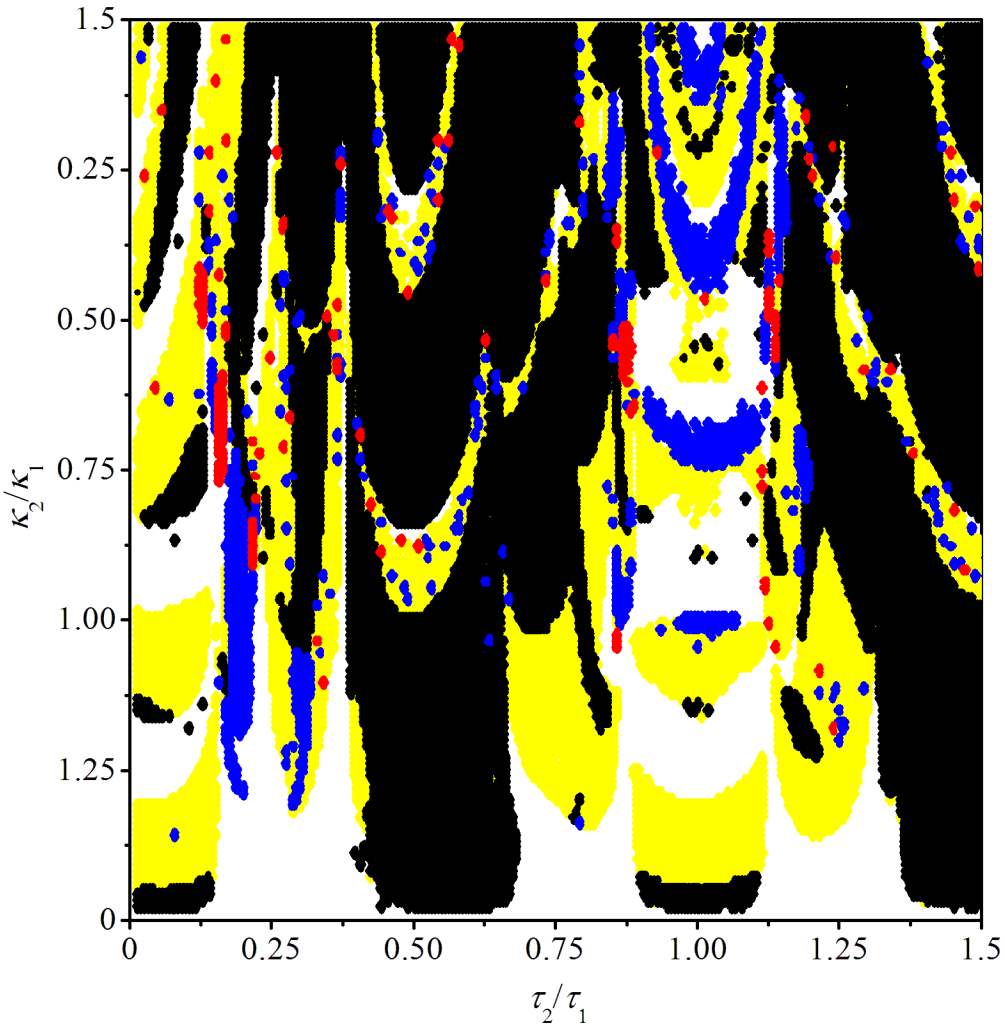

Figure 2.9: State digram in the parameter space of τ_2/τ_1 and κ_2/κ_1. Where $\tau_1 = 0.22$ ns and $\kappa_1 = 25$ ns^{-1}.

From figure 2.9 one can see the Arnold tongues of the steady state (black regions), and periodic regimes (yellow,blue and red regions). This means that the phases of the two external cavities are locked, so the laser motion becomes steady state or periodic orbits. The minima of the tongues occur when $\tau_2/\tau_1 = 1/4, 1/2, 3/4, \ldots$. It is remarkable that the diagram is symmetric around $\tau_2/\tau_1 = 1$. The asymmetry that may appear is due to multistability in the phase-locked regions. The addition of the second can stabilize the laser dynamics [Liu 1997] and from figure 2.9 it is clearly seen that the area corresponding to a stabilized dynamics (black region) is greater than any other regions.

2.3 Conclusions

In this chapter it is demonstrated that an external cavity in a semiconductor laser makes its dynamics richer. This is because optical feedback adds an additional degree of freedom to the semiconductor laser and thus periodic, quasi-periodic and chaotic orbits can appear. For stronger optical feedback, the stable and periodic regions tend to disappear and lead only to a chaotic behavior.

Introducing a second external cavity one can stabilize chaos due to phase locking of the two external cavities. Figure 2.9 shows the Arnold tongues, which are typical for a phase locking behavior.

Chapter 3

Synchronization of coupled external-cavity semiconductor lasers

Contents

This part of the thesis is devoted to a study of the dynamics of two coupled semiconductor lasers with optical feedback. It contains two sections. The first section describes the case when the lasers operate in a monostable regime. First we analyze the cases when both lasers operate in a CW regime, then in a periodic regime and finally in a chaotic regime. In the second section we study the case when the lasers operate in a bistable regime. The master laser can operate in a CW regime and the slave laser in a chaotic regime, or each laser operates in a different periodic regime. Scenarios for different combinations are studied.

3.1 Monostability domain

From the previous chapter, where the dynamics of an external-cavity semiconductor laser was studied, we showed that different dynamical regimes can be obtained. Lets first consider the case when both lasers operate in a CW regime. For this case feedback strength $\kappa = 2.5$ ns^{-1}, external round trip time $\tau = 0.43$ ns, and phase $\phi = 0$ are used. Note that the parameter values of the for both lasers are the same. Figure 3.1 shows the bifurcation diagram (black squares) of the slave laser output as a function of the coupling strength γ between the lasers. In the same figure, the frequency (color squares) at which periodic orbits oscillates is shown. The left y-axis corresponds to the intensity output (for the bifurcation diagram) of the SL and the right y-axis corresponds to the oscillating frequencies.

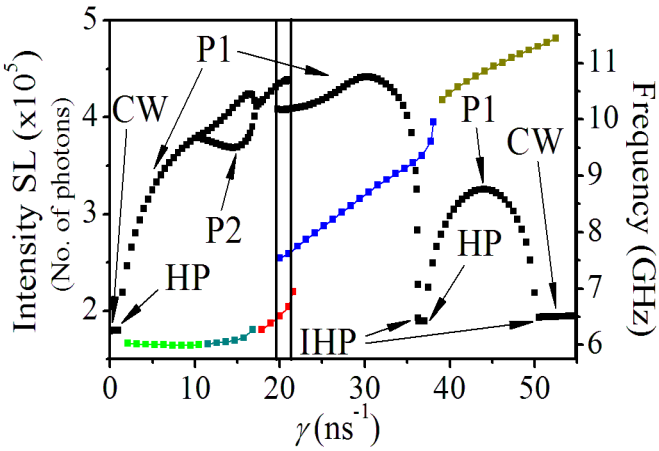

Figure 3.1: Bifurcation diagram (black squares) of the slave laser output as a sfunction of the coupling strength γ and oscillating frequency (color squares) of periodic orbits.

It is known that when optical injection between two semiconductor lasers without external cavities takes place, several types of bifurcations, such as Hopf, period doubling, etc. can be observed [Hwang 2000, Wieczorek 2000, Wieczorek 2005]. This behavior is shown in figure 3.1. When the coupling is $\gamma < 1$ ns^{-1}, there is a steady state emission (CW). When $\gamma \approx 1$ ns^{-1} there is a Hopf bifurcation that leads to periodic oscillations (period-1). At $\gamma \approx 10$ ns^{-1} there is a period doubling bifurcation, and the slave laser starts to oscillate in a period-2 regime. Between the Hopf and period doubling bifurcations, the oscillation frequency of the period-1 regime corresponds to the frequency of relaxation oscillations, this is $f_m = 6$ GHz. After the period doubling bifurcation occurs, the oscillating frequencies increase as the coupling increases. Then at $\gamma \approx 17.5$ ns^{-1} there is an inverse period-doubling bifurcation that leads to a period-1 regime. The two vertical lines indicate a bistable region of period-1 with different frequencies. For this case, at $\gamma \approx 19.7$ ns^{-1} and $\gamma \approx 21$ ns^{-1} there are saddle-node bifurcations. Then at $\gamma \approx 36.3$ ns^{-1} there is an inverse Hopf bifurcation leading to a CW regime and at $\gamma \approx 37$ ns^{-1} another Hopf bifurcation leads to a period-1 regime with higher frequencies. At $\gamma \approx 50$ ns^{-1} there is another inverse Hopf bifurcation, when $\gamma = 50$ ns^{-1}, this corresponds approximately 22% of the the master laser power injected into the slave laser.

In optically injected lasers without external cavities, the oscillation frequencies is the beating between the two laser frequencies. For the case of lasers with external-cavities, the oscillation frequency depends on the coupling parameter.

Now lets consider the case when the master and slave lasers are in a period 1 regime.

The parameters used for this case are: for the feedback strength $\kappa = 4$ ns^{-1}, round trip time $\tau = 0.4$ ns and the phase $\phi = \pi$. Figure 3.2 a) shows the bifurcation diagram of the slave laser intensity output as a function of the coupling strength γ, and figure 3.2 b) shows the cross-correlation between the master and slave lasers to measure the synchronization between them.

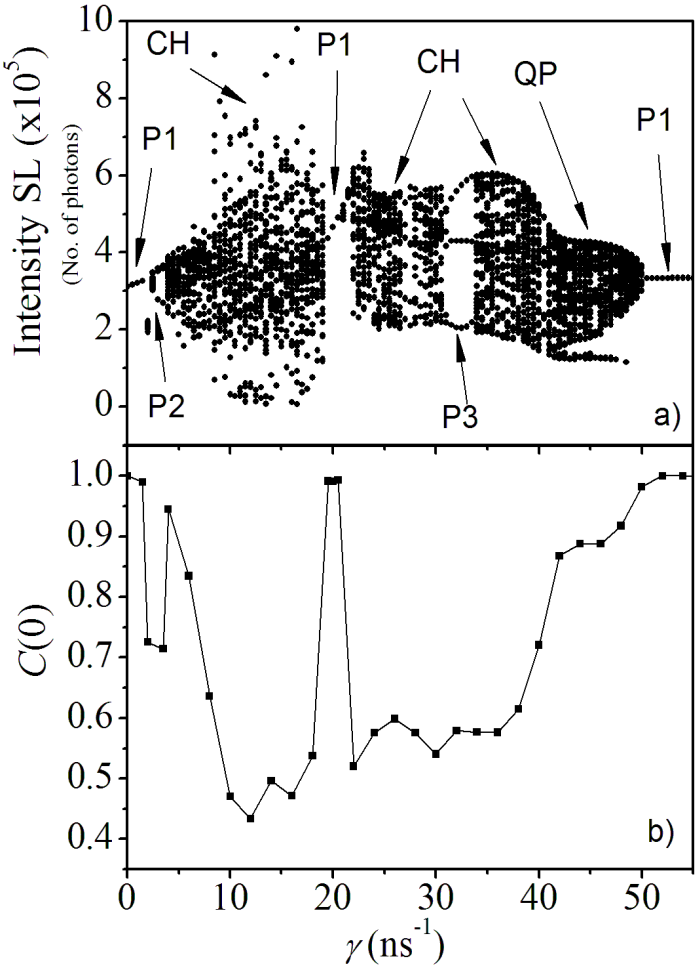

Figure 3.2: a) Bifurcation diagram of output intensity of slave laser and b) cross-correlation between master and slave lasers as a function of coupling strength γ.

From figure 3.2 a) it is clearly seen that rich dynamics is observed in the slave laser output. When the coupling $\gamma < 1.5$ ns^{-1} the laser behaves in a periodic regime, and the cross-correlation between the lasers is $C(0) = 1$. Then there is a period doubling route to chaos and the cross-correlation reaches its minimum at $\gamma \approx 12$ ns^{-1}. At $\gamma \approx 19.5$ ns^{-1}

there is crisis resulting in a period-1 regime and correlation is again $C(0) = 1$ indicating complete synchronization. Then there is an inverse-crisis bifurcation at $\gamma \approx 12$ ns^{-1}, where there is a chaotic regime and the cross-correlation drops. There is another crisis bifurcation at $\gamma \approx 31$ ns^{-1}, and a period-3 window appears when $31 < \gamma < 34$ ns^{-1}. Then there is a saddle-node bifurcation at $\gamma \approx 34$ ns^{-1} that leads to chaos. As the coupling strength is increased, the cross-correlation increases, for $41 < \gamma < 50$ ns^{-1} there is a quasi-periodic window and at $\gamma \approx 50$ ns^{-1} there is an inverse torus bifurcation. For $\gamma < 50$ ns^{-1} the slave laser behaves in a period-1 regime and has completely synchronized with the master laser.

Another way to analyze the laser dynamics, is a phase space plot. Figure 3.3 shows the laser trajectory in the $(E(t), iE(t), N(t))$, where $E(t)$ is the real part of the electric field, $iE(t)$ is the imaginary part of the electric field, and $N(t)$ is the population inversion, when $\gamma = 35$ ns^{-1}. From this figure it is clearly seen that the behavior is chaotic, since the trajectory visits all the points of the chaotic attractor while $t \to \infty$.

Figure 3.4 shows the trajectory in the phase space when $\gamma = 45$ ns^{-1}, the behavior is quasi-periodic. A limit tori is the attractor that corresponds to a quasi-periodic behavior because the frequencies are an irrational ratio. This was shown in figure 2.2 e) of chapter 2.

The next scenario for optical injection in monostable state is when both lasers are in a chaotic regime. For this case the parameters are feedback strength $\kappa = 25$ ns^{-1}, round trip time $\tau = 1$ ns, and the phase $\phi = 0$. The behavior of the slave laser output is always chaotic. Figure 3.5 shows the cross-correlation as a function of the coupling strength γ. When $\gamma < 5$ ns^{-1}, the cross-correlation is close to zero. For $\gamma > 5$ ns^{-1} the cross-correlation increases and finally at $\gamma \gtrsim 60$ ns^{-1} the lasers are completely synchronized.

Next we study how the cross-correlation between the master and slave laser changes when there is a small parameter mismatch between the parameters of the external cavities of the lasers, when both lasers are in a chaotic regime. The coupling strength is kept constant at $\gamma = 80$ ns^{-1}. Figure 3.6 a) shows the cross-correlation as a function of the mismatch between the feedback strengths. The feedback of the master laser is kept constant $\kappa_{\mathrm{m}} = 25$ ns^{-1} and the feedback κ_{s} for the slave laser is varied; the difference is given by $\Delta\kappa = \kappa_{\mathrm{s}} - \kappa_{\mathrm{m}}$. It can be seen that the cross-correlation slope is lower when the feedback strength of the slave laser is smaller than that of the master laser, this is $\kappa_{\mathrm{s}} < \kappa_{\mathrm{m}}$. On the other hand, if $\kappa_{\mathrm{m}} < \kappa_{\mathrm{s}}$, the cross-correlation drops more drastically. A feedback strength of $\kappa_{\mathrm{m}} = 25$ ns^{-1}corresponds to a reflectivity of $R_{\mathrm{ext}} = 1.6\%$ for

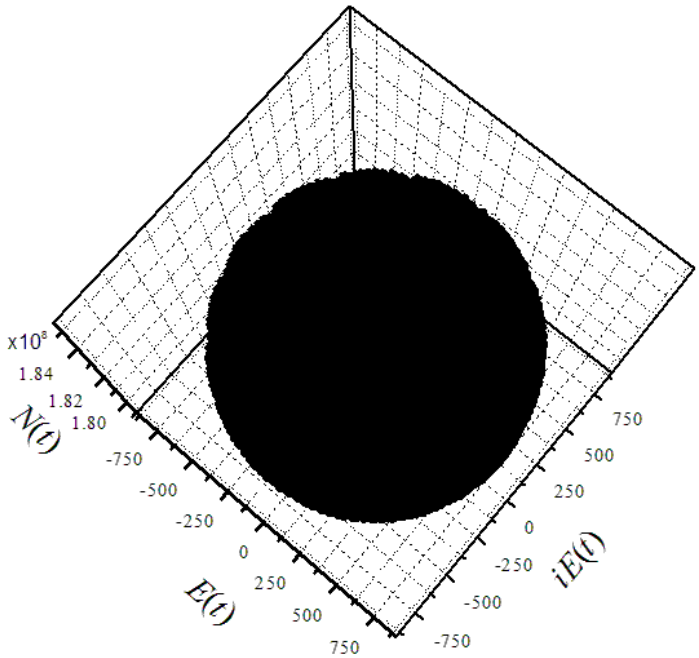

Figure 3.3: Chaotic trajectory in phase space for $\gamma = 35$ ns^{-1}.

the external cavity mirror. To have a cross-correlation of $C(0) \geq 0.99$ we need that $1.4\% \leq R_{\text{ext}} \leq 1.8\%$.

Figure 3.6 b) shows the cross-correlation as a function of the difference between the external round trip times. The external round trip time of the master laser is kept constant $\tau_{\text{m}} = 1$ ns, τ_{s} is the external round trip time for the salve laser, and the difference is given by $\Delta\tau = \tau_{\text{s}} - \tau_{\text{m}}$. This figure shows how sensitive the synchronization between the lasers is with respect to their external cavities round trip times. To have a cross-correlation of $C(0) \geq 0.99$ we need that $0.999 \leq \tau_{\text{s}} \leq 1.001$ ns. Since the media of the external cavity is considered to be air, whose index of refraction is about 1.0003; for $\tau_{\text{s}} = 1.001$ ns the air would have to change its index of refraction to about 1.001. For practical reasons changes in the air temperature can be neglected [Smith 2000]. On the other hand, the length of the external cavity can vary ± 0.15 mm.

Finally, figure 3.6 c) shows the cross-correlation when the phases are different. The phase of the master laser is kept constant to $\phi_{\text{m}} = 0$, and the phase of the slave laser (ϕ_{s}) is varied varied from $0 - 2\pi$. Complete synchronization can only be obtained when the lasers have the same phase. As mentioned in chapter one, the phase can be modified by applying an electric field to the external cavity [Pérez 2006, Tronciu 2008a, Tronciu 2008b].

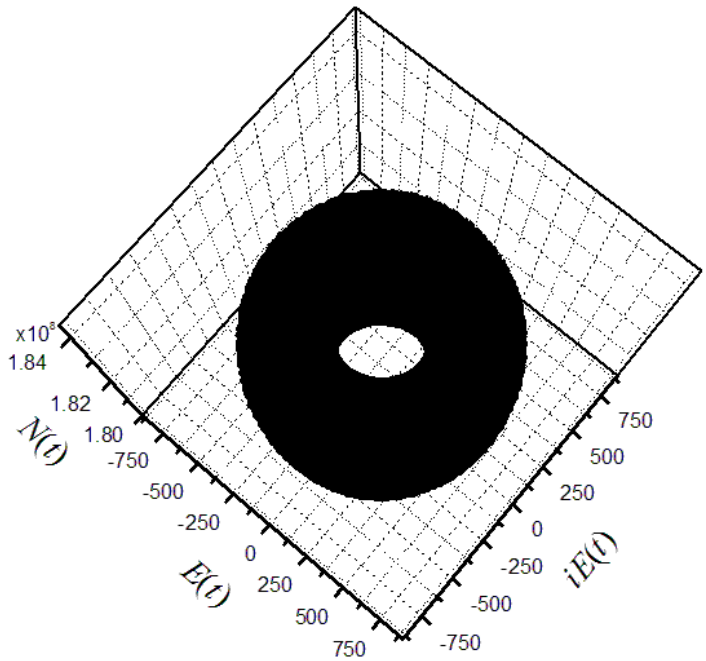

Figure 3.4: Quasi-periodic trajectory in phase space for $\gamma = 45$ ns^{-1}, where the torus is the attractor.

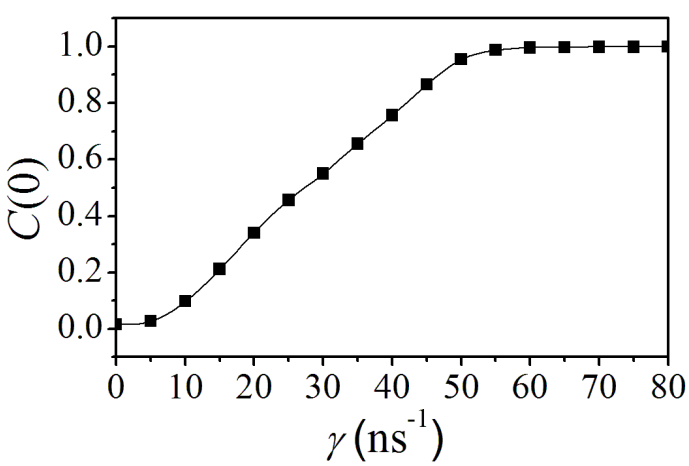

Figure 3.5: Cross-correaltion between master and slave lasers as a function of coupling strength γ.

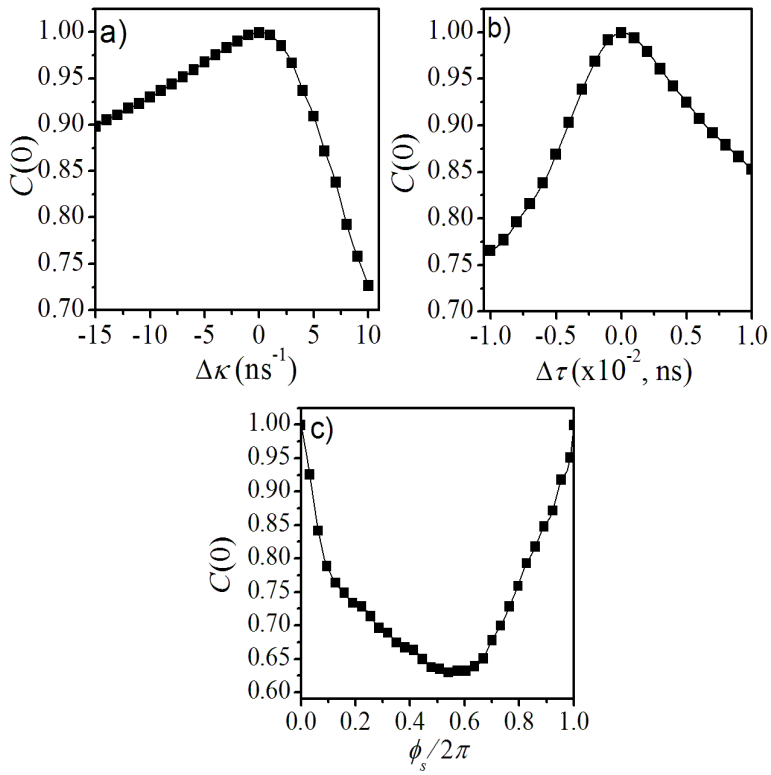

Figure 3.6: Cross-correlation when there is match in the external cavity parameters between the ML and SL in a) the feedback parameter b) external round trip time, and c) initial phase. ML parameters are kept constant and SL parameters are varied.

3.2 Bistability domain

First we study the case when CW and chaotic regimes coexist. The parameters used are: feedback strength $\kappa = 12.7$ ns $^{-1}$, external round trip time $\tau = 0.4$ ns, and phase $\phi = \pi$. A bistability. domain can be seen in the bifurcation diagram in figure 2.5 b). First consider the case when the master laser is in a CW regime and the slave laser in a chaotic regime. Figure 3.7 shows the bifurcation diagram (black squares) of the slave laser output and the frequency of the periodic orbits (red and blue squares) as a function of the coupling strength γ. The bifurcation diagram is very similar to that in figure 3.1, where both lasers were in a CW regime. At $\gamma \approx 4.5$ ns^{-1} there is a Hopf bifurcation leading to periodic orbits. There are saddle-node bifurcations at $\gamma \approx 18$ ns^{-1} and $\gamma \approx 19$ ns^{-1}, and between them there is bistability. Then at $\gamma \approx 19.75$ ns^{-1} there is another Hopf bifurcation that leads to period-1 orbits with higher frequencies, and at $\gamma \approx 44$ ns^{-1} there is an inverse Hopf bifurcation that leads to a CW. It is interesting to see that there is a large difference in the frequencies of the two different periodic windows.

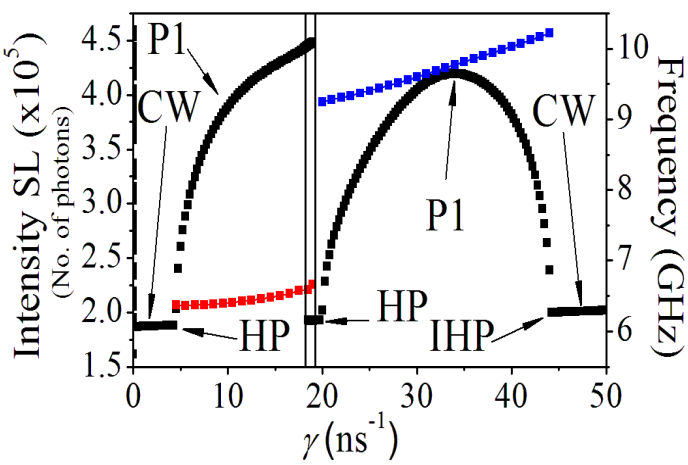

Figure 3.7: Bifurcation diagram (black squares) of slave laser intensity output and frequencies of the periodic orbits (red and blue squares) as a function of γ, when master laser is in CW and slave laser in chaotic regime.

Now let the master laser be in a chaotic regime and the slave laser in CW. For this case, as soon the lasers are coupled, the slave laser behaves in chaos. As the coupling strength increases, the cross-correlation between lasers increases and at $\gamma \geq 60$ ns^{-1}, the cross-correlation is $C(0) \approx 1$, which means complete synchronization. This behavior is similar to that when both lasers are chaotic.

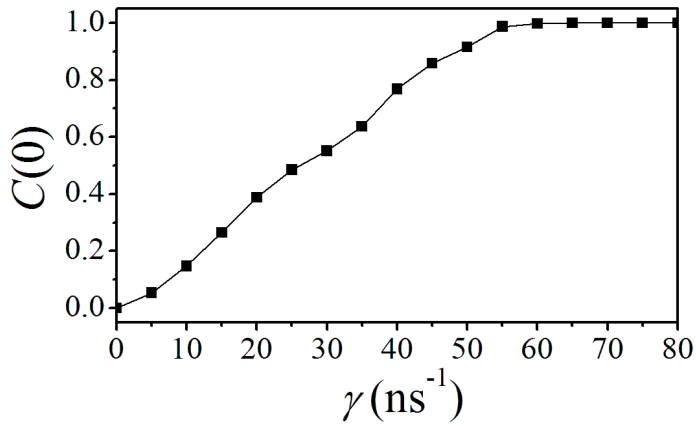

Figure 3.8: Cross-corraltion between master (chaotic) and slave (CW) lasers.

The next case is when CW and a periodic regime coexist. The parameters used for this case are: feedback strength $\kappa = 15.1$ ns $^{-1}$, external round trip time $\tau = 0.2$ ns, and phase $\phi = 0$. This is shown in the figure 2.5 a) where coexistence of a period-2 orbit with CW. The first case is when the master laser is in a CW regime and the slave laser in a period-2. The injection of the CW laser into the periodic laser causes CW, Hopf and inverse Hopf bifurcations. Figure 3.9 shows the bifurcation diagram (black squares) and frequencies (right y-axis and red squares) of the slave laser intensity as a function of the coupling γ. At $\gamma \approx 7$ ns $^{-1}$ there is a Hopf bifurcation that leads to period-1 orbits with higher frequencies. Then at $\gamma \approx 43$ ns $^{-1}$ there is an inverse Hopf bifurcation, and CW.

Now consider the case when the master laser is in a period-2 regime and the slave laser in the CW. Figure 3.10 a) shows the bifurcation diagram of the slave laser intensity, and figure 3.10 b) shows the cross-correlation between the master and slave lasers as a function of the coupling γ. For this case the dynamics is very rich; there is a chaotic regime which turns into quasi-periodic at $\gamma \approx 13\,\mathrm{ns}^{-1}$. At $\gamma \approx 47\,\mathrm{ns}^{-1}$ there is an inverse torus bifurcation that leads to period-2 and there is complete synchronization between the master and slave lasers. From figure 3.10 we can see that the cross-correlation resembles the dynamics. The lowest correlation is observed when the slave laser is chaotic, then it increases as the coupling is increased. Then, in the quasi-periodic regime it decreases, but it is not as low as in the chaotic regime. This case resembles when both lasers are in a periodic regime.

Next we consider the case when the lasers have different periodic orbits, that represents the richest dynamics. First the master laser is in a period-1 regime and the slave

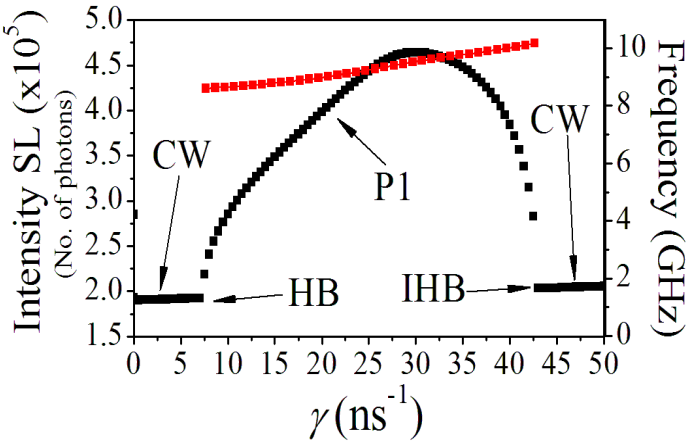

Figure 3.9: Bifurcation diagram (black squares) and frequencies (red squares) of the slave laser intensity output as a function of γ, when the master laser is in CW and the slave laser in a period 2 regime.

laser in a period-2. The parameters used for this case are: feedback strength $\kappa = 13.3$ ns $^{-1}$, external round trip time $\tau = 0.4$ ns, and phase $\phi = \pi$. The corresponding bifurcation diagram shown in figure 2.5 b). Figures 3.11 a) and b) show the bifurcation diagram of the slave laser intensity of and the cross-correlation between the master and slave lasers. For a very small coupling between the lasers, ($\gamma \approx 0.5$ ns^{-1}), chaos arises ending in crisis when $\gamma \approx 3.5$ ns^{-1} that results in a period-2 regime. At $\gamma \approx 8.5$ ns^{-1} a period-3 regime appears which turns into a quasi-periodic regime when $\gamma \approx 11.5$ ns^{-1}. As γ is increased, another quasi-periodic attractor appears in a saddle-node bifurcation. In the region of $17.5 < \gamma < 19.5$ ns^{-1}, which is found between the two horizontal lines, two quasi-periodic regimes exist. When $\gamma \approx 19.5$ ns^{-1}, the first quasi-periodic regime disappears and the second one continues to finally end up in an inverse torus bifurcation (at $\gamma \approx 43.5$ ns^{-1}) leading to a period-1 regime.

Finally, we consider the case when the master laser is in a period-2 and the slave laser in a period-1 regime. Figure 3.12 a) and b) show the bifurcation diagram of the slave laser output and the cross-correlation between the lasers. For very low coupling, $\gamma \approx 0.5$ ns^{-1}, the slave laser undergoes a torus bifurcation leading to a quasi-periodic regime, which is then converted into chaos at $\gamma \approx 2.5$ ns^{-1}. At $\gamma \approx 24$ ns^{-1} the dynamic turns quasi-periodic which ends at an inverse torus bifurcation at $\gamma \approx 50$ ns^{-1}, leading to a period-2 regime.

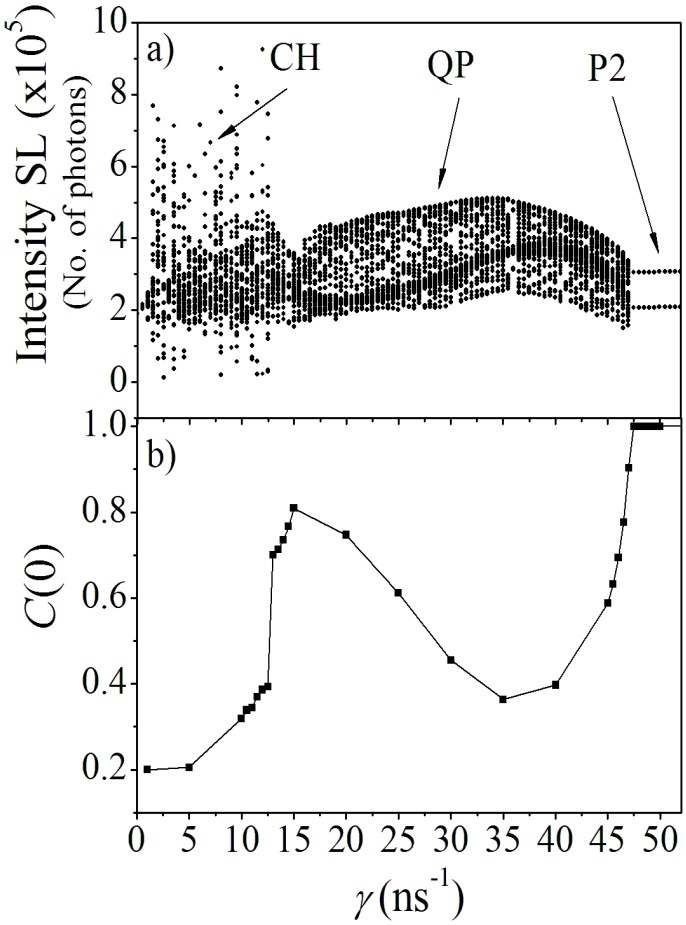

Figure 3.10: a) Bifurcation diagram of slave laser intensity and b) cross-correlation between master and slave lasers as a function of the coupling strength γ when the master is in a period-2 and the slave in a CW regime.

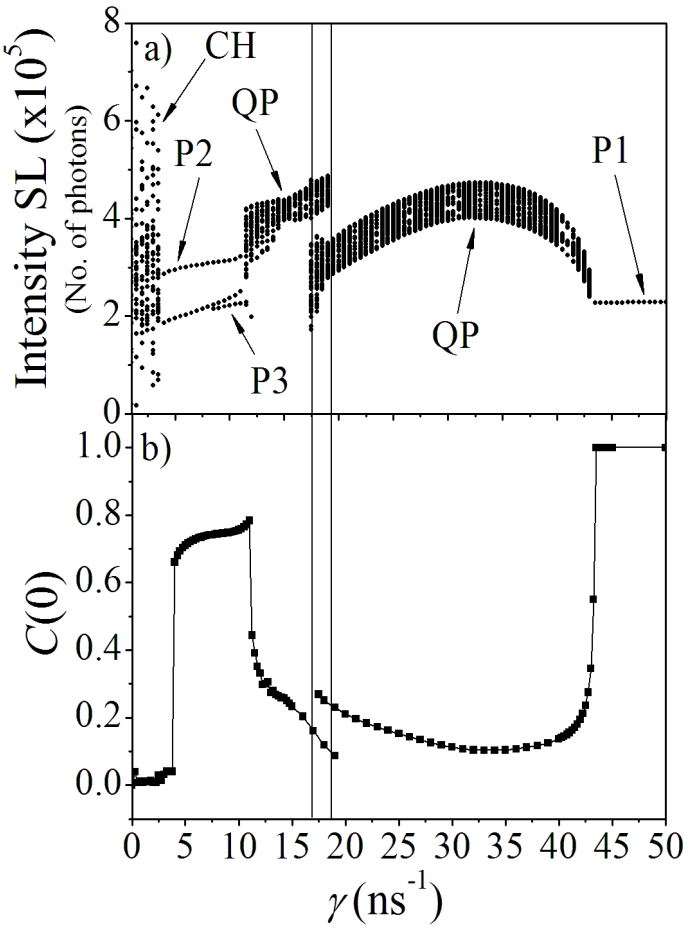

Figure 3.11: a) Bifurcation diagram of slave laser intensity and b) cross-correlation between the master and slave lasers as a function of the coupling strength γ when master laser is in period 1 and slave laser in a period 2.

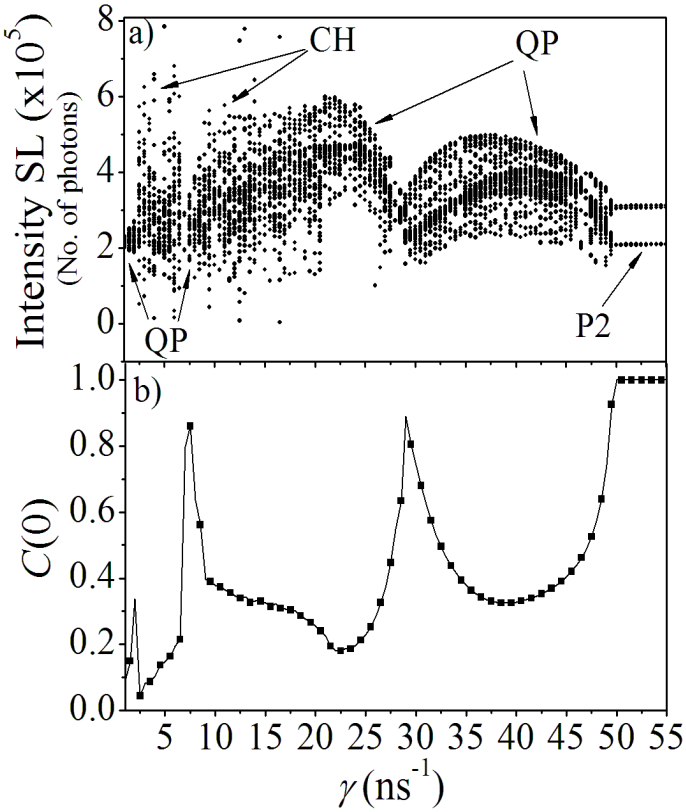

Figure 3.12: a) Bifurcation diagram of slave laser intensity of the slave laser and b) cross-correlation between master and slave lasers as a function of the coupling strength γ when the master laser is in a period-2 and the slave laser in a period-1.

3.3 Conclusions

In this chapter we studied the synchronization of two external-cavity semiconductor lasers through the analysis of bifurcation diagrams we have shown that the slave laser undergoes saddle-node, Hopf, period-doubling, torus, and crisis bifurcations, given rise to diverse dynamical regimes and bistability. Finally when the coupling is strong enough, the slave laser is synchronized with the master laser, that can be studied with the cross-correlation between the lasers.

Chapter 4

Secure optical communications

Contents

This section is dedicated to a study of secure optical communications based on complete and generalized synchronization. It contains two sub-sections. The first sub-section we study all-optical communication systems. The first part of this subsection is devoted to a study of one-channel optical systems, based on complete synchronization and in the second part we study a two-channel optical system based on complete and generalized synchronizations. In the second sub-section we study a two-channel optoelectronic communication system.

4.1 All-optical communication systems

4.1.1 One channel communication systems

One-channel communication systems consist in a master laser or transmitter, and a slave laser or receiver, both operating in a chaotic regime. The message is encrypted into the chaotic output of the master laser. To recover the message the slave laser should be synchronized with the master. The message can be added to the chaotic carrier either by chaos modulation or by chaotic masking (see figure 1.15 a)), or to the transmitter itself by shift keying (see figure 1.15 b)). Figure 4.1 shows the Q-factor of a transmitted message of 1 Gb/s as a function of the coupling between the transmitter and the receiver using chaotic modulation. The message amplitude corresponds to a modulation depth of the chaotic carrier of 2% for the blue curve and 4% for the green curve.

For a good transmission and good eye diagrams of the recovered message, the Q-factor should be around $Q \gtrsim 10$. Figure 4.2 shows Q-factors that correspond to different

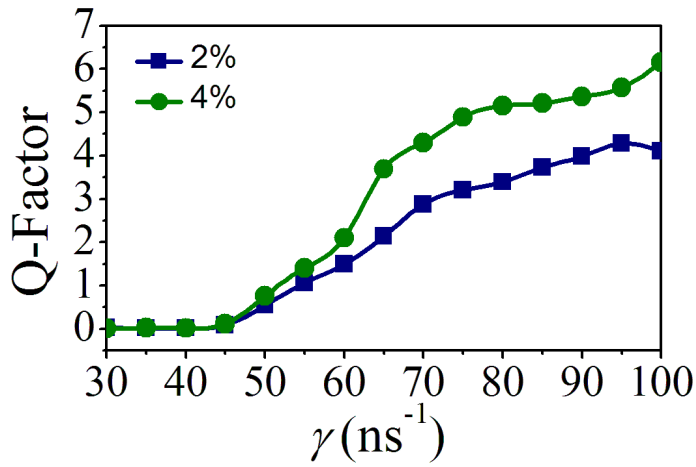

Figure 4.1: Q-Factor as a function of coupling parameter parameter γ using chaotic modulation.

eye diagrams, and figure 4.2 c) shows the open eye diagram corresponding to $Q = 10$.

For the case of shift keying (see figure 1.15 b)), the message is added to the pump current of the master laser, this is:

$$I(t) = I + em(t) \tag{4.1}$$

where $I = 29$ mA is the constant pump current, $e = 0.6$ (approximately 2% of the constant pump current) is the amplitude, and $m(t)$ is the message. For this method, the Q-factors are low, and the message transmission is not possible. Figure 4.3 shows the eye diagram for the 1Gb/s transmission when the coupling between the lasers is $\gamma = 70$ ns $^{-1}$ ($Q < 1$). For the case of chaos masking, the results are similar.

The reason that a good quality message cannot be recovered is due to the fact that the synchronization error between the transmitter and the receiver increases when the message is added. This is because the message is seen as an outside perturbation of the system that increases the synchronization error ($\langle$e$\rangle$). Figure 4.4 shows how the mean synchronization error increases when the message is added to the transmitter. The mean synchronization error is normalized to 1, where 1 indicates that there is no synchronization. The black curve with squares of figure 4.4 is the mean synchronization error when there is no message added to the system. It can be seen that when $\gamma \approx 60$ ns^{-1}, $\langle$e$\rangle$ is very close to zero, indicating complete synchronization. When the message is added, for chaotic modulation (brown curve and circles) the mean synchronization

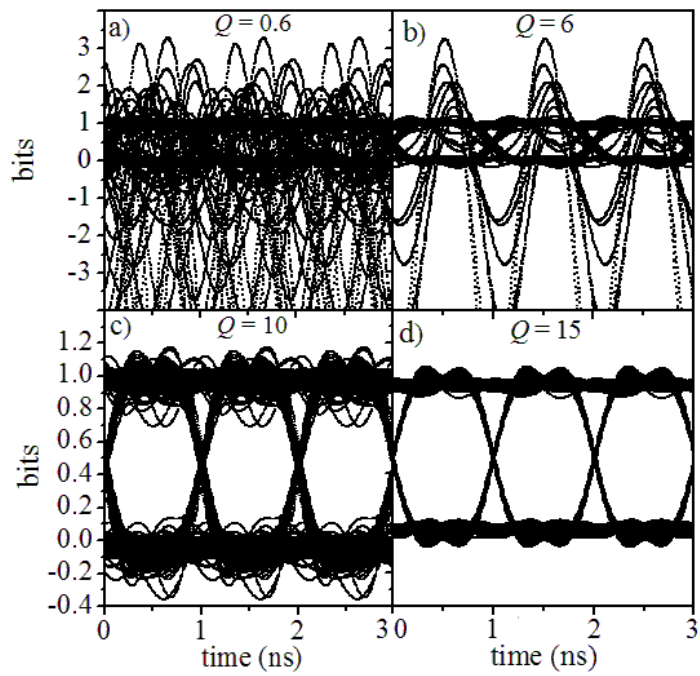

Figure 4.2: Eye diagrams and their corresponding Q-factors.

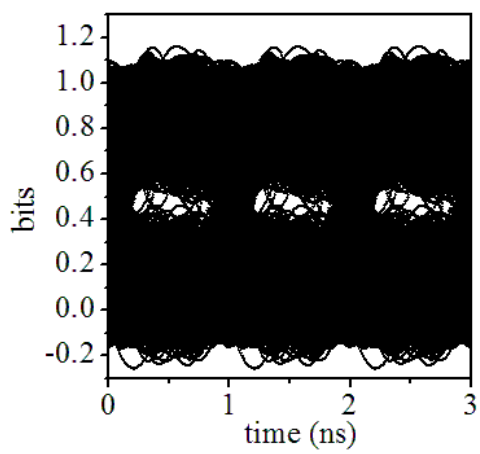

Figure 4.3: Eye diagram for shift keying, where $Q < 1$.

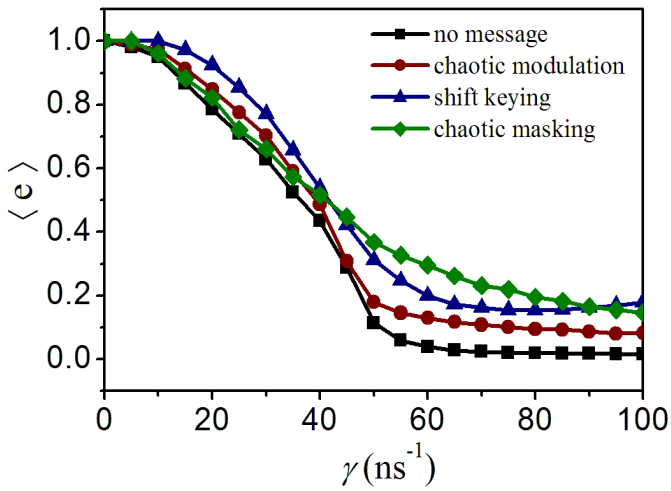

Figure 4.4: Mean synchronization error between the transmitter and the receiver.

error increases and for shift keying it is even higher (blue curve and triangles), and ⟨e⟩ for chaotic masking is the green curve with diamonds.

4.1.2 Two channel communication systems

To avoid the increase of error synchronization when the message is added, a two channel communication system is used. This system consists in a transmitter and a receiver, each one containing a master and a slave laser. Figure 4.5 a) shows a scheme of this system for chaotic masking and modulation, and figure 4.5 b) shows a scheme for shift keying. The master laser (ML1) in the transmitter has the same characteristics of the master laser (ML2) in the receiver, and ε is the coupling strength between this two lasers. Since these two lasers are identical, complete synchronization can be achieved with the appropriate coupling. The slave laser (SL1) in the transmitter has the same characteristics as the slave laser (SL2) in the receiver, i.e. they are identical. Now, the master laser (ML1) and the slave laser (SL1) in the transmitter have different characteristics, which means that complete synchronization is not possible, and only generalized synchronization can be obtained. The same is for the receiver, where ML2 and SL2 have different characteristics and only generalized synchronization is obtained, hence the signal in channel 1 is different to that in channel 2. $\gamma 1$ is the coupling strength between ML1 and SL1 in the receiver, and $\gamma 2$ is the coupling between ML2 and SL2 in the receiver.

Since ML1 and ML2 are completely synchronized, SL1 and SL2 are also completely synchronized, because of the generalized synchronization between the master (ML1 and

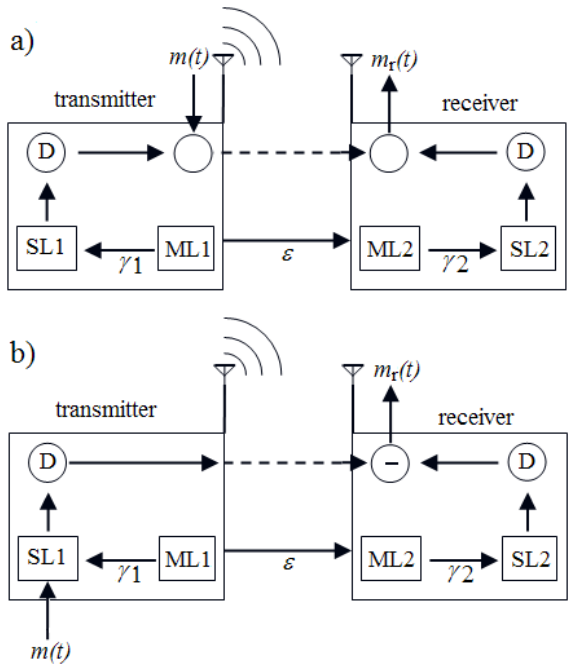

Figure 4.5: Scheme of a two channel communication system for a) chaotic masking and modulation, and b) shift keying.

ML2) and slave (SL1 and SL2) lasers in the transmitter and in the receiver. Since SL1 and SL2 are completely synchronized, a message added to SL1 can be recovered in the receiver by resting SL1 and SL2. In the scheme of figure 4.5, the outputs of the lasers are detected by a detector D. Once the optical signal is digitalized, the message is added to the electric signal (for the cases of chaotic masking and modulation) and then transmitted through an antenna. The message is received by an antenna in the receiver, and the electric signals from SL1 and SL2 are compared. The system can also be completely optical, the message can be added directly to the SL1 output, and sent to the receiver by optical fiber. Then the signal from SL2 is compared with the one from SL1.

In our case, the parameters of the master (ML1 and ML2) and slave (SL1 and SL2) lasers are different to achieve generalized synchronization between them. For ML1 and ML2, the feedback strength is $\kappa_{\mathrm{m}} = 25$ ns^{-1} and the external round trip time is $\tau_{\mathrm{m}} = 1$ ns. For SL1 and SL2, the feedback strength is $\kappa_{\mathrm{m}} = 20$ ns^{-1} and the external round trip time is $\tau_{\mathrm{m}} = 0.5$ ns. Another advantage of a two channel system is that bidirectional coupling between ML1 and ML2 is possible, without loss of security. Bidirectional coupling between the master lasers will lead to a lower mean synchronization error, and therefore a better synchronization between SL1 and SL2. For the case of bidirectional coupling, the length of the external cavities and the distance between ML1 and ML2 must satisfy the condition $l_{\mathrm{ML1}} + l_{\mathrm{ML2}} = L_{\mathrm{ML1}} + L_{\mathrm{ML2}}$ [Chiang 2005], where l_{ML1} is the length of the external cavity of ML1, where l_{ML2} is the length of the external cavity of ML2, L_{ML1} is the length from ML1 to ML2, and L_{ML2} is the length from ML2 to ML1.

Figure 4.6 shows the cross-correlation and the mean synchronization error between ML1 and ML2 as a function of their coupling ε, for the cases of unidirectional and bidirectional coupling. The black circles and the green diamonds correspond to the cross-correlation and the mean synchronization error for unidirectionally coupling. The brown triangles and the blue squares correspond to the cross-correlation and the mean synchronization error for bidirectional coupling. When there is bidirectional coupling, the coupling strength ε between ML1 and ML2 required to obtain complete synchronization is smaller. Even though the cross-correlation $C(0) \approx 1$, when $\varepsilon > 16$ ns^{-1} and $\varepsilon > 60$ ns^{-1} for bidirectional and unidirectional coupling, the mean synchronization error for bidirectional coupling is $\langle \mathrm{e} \rangle < 0.005$ and for unidirectional coupling $\langle \mathrm{e} \rangle < 0.025$.

The cross-correlation and the mean synchronization error between ML1 and SL1 as a function of the coupling ($\gamma 1$) between them are shown in figure 4.7. Similar behavior is observed for the lasers in the receiver, ML2 and SL2. One can see that complete synchronization can never be achieved for $\gamma 1 = 100$ ns^{-1}, the cross-correlation

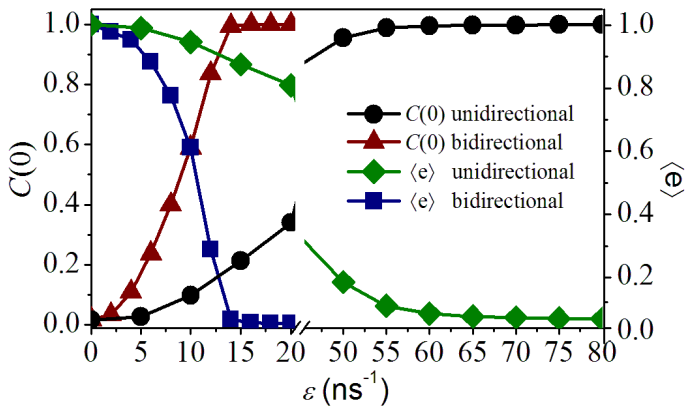

Figure 4.6: Cross-correlation and mean synchronization error between ML1 and ML2 as a function of coupling ε. The black circles and the green diamonds correspond to unidirectional coupling and the brown triangles and the blue squares to bidirectional coupling.

(green squares) is $C(0) \approx 0.84$, and the mean synchronization error (blue triangles) is $\langle e \rangle \approx 0.39$. The same results are found in unidirectional and bidirectional coupling.

Figure 4.8 shows the cross-correlation and the mean synchronization error between the slave laser (SL1) of the transmitter and the one (SL2) in the receiver as a function of the coupling strength between ML1-SL1 and ML2-SL2. These coupling strengths, $\gamma 1$ and $\gamma 2$, are varied equally. For the case of unidirectional coupling, a coupling strength between ML1 and ML2 is set to $\varepsilon = 80$ ns^{-1} and for bidirectional coupling $\varepsilon = 16$ ns^{-1}. The brown curve with triangles and the blue curve with squares correspond to the cross-correlation and the mean synchronization error for the case where there is bidirectional coupling between ML1 and ML2. The black curve with circles and the green curve with diamonds correspond to the cross-correlation and the mean synchronization error for the case of unidirectional coupling between ML1 and ML2. For the case of bidirectionally coupling the synchronization error between SL1 and SL2 is $\langle e \rangle < 0.01$.

Now lets look at message transmission using the two channel scheme. Figure 4.9 shows how the Q-factor depends on of the coupling parameter between ML1 (ML2) and SL1 (SL2). The coupling strengths $\gamma 1$ and $\gamma 2$, are varied equally. For the case of unidirectional coupling, a coupling strength between ML1 and ML2 is set to $\varepsilon = 80$ ns^{-1} and for bidirectional coupling $\varepsilon = 16$ ns^{-1}. Figure 4.9 a) corresponds to chaotic masking, this is when the message is added to the output signal of SL1 in the transmitter. The green curve with diamonds (unidirectional coupling) and the brown curve with squares (bidirectional coupling) correspond to a 1Gb/s transmission rate.

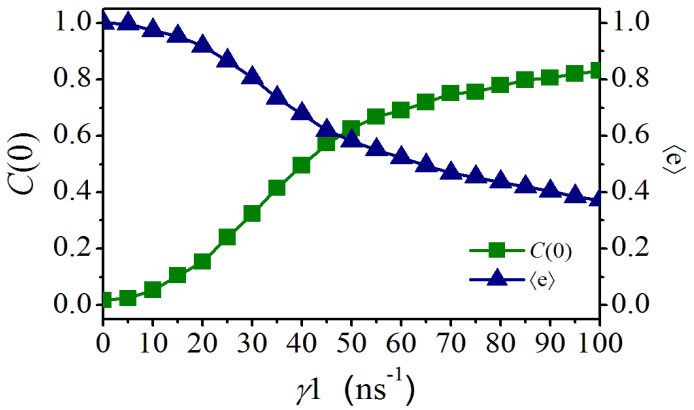

Figure 4.7: Cross-correlation (green squares) and mean synchronization error (blue triangles) between ML1 and SL1.

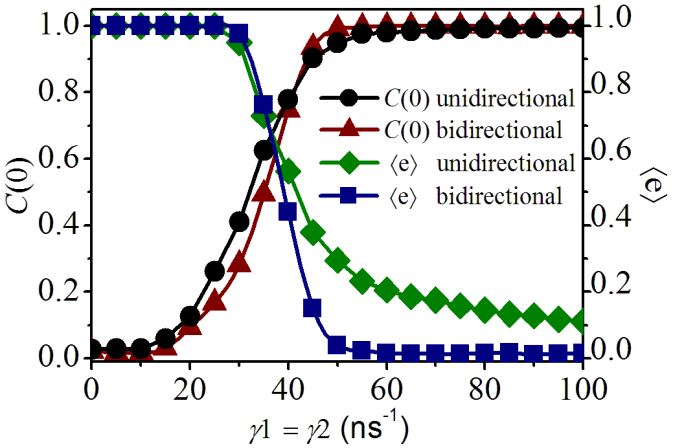

Figure 4.8: Cross-correlation and the mean synchronization error between SL1 and SL2 as a function of coupling $\gamma 1$ and $\gamma 2$. The black circles and the green diamonds correspond to unidirectional coupling and the brown triangles and the blue squares to bidirectional coupling.

The black curve with circles (unidirectional) coupling) and the blues curve with triangles (bidirectional coupling) correspond to a 5 Gb/s transmission rate. One can see that for the case of bidirectional coupling, a 5 Gb/s transmission rate is possible since the Q-factor is $Q \approx 10$ when $\gamma 1 = \gamma 2 > 80$ ns^{-1}.

Figure 4.9 b) shows the Q-factor when shift keying is used. In this case the message is added to the pump current of SL1 in the transmitter. The brown curve with squares corresponds to a 1 Gb/s transmission using bidirectional coupling between ML1 and ML2, and the green curve with squares to the case of unidirectional coupling. One can see that a good quality transmission is only possible using bidirectional coupling. For this case a 5 Gb/s transmission is not possible, since $Q < 2$, for both unidirectional and bidirectional coupling. For the 2-channel scheme chaotic modulation is not possible because of very low Q-factors are obtained. Figure 4.10 shows an eye diagram with $Q = 2.2$ when chaotic modulation is used, for bidirectional coupling and $\gamma 1 = \gamma 2 = 100$ ns^{-1}.

To check the robustness of this system, a parameter mismatch between the transmitter and the receiver is added. The coupling between ML1 and SL1 ($\gamma 1 = 80$ ns^{-1}) is kept constant and the coupling between ML2 and SL2 ($60 \leq \gamma 2 \leq 100$ ns^{-1}) is varied. This mismatch in the coupling parameters causes a difference between the cross-correlation of lasers in the transmitter and in the receiver. This difference in the cross-correlation affects synchronization between SL1 and SL2, thus affecting the quality of the transmitted message. The following figures show the mean synchronization error and Q-factor as functions of the difference between the cross-correlations of the lasers in the transmitter and the receiver, this is:

$$\delta C = C_{\mathrm{T}} - C_{\mathrm{R}} \tag{4.2}$$

where C_{T} is the cross-correlation between ML1 and SL1, and C_{R} is the cross-correlation between ML2 and SL2. For $\gamma 1 = 80$ ns^{-1}, the cross-correlation between ML1 and SL1 is $C_{\mathrm{T}} = 0.7781$. Figure 4.11 shows the mean synchronization error (blue squares) and Q-factor (green triangles) for a 1 Gb/s transmission rate when there is unidirectional coupling between ML1 and ML2 ($\varepsilon = 80$ ns^{-1}) and chaotic masking is used. As mentioned before, good transmissions are obtained when $Q \geq 10$, this corresponds to a mismatch of $|\gamma 1 - \gamma 2| \leq 2$ ns^{-1}.

Figure 4.12 shows the mean synchronization error (blue squares) and Q-factor for a 1 Gb/s (green triangles) and 5 Gb/s (brown circles) transmission rates for bidirectional coupling between ML1 and ML2 ($\varepsilon = 16$ ns^{-1}) using chaotic masking. For a 1 Gb/s transmission rate a mismatch of $|\gamma 1 - \gamma 2| \leq 12$ ns^{-1} is allowed for a good transmission. On the other hand, for a 5 Gb/s transmission rate there is no place for parameter

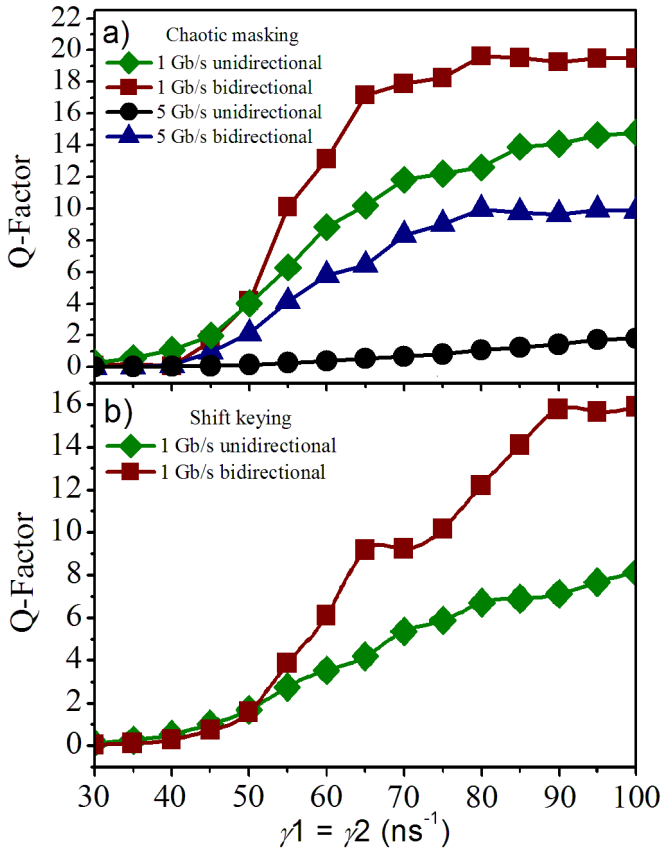

Figure 4.9: Q-factors when a) Chaotic masking is used. The brown curve with squares (bidirectional coupling) and the green curve with diamonds (unidirectional coupling) correspond to a 1 Gb/s transmission rate. The blue curve with triangles (bidirectional coupling) and the black curve with circles (unidirectional coupling) to a 5 Gb/s transmission rate. b) Shift keying, the brown curve with squares (bidirectional coupling) and the green curve with diamonds (unidirectional coupling) correspond to a 1 Gb/s transmission rate.

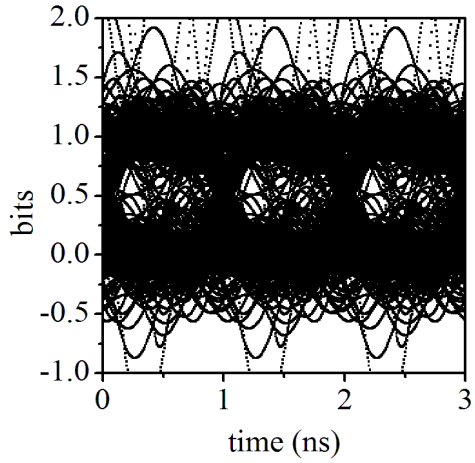

Figure 4.10: Eye diagram for a 1 Gb/s transmission rate using chaotic modulation, with bidirectional coupling, $\gamma 1 = \gamma 2 = 100$ ns^{-1}, and $Q = 2.2$.

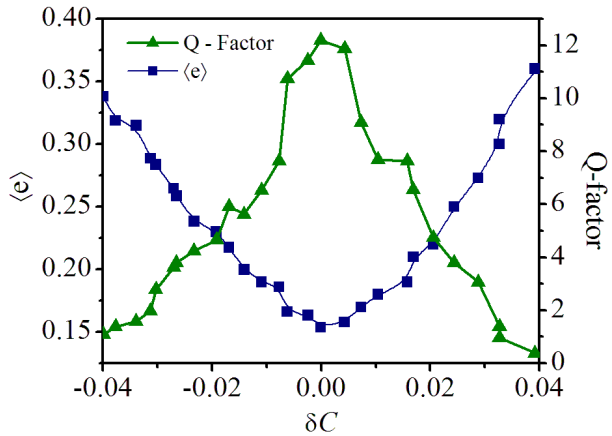

Figure 4.11: Mean synchronization error (blue squares) and Q-factor (green triangles) as a function of δC for unidirectional coupling using chaotic masking.

mismatch. From this figure it is also clear why a 5 Gb/s transmission rate is only possible when there is bidirectional coupling. For the case of bidirectional coupling, the mean synchronization error is $\langle e \rangle < 0.01$ when there is no parameter mismatch ($\delta C = 0$), and for unidirectional coupling we have that $\langle e \rangle > 0.15$.

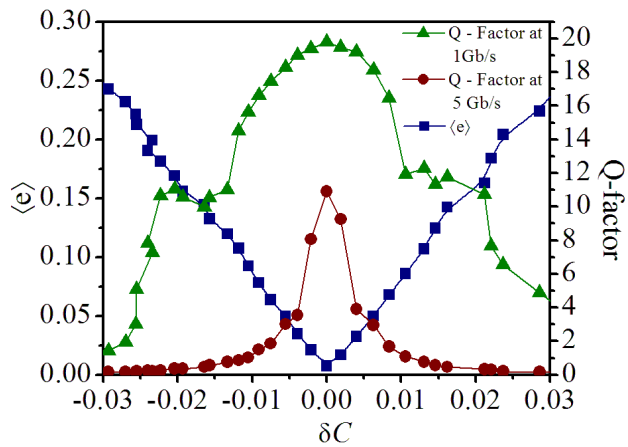

Figure 4.12: Mean synchronization error (blue squares) and Q-factor for 1 Gb/s (green triangles) and 5 Gb/s (brown circles) as a function of δC for bidirectional coupling using chaotic masking.

Next, shift keying is used. Figure 4.13 shows the mean synchronization error (blue squares) and Q-factor (green triangles) for a 1 Gb/s transmission rate for bidirectional coupling between ML1 and ML2 ($\varepsilon = 16$ ns^{-1}). A good transmission is possible when $0 < \gamma 1 - \gamma 2 < 9$ ns^{-1}. From this figure on can see that the curves are not symmetric around $\delta C = 0$, as the previous cases. This is due to the fact, that when the message is added to the pump current of SL1, there already exists a parameter mismatch when the bits "1" are being added to the system. This mismatch in the pump currents is then compensated by the mismatch between the coupling $\gamma 1$ and $\gamma 2$, so the curves of the mean synchronization error and Q-factor are shifted with respect to δC. Similar results for the previous cases are obtained if the parameter mismatch exists between other parameters.

4.2 Two channel optoelectronic communication systems

In the two channel optoelectronic communication system, the master lasers in the transmitter and in the receiver are replaced by chaotic electronic circuits. On the other hand, the slave lasers in the transmitter and in the receiver are replaced by semi-

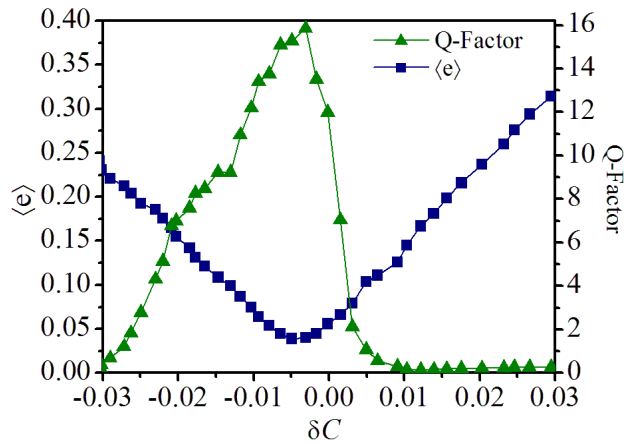

Figure 4.13: Mean synchronization error (blue squares) and Q-factor (green triangles) as a function of δC for bidirectional coupling using shift keying.

conductor lasers without optical feedback. For the chaotic electronic circuit a mathematical model that simulates a Rössler-like oscillator, as the one shown in figure 4.14 [Pisarchik 2005, Pisarchik 2008, Escobeza 2008, Pisarchik 2006] is used.

The scheme for this two channel system is shown in figure 4.15 a) for chaotic masking and modulation, and figure 4.15 b) for shift keying. R1 is the Rössler-like circuit used in the transmitter and R2 is the circuit used in the receiver. The Y output of the circuits is used to synchronize R1 with R2. Then, the X output of the circuits is used to modulate the pump current of the lasers (SL1 and SL2).

The Carroll model is used to simulate the electronic circuit shown in figure 4.14. This model represents a small modification of the Rössler system replacing the nonlinear element by a piecewise linear function. The equations for R1 can be written in the following dimensionless form:

$$\frac{dX_1}{dt} = -\varrho\left(\mu X_1 + \varsigma Y_1 + Z_1\right) \tag{4.3}$$

$$\frac{dY_1}{dt} = \varrho\left(X_1 + \nu Y_1\right) \tag{4.4}$$

$$\frac{dZ_1}{dt} = \varrho\left[g(X_1) - Z_1\right] \tag{4.5}$$

$$g(X_1) = \begin{Bmatrix} 0, & X_1 \leq 3 \\ \varkappa(X_1 - 3), & X_1 > 3 \end{Bmatrix} \tag{4.6}$$

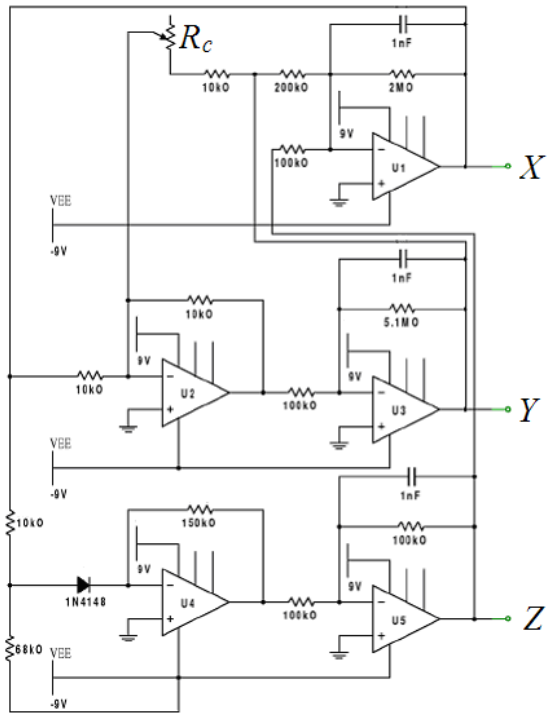

Figure 4.14: Rössler-like circuit.

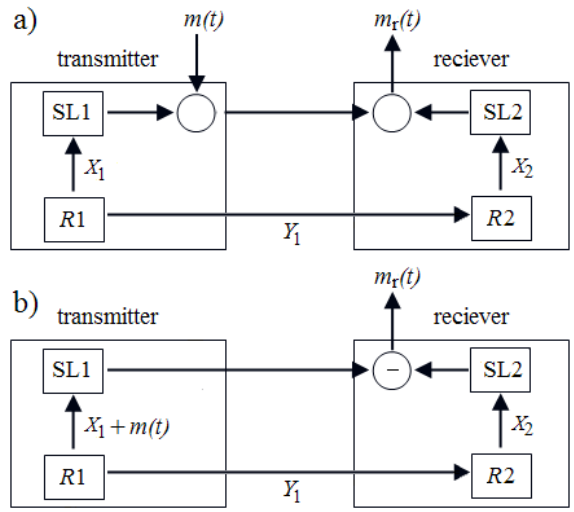

Figure 4.15: Scheme of the two channel optoelectronic communication system for a) chaotic masking and modulation, and b) shift keying.

where X_1, Y_1 and $Z_1$are the outputs of R1, $\varrho = 10^4 s^{-1}$ is the time factor and the other circuit parameters are $\mu = 0.05$, $\varsigma = 0.5$, $\varkappa = 15$, $\nu = r/R - 0.02$, $r = 10$ kΩ and $R = 80$ kΩ. Figure 4.16 shows the trajectory in the phase space of (X_1, Y_1, Z_1) for the above equations and parameters. from this figure the Rössler-like behavior is clearly seen.

The synchronization of the Rössler-like circuit in the receiver (R2) with the circuit in the transmitter (R1) can be achieved with the Pecora and Carroll [Boccaletti 2002] method. The model equations of the Rössler-like circuit in the receiver (R2) are:

$$\frac{dX_2}{dt} = -\varrho[\mu X_2 + \varsigma(Y_2 + \varepsilon(Y_1 - Y_2)) + Z_2] \tag{4.7}$$

$$\frac{dY_2}{dt} = [\varrho X_2 + \nu(Y_2 + \varepsilon(Y_1 - Y_2)] \tag{4.8}$$

$$\frac{dZ_2}{dt} = \varrho\,[g_2(X_2) - Z_2] \tag{4.9}$$

$$g_2(X_2) = \begin{Bmatrix} 0, & X_2 \leq 3 \\ \varkappa(X_2 - 3), & X_2 > 3 \end{Bmatrix} \tag{4.10}$$

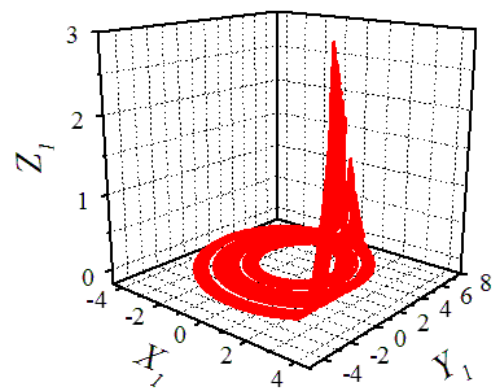

Figure 4.16: Trajectory in (X_1, Y_1, Z_1) phase space of the Rössler-like circuit.

where X_2, Y_2 and Z_2 are the outputs of R2, and ε is the coupling parameter, the rest of the parameters are the same as in R1. If $\varepsilon = 1$, there will be complete synchronization between R1 and R2. Figure 4.17 shows a graph, where X_1 vs. X_2 is plotted and complete synchronization exists between R1 and R2.

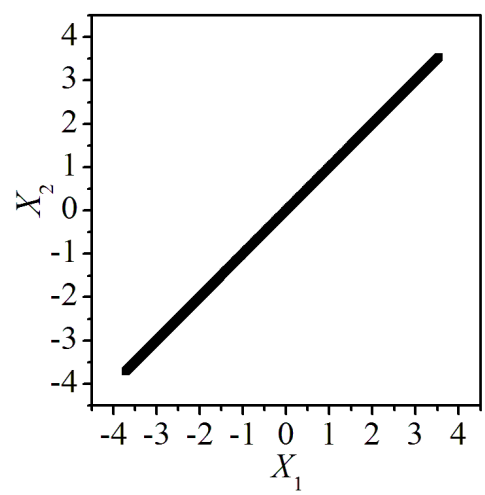

Figure 4.17: Plot showing complete synchronization between R1 and R2, when $\varepsilon = 1$

As mentioned before, X_1 is used to modulate the pump current of SL1 and X_2 is used to modulate the pump current of SL2. $(I(t) = 29 \times 10^{-3}/e_c + X_{1,2})$ Since the main frequency of the Rössler-like system ($f_R \approx 1.1$ kHz) is much lower than the frequency of the laser relaxation oscillations ($f_m \approx 6$ GHz), then the output intensity

of SL1 will behave the same as X_1, and SL2 as X_2. Figure 4.18 a) shows the behavior of the X_1 output and figure 4.18 b) the behavior of the SL1 output. It is clearly seen how SL1 follows R1. Since there exists complete synchronization between R1 and R2, complete synchronization exists between SL1 and SL2. So for this two channel communication system, one of the channels will have the X_1 behavior and the other one the Y_1 behavior. Each channel will have a different signal, similar to the two channel all optical communication system, but the bit transmission rate will be much slower due to the lower proper frequency of the Rössler-like system.

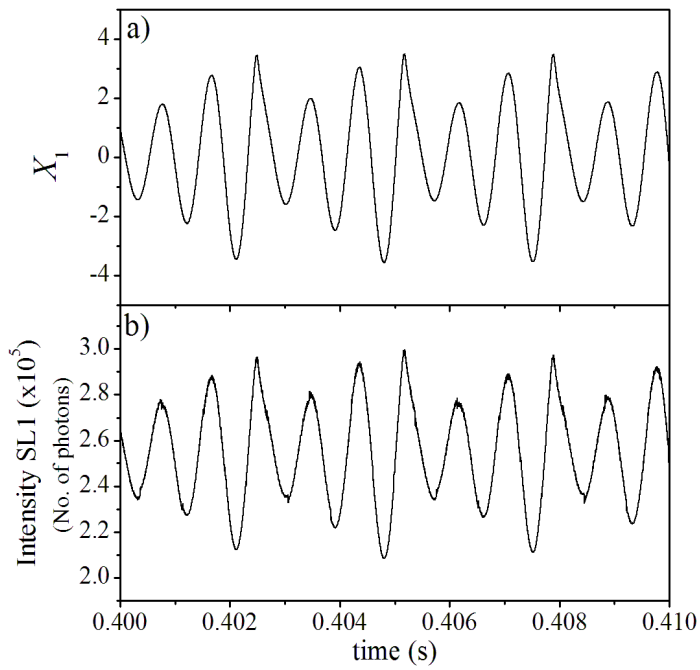

Figure 4.18: a) X_1 output from R1 and b) SL1 intensity output.

Figure 4.19 shows the eye diagrams for a 1kb/s transmission rate using a) chaotic modulation, b) chaotic masking and c) shift keying. For this communication system, the three methods are possible and the Q-factor is $Q \approx 19$ for all of them. It is important to take into consideration that noise was only consider for the lasers but not for the Rösler-like circuits.

Due to the fact that both lasers operate in a CW regime in the absence of the pump modulation, a parameter mismatch does not affect the synchronization between SL1 and SL2. Since both lasers follow the behavior of the X output, when the Rössler-circuits are synchronized, SL1 and SL2 will be synchronized too. Figure 4.20 a) shows a time

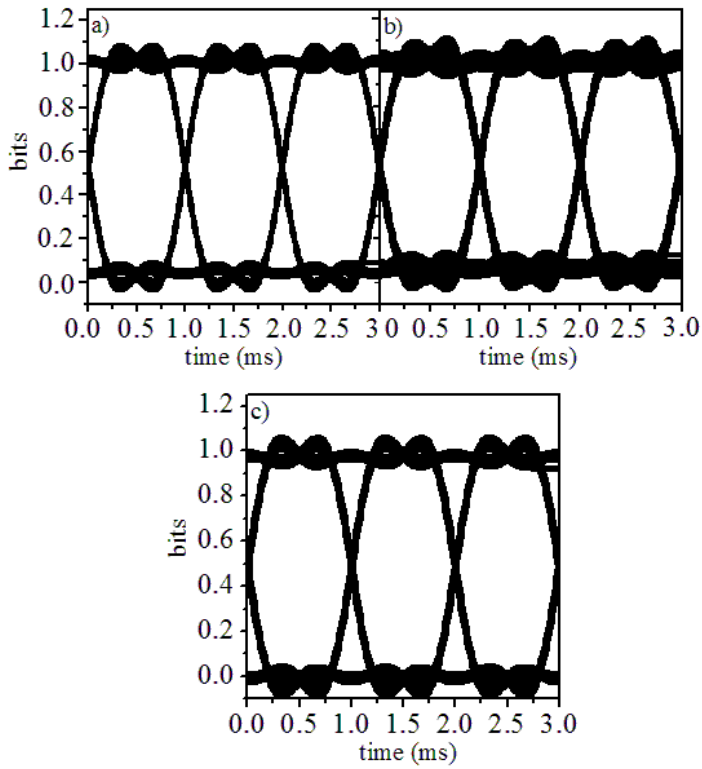

Figure 4.19: Eye diagrams for a 2 channel optoelectronic communication system for a 1 Kb/s transmission rate when a) chaotic modulation, b) chaotic masking, and c) shift keying are used.

series of the SL1 intensity with the parameters ($\alpha = 3$) we used until now, Figure 4.20 b) is the SL2 intensity when $\alpha = 2$. From this figure it is clearly seen that both lasers are synchronized even in the presence of parameter mismatch.

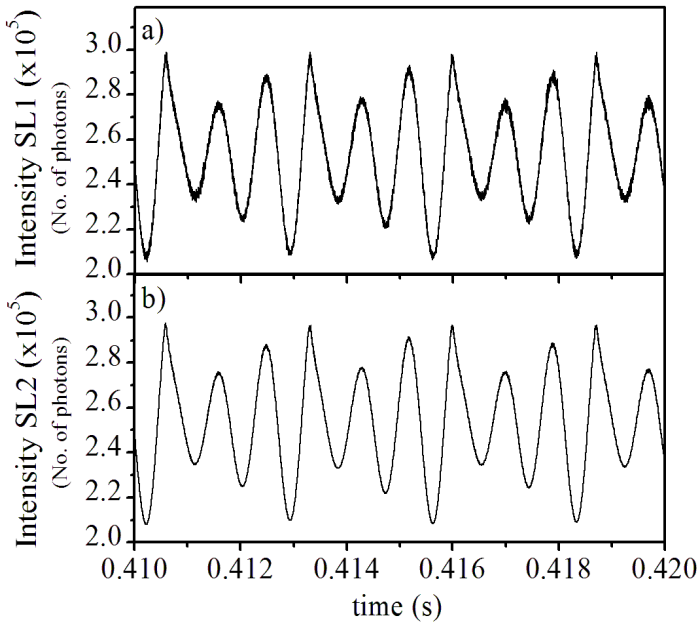

Figure 4.20: Time series of a) SL1 intensity output with $\alpha = 3$ and b) SL2 intensity output with $\alpha = 2$.

Since there is good enough synchronization between SL1 and SL2, message transmission is possible even in the presence of parameter mismatch between the lasers. The eye diagrams obtained with the parameter mismatch are similar to those shown in figure 4.19 and $Q \approx 19$. We performed simulations for $2 \leq \alpha \leq 4$ and obtained the same results. We did not introduced parameter mismatch between the Rössler-like electronic, since it is relatively easy to adjust parameters of one circuit to match those of the other to obtain complete synchronization.

This scheme allows to transmit at faster speeds but the communication system is not secure anymore. If the transmission speed is higher than the proper frequency of the system ($f_{\mathrm{R}} \approx 1.1$ kHz), an outsider will be able to identify the message in the chaotic carrier itself. Figure 4.21 a) shows a series of bits for 25kb/s transmission rate and figure 4.21 b) shows the SL1 output with the corresponding bits added using shift keying. From figure 4.21 b) one can identify the bits with out the need of a receiver.

Figure 4.21 c) shows the eye diagram of the recovered message and $Q \approx 10$. Similar results are obtained for chaotic masking and modulation.

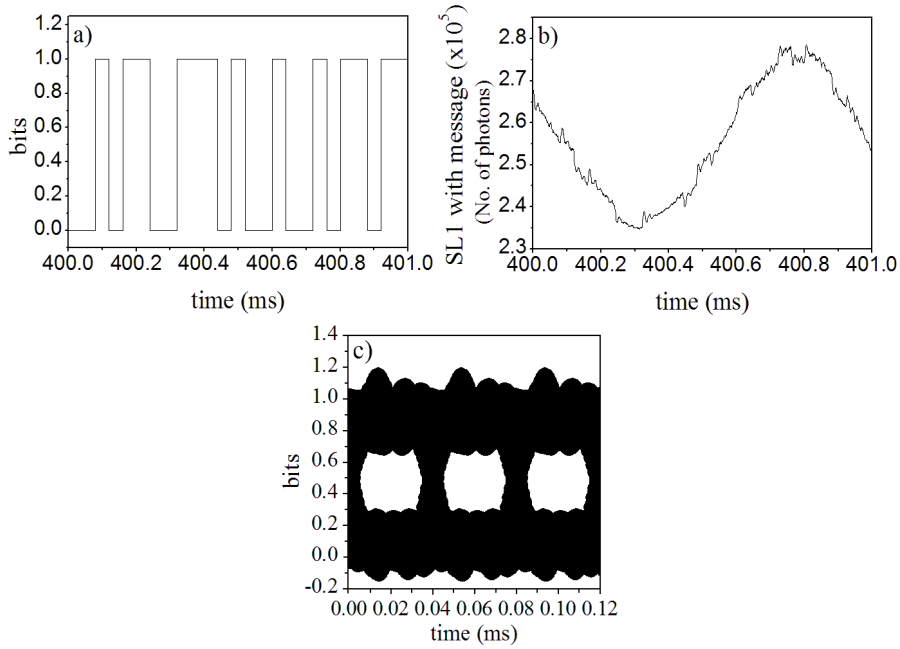

Figure 4.21: a) Time series of bits and b) SL1 output with the message added using shift keying, and C) eye diagram for a 25kb/s transmission rate.

4.3 Conclusions

In this chapter, we analyzed three different communication schemes. The first scheme consisted of a one channel communication system with a master laser acts as the transmitter and a slave laser acted as the receiver. In this scheme the same channel was used for two purposes: to synchronize the lasers and to transmit a message. Therefore the synchronization between the lasers was varied because the message acted as an outside perturbation that increases synchronization error between the lasers. Because of the large synchronization error, the quality of the recovered message was low. The highest Q-factor for this type of communication scheme was $Q \approx 6$.

The second scheme consisted in a 2 channel, all optical communication system based on complete and generalized synchronization. In this scheme the transmitter and the

receiver contained both a master laser and a slave laser. The master lasers were used to synchronize the transmitter with the receiver via one of the channels and the slave lasers were used to send a message through another channel. The master lasers in the transmitter and the receiver were completely synchronized, while the master and slave lasers were generalized synchronized. Since one channel was used to synchronize the lasers and another channel to transmit the message, the message does not affect the global synchronization between the transmitter and the receiver. Since the synchronization was not affected, the quality of the recovered message was very high. In the case of unidirectional coupling $Q \approx 12$ was obtained using the chaotic masking technique for a 1 Gb/s transmission rate. When bidirectional coupling was used between the master lasers was used, Q-factor of $Q \approx 20$ and $Q \approx 16$ where obtained using chaotic masking and shift keying for a 1 Gb/s transmission rate. For this scheme a 5 Gb/s transmission rate was obtained using chaotic masking. A good quality in the message recovery could not be obtained for the case of chaotic modulation.

The third scheme consisted of a 2 channel optoelectronic communication system. For this system a good quality revered message was obtained for the three different transmission techniques since $Q \approx 19$ for the three cases. This system was limited in the speed of the transmission rate, since the proper frequency of the Rössler-like circuit is around 1.1 kHz, that makes the transmission rate slow. On the other hand this system is very robust to parameter mismatch. In the presence of parameter mismatch between the lasers, the synchronization is not affected because they follow the X output of the circuits because the lasers work in a CW regime. However, the low transmission rate makes this system unpractical nowadays.

Chapter 5

General conclusions

The dynamics, synchronization and application of semiconductor lasers with optical feedback for secure communications were numerically investigated. Different dynamical regimes were observed. The dynamics depends on the feedback strength, the length of the external cavity, and the initial phase of the electric field from the external cavity Different routes to chaos, such as period doubling route to chaos and fixpoint-Period 1-Torus-Chaos route to chaos were found. When a second cavity was added to the semiconductor laser, a phase-locking phenomena occurs with the electric fields of the two external cavities. The Arnold tongues structure appears in the parameter space of the external cavity length. Adding a second cavity is one of the simplest ways to stabilize the dynamics of the laser and to eliminate the chaotic behavior.

When the optical signal of a semiconductor laser (master laser) was injected to another semiconductor laser (slave laser), synchronization between this two lasers can be observed. Different scenarios of synchronization where studied for different dynamical regimes: monostable and multistable regimes For both regimes, the slave laser can undergo into CW, chaotic, periodic and quasi periodic oscillations. When the coupling is strong enough, the slave laser orbit follows the master laser trajectory and they are completely synchronized. When both lasers are chaotic, the slave laser is completely synchronized with the master laser for strong coupling.

Taking advantage of chaotic synchronization between master and slave lasers, two different secure communication schemes where studied. The first scheme consisted of a one channel system used to synchronize the transmitter with the receiver and send a message. For this scheme, the recovered message at the receiver had a low quality factor. The other scheme consisted in a two channel system. For this system each channel had different signals. All-optical and an optoelectronic systems were studied. The all-optical system, which is based on generalized and complete synchronization, transmission rates of up to 5Gb/s were obtained with a good quality for message recovering. On the other hand the optoelectronic scheme had the advantage that it is robust to parameter mismatch, and the disadvantage is a low transmission speed due to the use of electronic circuits.

Appendix A

Fix points of the Lang-Kobayashi model

To obtain the fix points, it is easier to work with the normalized Lang-Kobayashi equations [Heil 2003, Haegeman 2002, Alsing 1996] given by:

$$\frac{dE(s)}{ds} = (1 + i\alpha)N(s)E(s) + \eta E(s-\theta)\exp(-i\Omega\theta) \tag{A.1}$$

$$T\frac{dN(s)}{ds} = P - N(s) - (1 + 2N(s))\,|E(s)|^2 \tag{A.2}$$

where E and N are the normalized Electric field and carrier inversion, the time is $s = \frac{t}{\tau_\mathrm{p}}$, where τ_p is the photon lifetime. $T = \frac{\tau_\mathrm{n}}{\tau_\mathrm{p}}$, where τ_n is the carrier lifetime. Ω is the dimensionless angular frequency. $\theta = \frac{\tau}{\tau_\mathrm{p}}$ is the ratio of the external cavity round trip time and the photon lifetime. P is the dimensionless pumping current above threshold. $\eta = \kappa\tau_\mathrm{p}$ is the feed back strength and α is the line width enhancement factor. Equation (A.1) and (A.2) are now transformed into polar coordinates [Davidchack 2001, Rottschafer 2005] by introducing $E(s) = E_0(s)\exp(i\varphi(s))$, which gives:

$$\frac{dE_0(s)}{ds} = N(s)E_0(s) + \eta E_0(s-\theta)\cos(\Omega\theta + \varphi(s) - \varphi(s-\theta)) \tag{A.3}$$

$$\frac{d\varphi(s)}{ds} = \alpha N(s) - \eta\frac{E_0(s-\theta)}{E_0(s)}\sin(\Omega\theta + \varphi(s) - \varphi(s-\theta)) \tag{A.4}$$

$$T\frac{dN(s)}{ds} = P - N(s) - (1 + 2N(s))E_0^2(s) \tag{A.5}$$

Fix points are found when $E(s) = E_\mathrm{c}\exp(i\psi s)$ and $N(s) = N_\mathrm{c}$, where E_c, N_c, and ψ are constant; introducing into equations (A.3), (A.4), and (A.5):

$$N_c = -\eta \cos(\Omega\theta + \psi\theta) \tag{A.6}$$

$$\psi = \alpha N_c - \eta \sin(\Omega\theta + \psi\theta) \tag{A.7}$$

$$E_c^2 = \frac{P - N_c}{1 + 2N_c} \tag{A.8}$$

Fix points in the phase space of ψ and N_c are given by the intersection of equations (A.6) and (A.7). For a $\eta = 0.25$, $\theta = 8$ and $\Omega\theta = 0$, the fix points are shown in figure A.1 a). If $0 \leq \Omega\theta \leq 2\pi$ then the fix points form an ellipse in the phase space of ψ and N_c as shown in figure A.1 b).

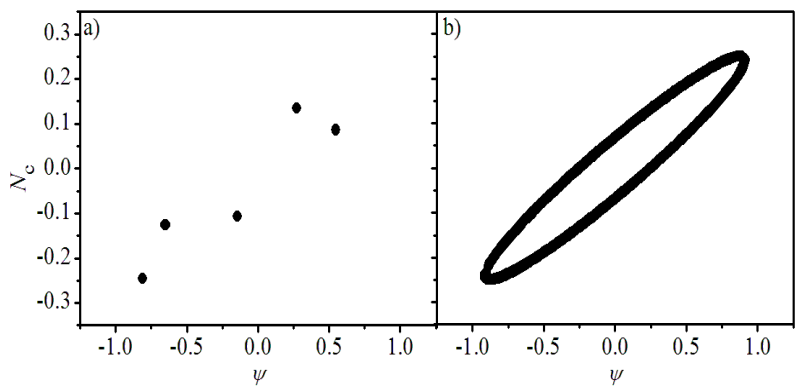

Figure A.1: Fix points when a) $\Omega\theta = 0$ and b) $0 \leq \Omega\theta \leq 2\pi$

Fix points in the phase space of E_c and N_c are obtained by solving equation (A.8). Figure A.2 shows the the fix points and a trajectory of the solution of equations (A.1) and (A.2) in the phase space of E_c and N_c when $\Omega\theta = 0$ and $P = 0.75$. The trayectory is always attracted to the maximum energy point which corresponds to the fix point with the largest E_c.

The stability of the fix points is given by the solution of the characteristic equation given by:

$$\det(A + B\exp(-\lambda\theta) - \lambda I) = 0 \tag{A.9}$$

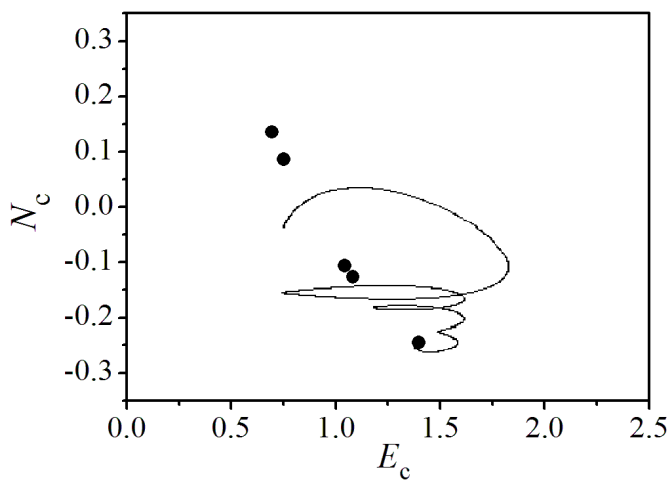

Figure A.2: Fix points and trajectory in the phase space of E_c and N_c for a semiconductor laser with 1 external cavity.

where λ are the eigenvalues, I is the identity matrix, A is:

$$\begin{bmatrix} N_c & -\eta E_c \sin(\psi\theta) & E_c \\ \frac{\eta}{E_c}\sin(\psi\theta) & -\eta\cos(\psi\theta) & \alpha \\ -\frac{2}{T}(1+2N_c)E_c & 0 & -\frac{1}{T}(1+2E_c^2) \end{bmatrix} \tag{A.10}$$

and B is given by:

$$\begin{bmatrix} \eta\cos(\psi\theta) & \eta E_c \sin(\psi\theta) & 0 \\ -\frac{\eta}{E_c}\sin(\psi\theta) & \eta\cos(\psi\theta) & 0 \\ 0 & 0 & 0 \end{bmatrix} \tag{A.11}$$

Equation (A.9) is a quasi-polynomial and has an infinite number of solutions.

For the case of two external cavities the analysis is very similar, just the feedback strength η_2 and external round trip time θ_2 of the second cavity have to be considered. The Fix points will know be obtained by the intersection of the following equations:

$$N_c = -\eta\cos(\Omega\theta + \psi\theta) - \eta_2\cos(\Omega\theta_2 + \psi\theta_2) \tag{A.12}$$

$$\psi = \alpha N_c - \eta\sin(\Omega\theta + \psi\theta) - \eta_2\sin(\Omega\theta_2 + \psi\theta_2) \tag{A.13}$$

$$E_c^2 = \frac{P - N_c}{1 + 2N_c} \tag{A.14}$$

Figure A.3 a) shows the fix points [Tronciu 2006, Würtenberger 2000] in the phase space of ψ and N_c when $\Omega\theta = 0$ and $\Omega\theta_2 = 0$, $\eta = 0.25$, $\eta_2 = 0.25$, $\theta = 22$ and $\theta_2 = 27$. If $0 \leq \Omega\theta \leq 2\pi$ and $\Omega\theta_2 = 0$ is kept constant, the fix points now form a pattern as the one shown in figure A.3 b).

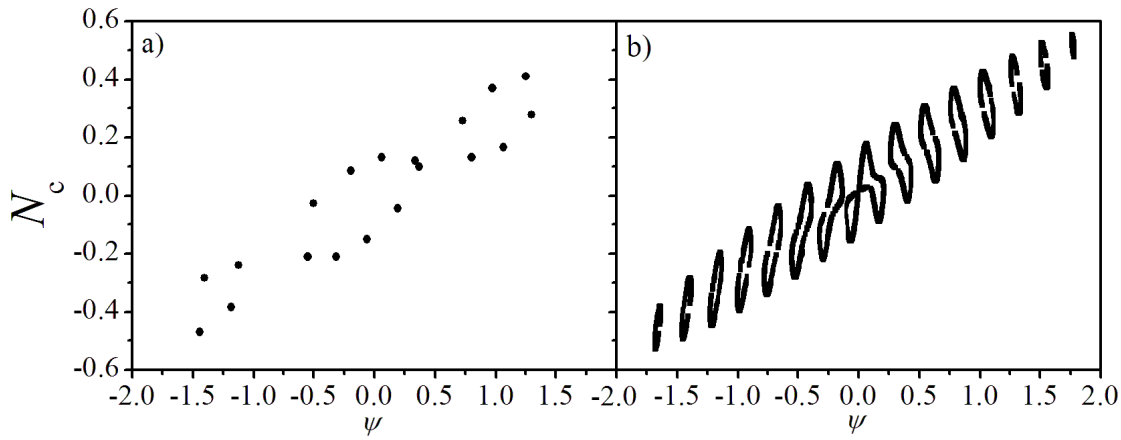

Figure A.3: Fix points when a) $\Omega\theta = 0$ and $\Omega\theta_2 = 0$, and b) $0 \leq \Omega\theta \leq 2\pi$ and $\Omega\theta_2 = 0$.

Fix points in the phase space of E_c and N_c are shown in figure A.4 for $P = 0.75$, and now the trajectory is not always attracted to the maximum energy point.

The stability of the fix points are given by the characteristic equation:

$$\det(A' + B\exp(-\lambda\theta) + C\exp(-\lambda\theta_2) - \lambda I) = 0 \tag{A.15}$$

where A' is given by:

$$\begin{bmatrix} N_c & -E_c(\eta\sin(\psi\theta) + \eta_2\sin(\psi\theta_2)) & E_c \\ \frac{1}{E_c}(\eta\sin(\psi\theta) + \eta_2\sin(\psi\theta_2)) & -\eta\cos(\psi\theta) - \eta_2\cos(\psi\theta_2) & \alpha \\ -\frac{2}{T}(1 + 2N_c)E_c & 0 & -\frac{1}{T}(1 + 2E_c^2) \end{bmatrix} \tag{A.16}$$

and C is:

$$\begin{bmatrix} \eta_2\cos(\psi\theta_2) & \eta_2 E_c\sin(\psi\theta_2) & 0 \\ -\frac{\eta_2}{E_c}\sin(\psi\theta_2) & \eta_2\cos(\psi\theta_2) & 0 \\ 0 & 0 & 0 \end{bmatrix} \tag{A.17}$$

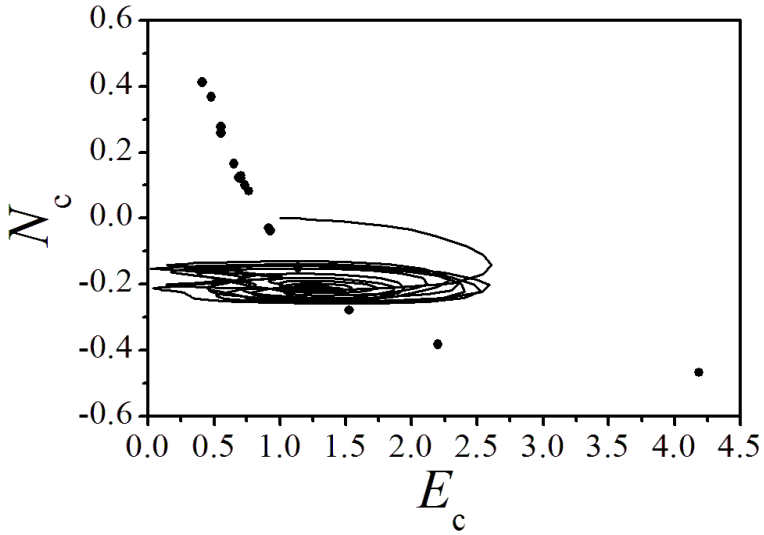

Figure A.4: Fix points and trajectory in the phase space of E_c and N_c for a semiconductor laser with 2 external cavities.

Appendix B

Vita and Publications

B.1 Vita

- 2002 B.Sc. Mechanical Engineering, University of Missouri-Rolla, USA
- 2006 M.Sc. Optics, Centro de Investigaciones en Óptica, A.C., Mexico

B.2 Publications

- F. R. Ruiz-Oliveras and A. N. Pisarchik, *Phase-Locking Phenomenon in a Semiconductor Laser with External Cavities*, Optics Express, No. 26, Vol. 14, 2006.
- Miguel C. Soriano, Flavio Ruiz-Oliveras, Pere Colet and Claudio R. Mirasso, *Synchronization properties of coupled semiconductor lasers subject to filtered optical feedback*, PRE 78, 046218, 2008.
- F. R. Ruiz-Oliveras and A. N. Pisarchik, *Synchronization of semiconductor lasers with coexisting attractors*, PRE 79, 016202, 2009.
- Flavio Ruiz-Oliveras, Miguel C. Soriano, Pere Colet and Claudio R. Mirasso, *Information Encoding and Decoding using Unidirectionally Coupled Chaotic Semiconductor Lasers subject to Filtered Optical Feedback*, IEEE-JQE, Vol. 45, No. 8, 2009.
- Alexander N. Pisarchik and Flavio R. Ruiz-Oliveras, *Optical Chaotic Communication Using Generalized and Complete Synchronization*, IEEE-JQE (accepted on september 9, 2009).

B.3 Patent

Alexander N. Pisarchik and Flavio R. Ruiz Oliveras, *Sistema de comunicación óptica usando caos*, patent pending, MX/A/2009/001860.

Bibliography

[3d] In Chaos-based communications using semiconductor lasers subject to feedback from an integrated double cavity. See EPAPS Document No. E-PLEEE8-78-105812 for a movie corresponding to figure 2.6. 31

[Aboites 2007] V. Aboites. In Lásers una introducción. Centro de Investigaciones en Óptica, A.C., 2007. 1

[Alsing 1996] P. M. Alsing, V. Kovanis, A. Gavrielides and T. Erneux. *Lang and Kobayashi phase equation*. PRA, vol. 53, no. 6, 1996. 79

[Beesley 1971] M. J. Beesley. In Lasers and their Applications. Taylor and Francis Ltd., London, services Electronics, Research Laboratory, Ministry of Defensei, 1971. 1

[Bennet 2002] Matthew Bennet, Michael F. Schatz, Heidi Rockwood and Kurt Wiesenfeld. In Huygen's clocks. Proc. R. Soc. Lond. A, Vol. 458, No. 2019, 2002. 16

[Besnard 1993] P. Besnard, B. Meziane and G. N. Stephan. *Feedback Phenomena in a Semiconductor Laser induced by distant reflectors*. IEEE-JQE, vol. 29, no. 5, 1993. 15

[Boccaletti 2002] S. Boccaletti, J. Kurths, G. Osipov, D. L. Valladares and C. S. Zhoul. *Synchronization of chaotic systems*. Physics reports, vol. 366, 2002. 17, 69

[Breed 2005] Garry Breed. In Analyzing signals using the eye diagram. High Frequency Electronics, Summit Technical Media, 2005. 26

[Buldú 2009] J. M. Buldú, J. García-Ojalvo, Claudio R. Mirasso, M. C. Torrent and J. M. Sancho. *Effect of external noise correlation in optical coherence resonance*. PRE, vol. 64, 051109, 2009. 11

[Chiang 2005] Margaret C. Chiang, How-Foo Chen and Jia-Ming Liu. *Experimental Synchronization of Mutually Coupled Semiconductor Lasers with Optoelectronic Feedback*. IEEE-JQE, vol. 41, no. 11, 2005. 60

[Cohen 1991] Julius S. Cohen and Daan Lenstra. *The Critical Amount of Optical Feedback for Coherence Collapse in Semiconductor Lasers*. IEEE-JQE, vol. 27, no. 1, 1991. 15

[Colet 1998] Pere Colet and Rajarshi Roy. *Digital communications with synchronized chaotic lasers*. Optics Lett., vol. 19, 1998. 15

[Davidchack 2001] Ruslan. L. Davidchack, Ying-Cheng Lai, Athanasios Gavrielides and Vassilios Kovanis. *Regular dynamics of low frequency fluctuations in external cavity semiconductor lasers.* PRE, vol. 63, 056206, 2001. 79

[Dutton 1998] Harry J. R. Dutton. In Understanding optical communications. IBM, 1998. 21

[Escobeza 2008] Jesús Ricardo Sevilla Escobeza. In Diseño de un arreglo experimental basado en un circuito electrónico para el estudio de sincronización de redes caóticas. Bachelor in mechantronics engineering thesis, Centro Universitorio de los Lagos, 2008. 67

[Fleming 1981] M. W. Fleming and A. Mooradian. *Fundamental line broadening of single-mode (GaAl)As diode lasers.* Appl. Phys. Lett., vol. 38, no. 7, 1981. 10

[García-López 2005] J. H. García-López, R. Jaimes-Reátegui, A. N. Pisarchik, C. Medina-Gutierréz, J. C. Jiménez-Godinez, A. U. Murguía-Hernandez and R. Valdivia. In Novel communication scheme based on chaotic Rössler circuits. J. Phys. Conf. Series, Vol. 32, 2005. 24

[García-López 2008] J. H. García-López, R. Jaimes-Reátegui, R. Chiu-Zarate, D. Lopez-Mancilla, R. Ramirez-Jiménez and A. N. Pisarchik. *Secure computer communication based on chaotic Rössler oscillators.* Open Elec. and Electronic Eng. J., vol. 32, 2008. 24

[Giudici 1997] M. Giudici, C. Green, G. Giacomelli, U. Nespolo and J. R. Tredicce. *Andronov bifurcation and excitability in semiconductor laser with optical feedback.* PRE, vol. 55, 6414, 1997. 15

[Gouaux 1998] Flore Gouaux, Noel Servagent and Thierry Bosch. *Absolute distance measurement with an optical feedback interferometer.* App. Optics, vol. 37, no. 28, 1998. 15

[Haegeman 2002] B. Haegeman, K. Engelborghs, D. Roose, D. Pieroux and T. Erneux. *Stability and rupture of bifurcations bridges in semiconductor lasers subject to optical feedback.* PRE, vol. 66, 046216, 2002. 79

[Heil 2001] T. Heil, Ingo Fischer and Wolfgang Elsässer. *Chaos synchronization and spontaneous symmetry breaking in symmetrically delay-coupled semiconductor lasers.* PRL, vol. 86, no. 5, 2001. 11

[Heil 2002] Tilmann Heil, Josep Mulet, Ingo Fischer, Claudio R. Mirasso, Michael Peil, Pere Colet and Wolfgang Elsässer. *On/off phase shift keying for chaos-encrypted communication using external-cavity semiconductor lasers.* IEEE-JQE, vol. 38, no. 9, 2002. 11

[Heil 2003] T. Heil, I. Fischer, W. Elsässer, K. Green B. Krauskopf and A. Gavrielides. *Delay dynamics of semiconductor lasers with short external cavities: Bifurcation scenarios and mechanisms.* PRE, vol. 67, 066214, 2003. 79

[Henry 1982] Charles H. Henry. *Theory of the linewidth of Semiconductor Lasers.* IEEE-JQE, vol. Q-18, no. 2, 1982. 10

[Hwang 2000] S. K. Hwang and J. M. Liu. *Dynamical characteristics of an optically injected semiconductor laser.* Optics Comm., vol. 183, 2000. 42

[Jesper 1992] M. Jesper, T. Bjarne and M. Jannik. *Chaos in semiconductor laser with optical feedback: theory and experiment.* IEEE-JQE, vol. 28, no. 1, 1992. 15

[Kanakidis 2003] D. Kanakidis, A. Argyris and D. Syvridis. *Performance characterization of high-bit-rate optical chaotic communication systems in a back to back configuration.* J. of Lightwave Tech., vol. 21, 2003. 26

[Kobayashi 1976] K. Kobayashi. *Improvements in direct pulse code modulation of semiconductor lasers by optical feedback.* Trans. IECE, vol. E-59, 1976. 14

[Lang 1980] Roy Lang and Kohro Kobayashi. *External Optical Feedback Effects on Semiconductor Injection Laser Properties.* IEEE-JQE, vol. QE-16, no. 3, 1980. 14

[Lenstra 1985] D. Lenstra, B. H. Verbeek and A. J. den Boef. *Coherence Collapse in Single-Mode Semiconductor Lasers Due to Optical Feedback.* IEEE-JQE, vol. 21, no. 6, 1985. 15

[Liu 1997] Yun Liu and Junji Ohtsubo. *Dynamics and chaos stabilization of semiconductor lasers with optical feedback from an interferometer.* IEEE-JQE, vol. 33, no. 7, 1997. 39

[Liu 2002] Y. Liu, Y. Takiguchi, P. Davis, T. Aida, S. Saito and J. M. Liu. *Experimental observation of complete chaos synchronization in semiconductor lasers.* App. Phys. Lett., vol. 80, no. 23, 2002. 18

[Locquet 2002] A. Locquet, C. Masoller and C. R. Mirasso. *Synchronization regimes of optical-feedback-induced chaos in unidirectionally coupled semiconductor lasers.* PRE, vol. 65, 056205, 2002. 18

[Locuet 2002] A. Locuet, C. Massoller, P. Mégret and M. Blondel. *Comparison of two types of synchronization of external-cavity semiconductor lasers.* Optics Lett., vol. 27, no. 1, 2002. 11

[Luo 2000] L. Luo, P. L. Chu, T. Whitbread and R. P. Peng. *Synchronization and coherent combining of two pulsed fiber lasers.* Chin. Opt. Lett., vol. 7176, no. 213, 2000. 18

[Masoller 1997] C. Masoller. *Implications of how the linewidth enhancement factor is introduced on the Lang and Kobayashi model.* IEEE-JQE, vol. 33, no. 5, 1997. 10

[Maurer 1980] J. Maurer and L. Libchaber. *Effect of the Prandtl number on the onset of turbulence in liquid 4He.* J. Phys. Lett, vol. 21, no. 41, 1980. 31

[Meucci 2006] R. Meucci, F. Salvadori, M. V. Ivanchenko, K. A. Naimee, C. Zhou, F. T. Arecchi, S. Boccaletti and J. Kurths. PRE, vol. 74, 066207, 2006. 18

[Mirasso 1996] C. R. Mirasso, P. Colet and P. Garcia Fernandezi. *Synchronization of Chaotic Semiconductor Lasers: Application to Encoded Communications.* IEEE, Phot. Tech. Lett., vol. 8, 1996. 14, 18

[Mirasso 2000] Claudio R. Mirasso. In Applications of semiconductor lasers to secure communications. Nonlinear Laser Dynamics: Concepts, Mathematics, Physics, and Applications International Spring School, AIP, Conference Proceedings, Vol. 548, 2000. 19

[Murakami 2002] Atsushi Murakami. *Synchronization of chaos due to linear response in optically driven semiconductor lasers.* PRE, vol. 65, 056617, 2002. 18

[Nagashima 1999] Hiroyuki Nagashima and Yoshikazu Baba. In Introduction to Chaos: Physics and mathematics of chaotic phenomena. Institute of Physics Publishing, Bristol and Philadelphia, Shizouka University, 1999. 29

[Ohtsuko 2006] J. Ohtsuko. In Semiconductor Lasers: Stability, Instability and Chaos. Springer Series in Optical Sciences, Vol. 111, Springer-Verlag, 2006. 15, 29

[Osinski 1987] M. Osinski and J. Buus. *Linewidth broadening factor in semiconductor lasers–An overview.* IEEE-JQE, vol. 23, no. 1, 1987. 10

[Pecora 1990] L. M. Pecora and T. L. Carol. *Synchronization of chaotic systems.* PRL, vol. 64, 821, 1990. 16

[Pérez 2006] Toni Pérez, Mindaugas Radziunas, Hans-Jurgen Wunsche, Claudio Mirasso and Fritz Henneberge. *Synchronization properties of two coupled multi-section semiconductor lasers emitting chaotic light.* IEEE, Phot. Tech. Lett., vol. 18, no. 20, 2006. 31, 45

[Petermann 1991] K. Petermann. In LD modulation and noise. Kluwer, Dordrecht, 1991. 14

[Peterson] Ivars Peterson. In http://www.phschool.com/science_news /articles/staying_in_step.html. 16

[Pisarchik 2005] A. N. Pisarchik and R. Jaimes-Reátegui. In Homoclinic orbits in a piecewise linear Rössler-like circuit. Journal of Physics: Conference Series, 23, 2005. 67

[Pisarchik 2006] A. N. Pisarchik, R. Jaimes-Reátegui, J. R. Villalobos-Salazar, J. H. García-López and S. Boccalett. *Synchronization of chaotic systems with Coexisting Attractors*. PRL, vol. 96, no. 24, 2006. 67

[Pisarchik 2008] A. N. Pisarchik, R. Jaimes-Reátegui and J. H. García-López. *Synchronization of multistable systems*. Int. J. of Bifur. and Chaos, vol. 18, no. 6, 2008. 67

[Ravelet 2004] F. Ravelet, L. Marié, A. Chiffaudel and F. Daviaud. *Multistability and Memory Effect in a Highly Turbulent Flow: Experimental Evidence for a Global Bifurcation*. PRL, vol. 93, 164501, 2004. 31

[Revuelta 2002] Josè Revuelta, Claudio R. Mirasso, Pere Colet and Luís Pesquera. *Criteria for synchronization of coupled chaotic external-cavity semiconductor lasers*. IEEE, Phot. Tech. Lett., vol. 14, no. 2, 2002. 12

[Rogister 1999] F. Rogister, P. Mégret, M.Blondel O. Deparis and T. Erneuxi. *Suppression of low-frequency fluctuations and stabilization of a semiconductor laser subjected to optical feedback from a double cavity: theoretical results*. Optics Lett., vol. 24, no. 17, 1999. 15

[Rogister 2000] F. Rogister, D.W. Sukow and A. Gavrielidis. *Experimental demonstration of suppression of low-frequency fluctuations and stabilization of an external-cavity laser diode*. Optics Lett., vol. 25, no. 11, 2000. 15

[Rogister 2001] F. Rogister. *Nonlinear Dynamics of Semiconductor Lasers Subject to Optical Feedback*. PhD thesis, Faculté Polytechnique de Mons, 2001. 5

[Rottschafer 2005] Vivi Rottschafer and Bernard Krauskopf. In The ECM-backbone of the Lang-Kobayashi equations: a geometric picture. http://hdl.handle.net/1983/478, ROSE, 2005. 79

[Roy 1994] R. Roy and K. S. Thornburg Jr.l. *Experimental synchronization in chaotic lasers*. PRL, vol. 72, 1994. 16

[Ruiz-Oliveras 2005] F. R. Ruiz-Oliveras and A. N. Pisarchik. In Control of self-oscillations in a diode laser with external cavity. J. Phys. Conf. Series, Vol. 32, 2005. 15

[Ruiz-Oliveras 2006a] F. R. Ruiz-Oliveras and A. N. Pisarchik. *Phase-locking phenomenon in a semiconductor laser with external cavities.* Optic Express, vol. 14, no. 26, 2006. 34

[Ruiz-Oliveras 2006b] Flavio Ruiz-Oliveras. In Dinámica de láseres de semiconductor con cavidades externas. Master thesis, Centro de Investiagciones en Óptica, A.C., 2006. 34

[Ruiz-Oliveras 2009] F. R. Ruiz-Oliveras and A. N. Pisarchik. *Synchronization of semiconductor lasers with coexisting attractors.* PRE, vol. 79, 016202, 2009. 31

[Saford 1988] E. L. Saford and J. A. McCann. In Fiberoptics and Laser Handbook. 2nd Edition, McGraw-Hill, 1988. 1

[Salathe 1979] R. P. Salathe. *Diode lasers coupled to external resonators.* Appl. Phys., vol. 20, no. 1, 1979. 15

[Sale 1995] T. E. Sale. In Vertical Cavity Surface Emitting Lasers, Optoelectronic series: 2. John Wiley & Sons inc. New York, 1995. 10

[Saleh 1991] B.E.A. Saleh and M.C. Teich. In Fundamental of Photonics. Wiley, Florida, 1991. 8

[Siegman 1986] A. E. Siegman. In University Science Books. University Science Books, 1986. 1, 12

[Singh 1995] J. Singh. In Semiconductor Optoelectronics: Physics and Technology. McGraw-Hill Inc., 1995. 8

[Sivaprakasam 2002] S. Sivaprakasam, Paul S. Spencer, P. Rees and K. Alan Shore. *Regimes of chaotic synchronization in external-cavity laser diodes.* IEEE-JQE, vol. 38, no. 9, 2002. 18

[Smith 2000] Warren J. Smith. In Modern Optical Engineering. McGraw Hill, SPIE presst, 2000. 45

[Soriano 2006] M. C. Soriano. In Aspects of feedback and noise in Vertical-Cavity Surface-Emitting Lasers. PhD thesis, Vrije Universiteit Brussel, 2006. 5

[Soriano 2008] Miguel C. Soriano, Flavio Ruiz-Oliveras, Pere Colet and Claudio R. Mirasso. *Synchronization properties of coupled semiconductor lasers subject to optical feedback.* PRE, vol. 78, 046218, 2008. 17

[Strogatz 1994] Steven H. Strogatz. In Nonlinear dynamics and chaos: with applications to physics. Addison Wesley, 1994. 29

[Sugawara 1994] T. Sugawara, M. Tachikawa, T. Tsukamoto and T. Shimizu. *Two different routes to chaos in a two-mode CO2 laser with a saturable absorber.* PRL, vol. 72, 3502, 1994. 18

[Terry 2001] J. R. Terry and G. D. VanWiggeren. *Chaotic communication using generalized synchronization.* Ch. Sol. and Fractals, vol. 12, 2001. 25

[Thyagarajan 1981] K. Thyagarajan and A. K. Ghata. In Laser Theory and Application. Plenum Press, New Delhi, 1981. 1

[Tronciu 2006] V.Z. Tronciu, H. J. Wunsche, M. Wolfrum and M. Radziunas. *Semiconductor laser under resonant feedback from a Fabry-Perot resonator: stability of continuos-wave operation.* PRE, vol. 73, 046205, 2006. 82

[Tronciu 2008a] V. Z. Tronciu, I. V. Ermakov, Pere Colet and Claudio R. Mirasso. *Chaotic dynamics of a semiconductor laser with double cavity feedback: applications to phase shift keying modulation.* Opt. Comm., vol. 281, no. 18, 2008. 31, 45

[Tronciu 2008b] V. Z. Tronciu, Claudio R Mirasso and Pere Colet. In Chaos-based communications using semiconductor lasers subject to feedback from an integrated double cavity. Journal of Physics B: Atomic, Molecular, and Optical Physics, 2008. 31, 45

[van Tartwijk 1995] G. H. M. van Tartwijk and D. Lenstra. *Semiconductor lasers with optical injection and feedback.* Quantum Semiclass. Opt., no. 7, 1995. 14

[Vicente 2005] Raúl Vicente, José Daudén, Pere Colet and Raúl Tora. *Analysis and characterization of the hyperchaos generated by a semiconductor laser subject to a delayed feedback loop.* IEEE-JQE, vol. 41, no. 4, 2005. 12

[Vicente 2008] Raúl Vicente, Ingo Fischer and Claudio R. Mirasso. *Synchronization properties of three-delay-coupled semiconductor lasers.* PRE, vol. 78, 066202, 2008. 11

[Wang 1994] W. M. Wang, K. T. V. Grattan, A. W. Palmer and W. J. O. Boylei. *Self-mixing interference inside a single-mode diode laser for optical sensing applications.* J. Lightwave technol., vol. 12, 1994. 14

[Weiss 1991] C.O. Weiss and R. Vilaseca. In Dynamics of Lasers. VCH, Weinheim, 1991. 15

[Wieczorek 2000] S. Wieczorek, B. Krauskopf and D. Lenstra. *Mechanisms for multistability in a semiconductor laser with optical injection.* Optics Comm., vol. 183, 2000. 42

[Wieczorek 2005] S. Wieczorek, B. Krauskopf, T.B. Simpson and Daan Lenstra. *The dynamical complexity of optically injected semiconductor lasers.* Phys. Reports, vol. 416, 2005. 42

[Wilson 1998] John Wilson and John Hawkes. In Optoelectronics An Introduction. Prentince Hall Europe, NewCastle, 1998. 8

[Würtenberger 2000] Sandra E. Würtenberger. In Unterdrückung und kontrolle chaostischer instabilitäten von halbleiterlasern unter externer optischer rückkopplung. Diplomarbeit, Technische Universität Darmstadt, 2000. 82